Summer 2014

A numerical procedure to design the optimal axial balance in external gear machines and its potential in formulating novel efficient design solutions

Divya Thiagarajan
Purdue University

Graduate School ETD Form 9
(Revised 01/14)

PURDUE UNIVERSITY
GRADUATE SCHOOL
Thesis/Dissertation Acceptance

This is to certify that the thesis/dissertation prepared

By Divya Thiagarajan

Entitled
A Numerical Procedure to Design the Optimal Axial Balance in External Gear Machines and its Potential in Formulating Novel Efficient Design Solutions

For the degree of Master of Science in Mechanical Engineering

Is approved by the final examining committee:

ANDREA VACCA

MONIKA IVANTYSYNOVA

FARSHID SADEGHI

To the best of my knowledge and as understood by the student in the *Thesis/Dissertation Agreement. Publication Delay, and Certification/Disclaimer (Graduate School Form 32)*, this thesis/dissertation adheres to the provisions of Purdue University's "Policy on Integrity in Research" and the use of copyrighted material.

Andrea Vacca

Approved by Major Professor(s): _____

_____

Approved by: David Anderson 07/02/2014

Head of the Department Graduate Program Date

A NUMERICAL PROCEDURE TO DESIGN THE OPTIMAL AXIAL BALANCE IN EXTERNAL GEAR MACHINES AND ITS POTENTIAL IN FORMULATING NOVEL EFFICIENT DESIGN SOLUTIONS

A Thesis

Submitted to the Faculty

of

Purdue University

by

Divya Thiagarajan

In Partial Fulfillment of the

Requirements for the Degree

of

Master of Science in Mechanical Engineering

August 2014

Purdue University

West Lafayette, Indiana

To my family

ACKNOWLEDGEMENTS

Firstly, I would like to thank Prof. Andrea Vacca for giving me this wonderful opportunity to work in his research team and for being one of the best possible advisors that anybody could hope for. This work would not have been possible without his constant support, enthusiasm and patience over the past two years. I would also like to thank my committee members, Prof. Monika Ivantysynova for her valuable comments and guidance throughout my time at Maha and Prof. Farshid Sadeghi for giving me the best possible introduction to lubrication in his class at Purdue.

I would like to specially thank Sujan for being a wonderful mentor and helping me familiarize with his work. I will always cherish the many interesting discussions that we had and the useful suggestions that he had given has helped me shape my work. I would also like to thank all my labmates, Ram, Pulkit, Tim, Sid, Gabriele, Guido, Davide, Matteo, Natalie, Ashley, Rene, Meike, Andrew, Paul and others who have made Maha such a fun and interesting place to come to work every day. My acknowdgement for the lab will not be complete without thanking Susan, Connie and Anthony for their help in making all our lives in graduate school so much easier and their enthusiasm in spreading the cheer in the lab.

I would like to take this opportunity to thank my parents and my brother, to whom I dedicate this thesis, for their strong support and love throughout my life.

TABLE OF CONTENTS

Page

Page

Page

LIST OF TABLES

Table Page

LIST OF FIGURES

Figure Page

Figure Page

Figure Page

Figure Page

Figure Page

Figure Page

Figure Page

Figure Page

Figure Page

NOMENCLATURE

Symbols

h - Film thickness, m

X – Cartesian X coordinate, m

Y – Cartesian Y coordinate, m

λ, ξ- Lame's coefficients

μ - Kinematic viscosity of working fluid, Pa-s

A – Area, m^2

p – Pressure, Pa

ρ – Density, kg/m^3

v – Cartesian velocity vector, m/s

M – Moment, N-m

Q – Volumetric flow rate, m^3/s

ω – Angular velocity, rad/s

T – Torque, Nm

τ_{zx} – Shear stress in XY plane in the X direction, N/m^2

P – Power Loss, Nm/s

O – Order of magnitude

N – Number of operating conditions

$\boldsymbol{\Delta}$A – Step size of design parameter, m^2

$\boldsymbol{\Delta}$Y – Step size of design parameter Y, m

V – Volume, m^3

Subscripts

t – Top surface

b – Bottom surface

ref – Reference

max – Maximum

min – Minimum

avg – Average

$loss, shear$ – Losses due to fluid shear

$loss, leak$ – Losses due to leakages

Acronyms

EGM – External Gear Machine

LP – Low Pressure

HP – High Pressure

TSV – Tooth Space Volume

EHD – Elastohydrodynamic

FSI – Fluid Structure Interaction

FVM – Finite Volume Method

HYGESim – Hydraulic Gear Machine Simulator

CFD – Computational Fluid Dynamics

CV – Control Volume

FV – Finite Volume

PDE – Partial Differential Equation

STL – Stereo lithography

CAD – Computer Aided Design

GNI – Gap Non-uniformity Index

OC – Operating Condition

wrt – with respect to

ABSTRACT

Thiagarajan, Divya. M.S.M.E., Purdue University, August 2014. A Numerical Procedure to Design the Optimal Axial Balance in External Gear Machines and its Potential in Formulating Novel Efficient Design Solutions. Major Professor: Andrea Vacca, School of Mechanical Engineering.

A novel numerical procedure to design the optimal axial balance in external gear machines (EGMs) has been formulated and developed in the present study. Lateral lubricating interfaces exist between the lateral bushes and the rotating gears in pressure compensated designs of EGMs and play a significant role in minimizing power losses arising from fluid shear stress and leakages from the gap. Moreover, lateral bushes in pressure compensated designs of EGMs perform significant functions of sealing the tooth space volumes while they transfer fluid from the inlet to the outlet port.

The losses from the lateral gap from these two opposing sources can be minimized by designing an optimal balance area on the side of the lateral bushes which do not face the gears, while simultaneously ensuring that proper pressure is established at the high pressure port of the EGM. This condition is termed as the ‘axial balance’ of the machine, which is significant in improving its reliability and reducing wear in the EGM under consideration.

To determine the optimal axial balance which minimizes the power losses associated with the lubricating gap in all operating conditions, all the static and hydrodynamic forces acting on the lateral bushes have to be considered. This delicate aspect of external gear units design is usually addressed through empirical procedures which rely heavily on experience, expertise and expensive experimental trial and error. In this research, the proposed method is fully automatic and leverages the previous work of modeling the lateral lubricating

interface between gears and lateral bushes in the author's research group at Purdue. The developed procedure has a significant potential to virtually design the axial balance in a variety of EGM designs, results for which are presented in the current study. Furthermore, the possibilities of using the developed procedure to design new efficient solutions is demonstrated in this research by applying this method to design a micro surface shaping effect, by introducing a linear sloping wedge on either side of the gear teeth. Optimal axial balance configurations are determined for these effects which further improves the efficiency of the reference EGM chosen for the purpose of this study.

CHAPTER 1. INTRODUCTION

1.1 Introduction to External Gear Machines

External gear machines (EGMs) are one of the widely used positive displacement machines today with its applications in agricultural, earthmoving and construction machinery, aerospace, automotive and other industries. The popular use of these hydrostatic units is owing to their reliability, compact nature, good efficiencies, comparatively low costs and simplicity in manufacturing. EGMs are primarily characterized by very few internal components to achieve the function of a positive displacement machine. Typically, these machines can function both as a pump as well as a motor. Reference cases of a pump configuration is presented in this research study although similar considerations can be applied to motors as well.

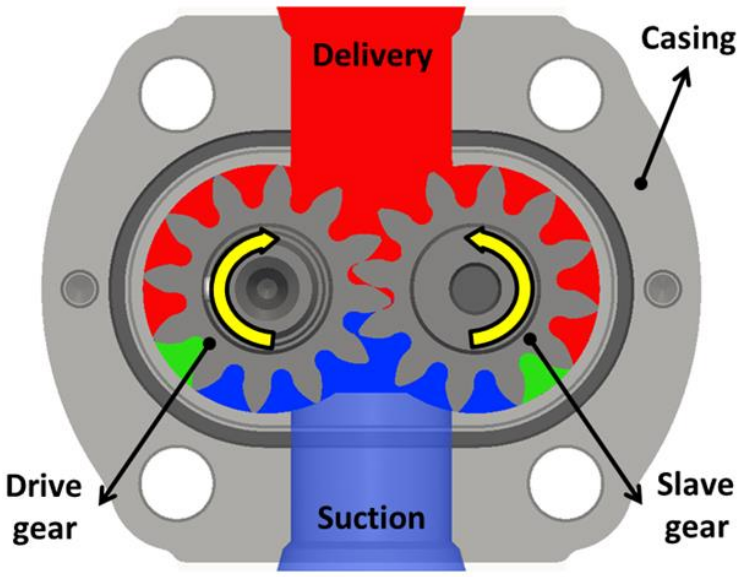

Figure 1: Schematic illustration of operation of an EGM representing the displacement of the hydraulic fluid at low pressure near the suction port to the delivery port at high pressure due to the meshing of the gears. The colors blue, green and red shown in the figure represent low, intermediate and high pressures of the fluid respectively.

External gear pumps have a relatively simple principle of operation where the fluid is transferred from the suction port to the delivery port at high pressure by the meshing action of the rotating gears. This working principle of an external gear pump is illustrated in Figure 1. While the gears are driven by the mechanical power from a shaft, the tooth space volumes (TSVs) between the gear teeth play the role of displacement chambers and transfer the hydraulic fluid between the inlet and the outlet ports.

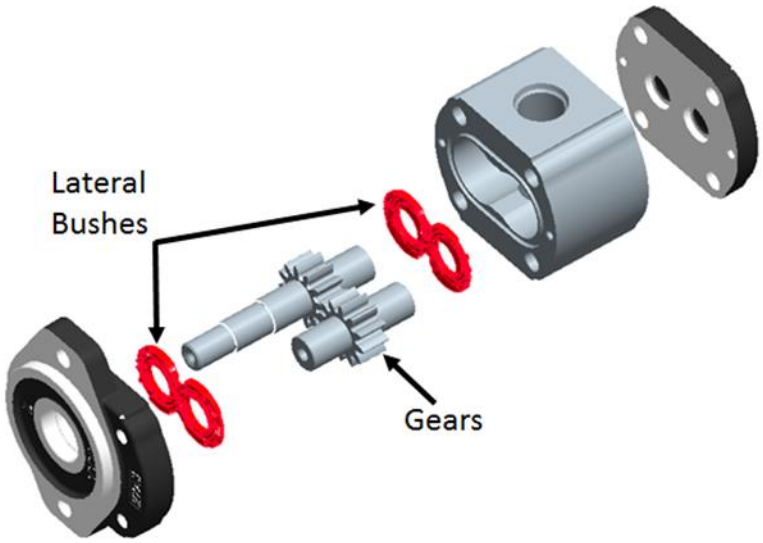

Figure 2: Exploded view of the main components of a typical EGM.

Currently available designs of external gear machines include both pressure compensated designs with lateral bushes and non-pressure compensated designs without the lateral bushes. Non-pressure compensated EGM designs are typically suitable for low pressure applications, usually less than 100 bar. However, since the focus of the present research is on designing the axial balance for pressure compensated EGM designs.

The main components of a pressure compensated EGM are shown in an exploded view in Figure 2. It can be seen from the figure that the driver and the driven gears are flanked by lateral bushes on either side. Lateral bushes constitute some of the critical aspects of designing an EGM.

Usually, there are two broad variations in the design of these lateral elements, one which is referred to as the pressure plates (as shown in Figure 3(A)) and the other design called

as the bearing blocks (as illustrated in Figure 3(B)). The latter design of the lateral bushing additionally includes the journal bearing through which the gear shaft passes.

Figure 4(A) and Figure 4(B) shows the pressure plate design of the lateral bushing with its side facing the gears and away from the gears respectively. It can be observed from Figure 4(B) that the 'relief grooves' machined on these plates near the suction (low pressure relief groove) and the delivery (high pressure relief groove) ports are responsible for ensuring that there are no trapped volumes when the gear TSVs enter into the meshing zone and thus preventing pressure peaks and cavitation. Another important function of the lateral bushes is to seal the TSVs while preventing leakages as the fluid is transferred from the delivery to the suction port. The bearing block design of the lateral bushing additionally includes the journal bearing which the gear shaft passes and thus provides structural support to the shaft in addition to the functions described above.

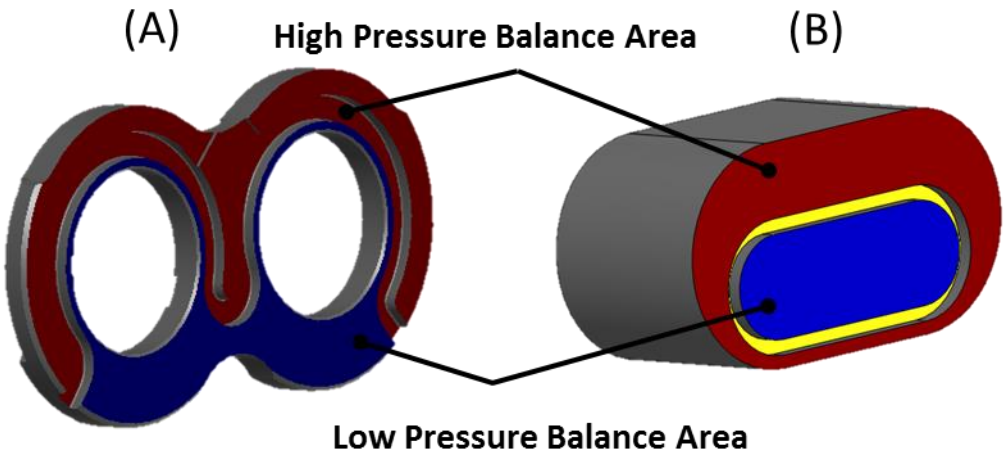

Figure 3: Figure showing the different kinds of lateral bushing designs (A) Pressure plate type design (B) Bearing block design (journal bearing through the gear shaft not shown here).

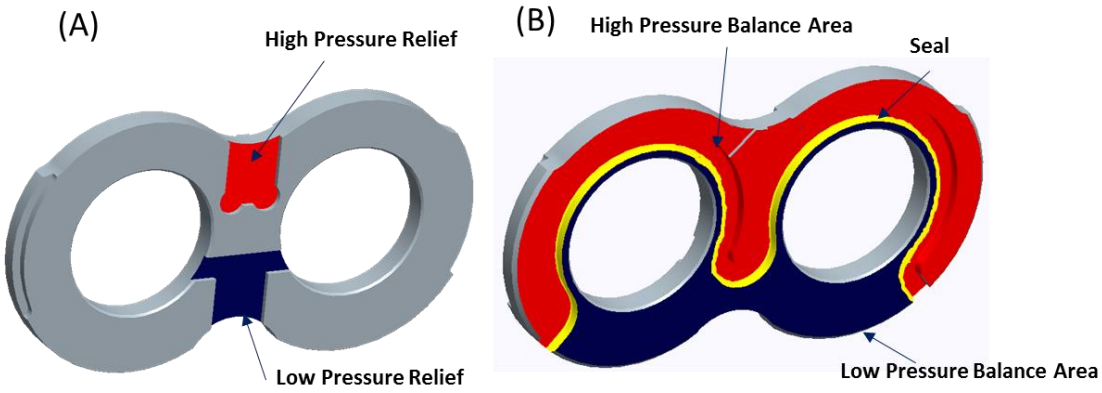

Figure 4: (A) Side of the lateral bushing facing the gears (B) Side of the lateral bushing facing away from the gears.

The final component in an EGM is the casing, which is also responsible for sealing the TSVs, especially in preventing leakage flow over the tooth tips and also providing the outer structural framework to the gears as well as the lateral bushes. Although an EGM has a working principle of operation which is relatively simple to understand, each of the main components of an EGM as outlined earlier perform multiple functions which increases the complexity in the process of designing the machine.

1.2 Lateral Lubricating Interfaces

In common designs of EGMs, the lubricating gaps in the machine can be classified primarily into radial and lateral gaps. The focus of this study is on the lateral lubricating gaps present in the clearance between the lateral bushes and the gears. Two such lateral lubricating interfaces as shown in Figure 5, exist on either side of the gears, between the driver and driven gears and the lateral bushes. In general, apart from aiding the sealing function of the lateral bushes to prevent leakages, these lubricating gaps are significantly responsible for supporting bearing loads in the machine. Thus, these lubricating interfaces form one of the most important aspects of the EGM design.

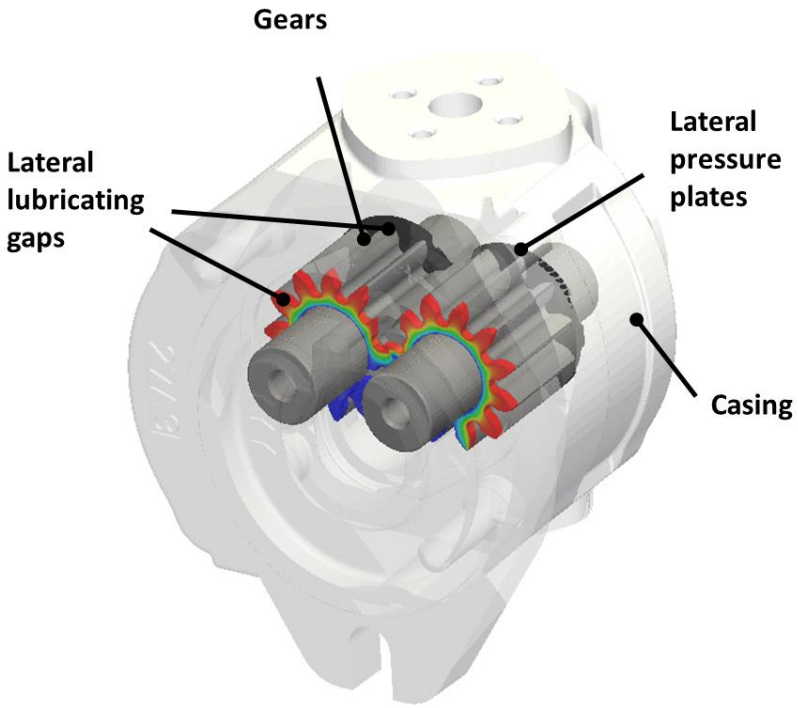

Figure 5: Representation of lateral lubricating interfaces existing between the gears and lateral bushes in EGM.

Two main opposing sources of power losses are present in these interfaces. One source of power loss arises due to the viscous friction in the fluid while the other source of power losses is due to the lateral leakages from these interfaces. The losses due to viscous friction increase with low gap heights in the interface whereas the lateral leakages increase with increasing lubricating film thicknesses between the gears and the lateral bushes. An optimal design of the floating axially balanced lateral bushes can help us in reducing the total power loss from the lateral gap and this represents one of the main goals of the present research study.

1.3 Research Objectives

Minimizing the total power losses thus involves careful consideration of both the opposing sources of power losses and this can be achieved by designing the balance area (as shown in Figure 3) on the side of the lateral bushing facing away from the gears. From a simplified perspective, we can achieve an optimal design of the lateral lubricating interface itself by designing the area on the rear side of the lateral bushing which is responsible for creating the condition ‘axial balance’ of the lateral bushes. This condition refers to the force balance

achieved on the lateral bushing considering both hydrostatic and hydrodynamic forces which will be later explained in this paper. Thus, designing an optimum axial balance condition comprises a critical aspect of an EGM design.

The design of these axially balanced lateral bushes is thus a very delicate process which involves consideration of not only all the forces acting on the lateral bushes, but also the physical effects of the lateral lubricating interfaces which couples the fluid flow and the elastic deformation of the solid components involved, namely the gears and the bushes themselves. Currently, such a challenging procedure is carried out in industries using empirical procedures and is largely based on skills and experience of the designer and requires expensive and time consuming trial and error experiments.

The present work involves developing an automatic numerical procedure to design the optimal balance area on the lateral bushing by coupling this optimization with an advanced fluid structure interaction (FSI) lateral lubricating gap model which comprehensively incorporates the effects of both the fluid and the physical solid domains. The original contributions of this research includes formulating and developing this optimization procedure and coupling it to a FSI-EHD lateral gap model and EGM simulation model which was previously developed and validated in the author's research team [1], [2]. Besides minimizing the power losses from the lateral lubricating interface, the procedure also prevents excessive relative tilts between the bushes and the gears, which would promote metal contacts and consequently material wear and an additional objective function was defined in this study to take care of this particular aspect of the design as a part of this research.

Original contributions of this work also include adapting this procedure for different EGM designs, micro-surface shaping effects and a wide range of operating conditions of an EGM. The capability of the procedure to design the optimal axial balance for a variety of features and designs of EGMs is demonstrated in this paper by considering certain selected cases which involve adding a wedged profile to the surface of the gears.

The procedure developed in this research has immense potential to virtually design efficient EGMs carefully considering all the physical effects of lateral lubricating interface and also represents a tool to explore novel and modified EGM designs.

CHAPTER 2. LITERATURE OVERVIEW

In this section, the literature related to different aspects of the present research study has been covered by classifying it into relevant sections. Since numerical modeling of EGMs plays an important role in design optimization, modeling efforts developed for these machines along with the literature related to optimization of components in fluid power are presented in this chapter.

2.1 Modeling of EGMs

Modeling of external gear machines has witnessed several developments in the past and the impact of the various modeling efforts have resulted in improving efficient designs of such machines. Numerical modeling of the lateral lubricating interface considering the effects operating conditions and lateral bushing tilt angles along with experimental considerations have been studied in the works of Koc.et al, Borghi et al [3-7]. In these works, an attempt was also made to use the developed numerical model to design the balance area by assigning numerical values to certain design parameters of the area. A FVM model of the lateral gaps integrated with a larger simulation tool for the entire EGM was presented in the studies of Zecchi and Vacca [8]. The work of Morgridge et al [9] incorporates EHD (ElastoHydroDynamic) effects and surface roughness considerations in a simplified single tooth gear model. However, all the research works mentioned used simplified assumptions of lubricant film thicknesses and bushing tilts and did not consider effects of including the elastic deformation of the solid components while solving for the pressure field generated in the lubricating gap.

The first EGM lateral lubricating interface model capable of predicting the film thickness was presented in research works of Dhar and Vacca [10] as an integral part of a larger complete EGM simulation tool. However, this work made an assumption of rigid solids,

and a first fluid structure interaction model of EGM lateral gaps, considering elastohydrodynamic effects while predicting film thickness was presented in the works of Dhar et al[11] and [12]. Also, the same authors in [12] also included a detailed experimental validation confirming that EHD effects are indeed of paramount importance to correctly predict the lubricating film thickness in the EGM lateral gaps. Thermal deformation effects of the lateral bushes and the gears were fully coupled to this FSI-EHD lateral gap model and the numerical prediction of the film thickness from this model was validated with direct experimental measurements of film thickness values in the work of Dhar [1]. This lubricating gap model, the most advanced of its kind till date, forms an integral part of the present study for evaluating the fully coupled effects of the solid and fluid domains in the lateral gap on the design optimization work presented in this study. Thus, the details of this model are further discussed in CHAPTER 3.

On the other hand, analysis of the flow delivered from an EGM was first studied with the help of graphical methods in the work of Beecham [13] and with analytical approaches in the studies of Bonacini, Manring and Kasaragadda, Fielding et al[14-16]. The effects of the designing various relief grooves and their profiles on the efficiency, pressure peaks and cavitation in EGMs by analyzing the fluid flow have been studied in the works of Casoli et al [17, 18]. Analysis of different forces acting on the moving parts of the machine with both analytical and numerical solutions have been presented by Ivantysyn and Ivantysynova, Falfari and Pelloni, Zardin and Borghi respectively in [19-21]. There has also been studies related to the flow field in EGMs using CFD applications by Wustmann et al, Simerics Inc, del Campo et al [22-24].

However, most of these works focused mainly on a carrying out detailed analysis on specific aspect of operation of the EGMs. The development of the simulation tool HYGESim (HYdraulic GEar machine Simulator) focused on modelling accurately the various phenomena associated with the operation of an EGM to provide a complete simulation model of the machine. Formulation, development and experimental validation of HYGESim has been presented previously in the works of Vacca and Gudetti, and Casoli et al [2,25]. Since the present work involves using the various sub models in the larger framework of HYGESim, the model will be briefly discussed in CHAPTER 3.

2.2 Design Optimization of Components in Positive Displacement Machines

Sophisticated optimization techniques developed and evolved over the last few decades have proved to be a class of very valuable tools in designing various engineering components. In particular, optimization techniques have been applied in designing various components of positive displacement machines in quite a few significant works.

In the case of EGMs, optimization approaches for efficient design of lateral bushes and gears have been presented in previously by Huang et al, Wang et al and Devendran, Vacca [26-30]. Similar multi-objective optimization tools for reducing noise generation in axial piston machines have been developed in the works of Seeniraj and Ivantysynova, Kim and Ivantysynova, Ericson et al [31-34]. However all these design optimization tools did not consider the fluid flow and the highly coupled physics of the FSI phenomena present in the lubricating interfaces of these machines. The present study represents a first of its kind design tool in positive displacement machines, which couples an automatic optimization procedure to a FSI-EHD model for lubricating gaps and thus fully accounting for the physical effects of the lateral lubricating interface in the design process.

2.3 Effects of Micro-Surface Shaping on Lubrication Performance

The present research also has the potential to aid in novel efficient designs of EGMs. The novel designs considered for this study include adding a linear sloping micro wedge to the surface of the gears and literature related to this aspect of the present research is discussed here. Surface texturing and the effect of adding micro surface shapes on the lubrication performance of conformal contacts have been explored previously in Nanbu et al, Wang et al. , Krupka et al [35-38]. Similar ideas can be applied to improve the lubrication performance of positive displacement machines. The possibility of using an advanced numerical model which incorporated the effects of EHD while predicting the fluid film thickness in lubricating gaps of positive displacement machines as a design tool for analyzing surface shaping effects was first investigated by Baker and Ivantysynova [39]. This work resulted in the design of a micro shaped surface (waved valve plate) which was shown to significantly reduce the power losses in the cylinder block valve plate interface in swash plate type axial piston machines. In EGMs, the possibilities of promoting efficient designs with novel surface shaping by adding linear sloping wedge and waved features on

the gears and shot peening effects on the gears and lateral bushes were demonstrated in the work of Dhar [1]. All such analysis were performed using the FSI-EHD lateral gap model Dhar, Vacca [12] which is also an integral part of the present study. The wedged gears were found to show a significant potential in reducing the power losses from the lateral gap. However, this work only explored the wedged designs with the original balance area design of the reference EGM and which might not be the optimal design for the texturing features introduced in the gap. Also, in the same work, only a certain specified wedge depth on the gears was considered as a part of that study and other variations were not explored. The optimization procedure presented in the current research work offers a potential to analyze the variations of these wedge depths on the gears by optimizing the axial balance for each of those cases. Furthermore, the procedure also offers the possibility of achieving further improved reduction in power losses from the lateral gap with the help of an optimal axial balance for each of the configurations of the wedged gears. Such a potential possessed by the procedure is analyzed and discussed in CHAPTER 6.

Moreover, the idea of adding linear sloping wedge profiles to the surface of the gears promotes the possibility of having EGMs with an extended field of operation, especially at much lower minimum shaft speeds. The potential of using the developed optimization tool to design the optimal axial balance of EGMs with such extended range of operating conditions is also investigated in 6.3.4.

CHAPTER 3. BASIC NUMERICAL MODELS FOR AXIAL BALANCE ANALYSIS

In the present section, an overview of the simulation models used in this work will be discussed. The research study performed in this paper utilizes the sub models of a EGM simulation tool HYGESim [2] as a calculation core for evaluating the designs generated in the optimization procedure. The framework of HYGESim consisting of several submodels and their interaction with each other is shown in Figure 6. The entire simulation tool models different aspects of an EGM operation which include displacement of fluid through the TSVs, features of the meshing process, internal pressure peaks and cavitation, port flow oscillations, radial motion of the gears, radial balance of forces, and the flow features in the lateral gaps and axial balancing of floating bushes and gears.

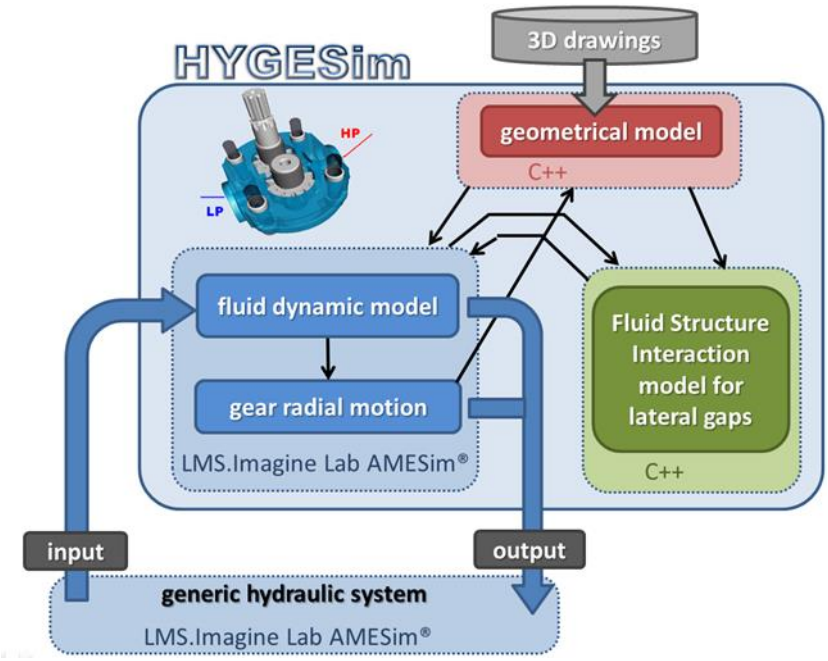

Figure 6: Framework of HYGESim with all its sub models.

The fluid structure interaction model of the lateral gaps forms the main calculation core of the developed optimization algorithm and hence will be given a detailed description in this

paper. The lateral gap model also utilizes the fluid dynamic model of HYGESim to set the pressure boundary conditions and the geometric model to calculate the input area volumes, as shown in Figure 6. These two models will be explained briefly in the following subsections.

3.1 HYGESim Simulation Tool

In the present section, a brief overview of the two sub models of HYGESim, namely the fluid dynamic model and the geometric model, which interact with the lateral gap model is presented. While the fluid dynamic model, developed inside the LMS Imagine Lab AMESim® environment with custom and standard component libraries in C language, is responsible for the simulation of flow through the TSVs, the geometric model evaluates the radial motion of the gears with the help of a standalone application.

3.1.1 Fluid Dynamic Model of HYGESim

The fluid dynamic model works in a co-simulation manner with the lateral lubricating gap model to set the pressure boundary conditions needed for the latter. Using a lumped parameter approach, the fluid dynamic model characterizes the flow through the entire EGM. The EGM is divided into multiple control volumes (CVs) as shown in Figure 7. The TSVs which also form a part of the CV classified are shown in the same figure for both the driver and driven gears.

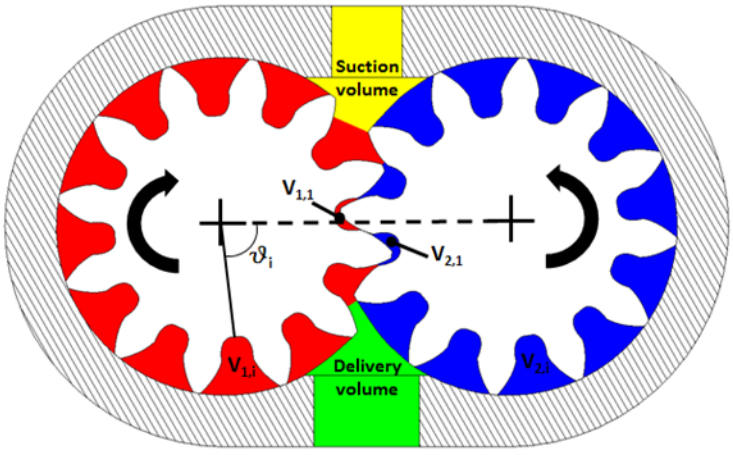

Figure 7 : Control Volumes specified in the fluid dynamic model of HYGESim.

The flows between the several control volumes, such as between adjacent CVs in the meshing zone, are modeled using the orifice equation,

$$\dot{m_{i,j}} = \frac{(p_i - p_j)}{|(p_i - p_j)|} \cdot \rho|_{p=\overline{p_{i,j}}} \cdot \alpha \cdot \Omega_{i,j} \cdot \sqrt{\frac{2 \cdot (p_i - p_j)}{\rho|_{p=\overline{p_{i,j}}}}}, \tag{3.1}$$

where, $\dot{m_{i,j}}$ represents the flow rate from the i[th] to the j[th] TSV and $\Omega_{i,j}$ represents the area of the connection between the two CVs.

A laminar flow equation (fully developed laminar flow, considering the relative motion between surfaces) is used to calculate the leakages across the tooth – tip,

$$\dot{m_{i,j}} = \rho \left[-\frac{h^3}{12\mu} \frac{(p_i - p_j)}{L} + \frac{hu}{2} \right] \cdot b, \tag{3.2}$$

where, $\dot{m_{i,j}}$ is the laminar flow from the i[th] to the j[th] TSV of the same gear through the gap between the tooth tip and the casing, u is the velocity of the wall, L is the gap length and b is the gap width.

The FSI model determines the net flow between each volume and the lateral gap using the flow field in the gap. Based on the flow between the adjacent TSVs, assuming conservation of mass and fluid state equation, the rate of change of pressure in the CV can be obtained using a pressure build-up equation,

$$\frac{dp_i}{dt} = \frac{1}{V_i} \frac{dp}{d\rho}\Big|_{p=p_i} \cdot \left[\sum \dot{m_{in,i}} - \sum \dot{m_{out,i}} - \rho|_{\rho=\rho_i} \left(\frac{dV_i}{dt} - \frac{dV_{var,i}}{dt} \right) \right]. \tag{3.3}$$

Further details of the fluid dynamic model and its outputs can be found in [2].

The co-simulation approach developed in [40] which involves the interaction between the FSI model and the fluid dynamic model where the exchange of pressure-leakage information between these two models occurs iteratively until convergence is reached. The fluid dynamic model helps in setting the pressures in the TSVs of the EGM and at the suction and delivery ports for the gap model. An example of this as a particular TSV travels one revolution from LP port to the HP port along with the delivery pressure at the HP port is shown in Figure 8. The convention for the shaft angle used is shown in Figure 7. As can

be seen, the pressures are varying according to the angle of rotation of the TSV, and this leads to variable loads on the lubricating interface.

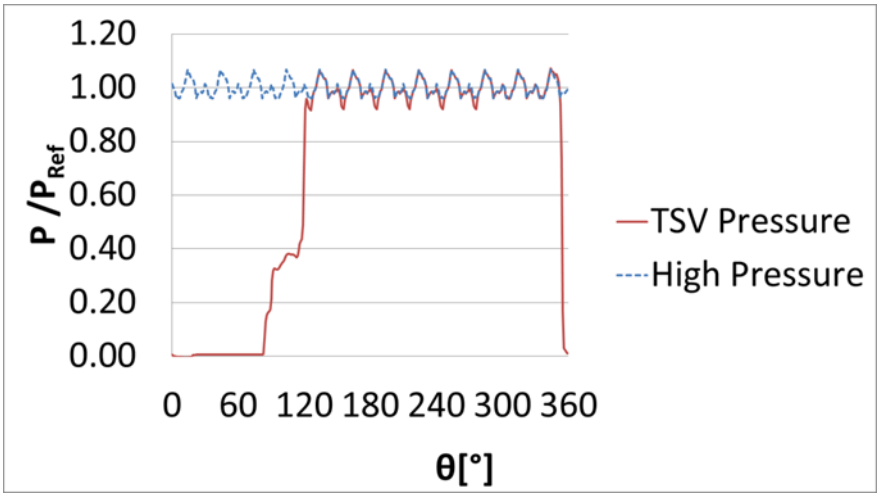

Figure 8: Typical pressure in a TSV and at the delivery (high pressure) port as predicted by HYGESim.

3.1.2 Geometric Model of HYGESim

The geometric model is responsible for the calculation of several relevant geometrical areas of volumes for input to both the FSI model as well as the fluid dynamic model. The equations (Eqns. 3.1, 3.2, 3.3) introduced to model the flow between the TSVs in the fluid dynamic model require the knowledge of the volumes of the TSVs as well as the area of the connections between them.

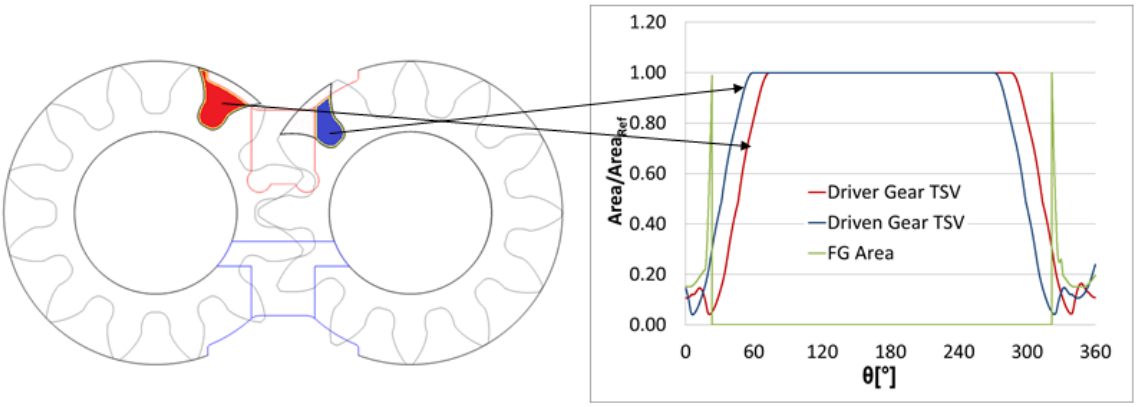

Figure 9: Areas of the tooth spaces provided by the geometric model to the lateral lubricating gap model.

Since these are based on the actual CAD drawings of EGMs, the geometric model, and consequently the whole procedure, can work for any given geometry of EGMs (for

example, shapes or relief grooves, teeth, etc…). The typical outputs from the geometric model which include the TSV areas of the gears as they undergo one revolution are shown in Figure 9. The TSV area information is, in particular, provided to the FSI model and is used to estimate the forces acting on the bushing which is used both to calculate the force balance on the bushing as well as to calculate its deformation.

3.2 Fluid Structure Interaction Model of the Lateral Lubricating Gaps

The FSI model for the lateral lubricating interfaces in EGMs forms the core simulation tool used for the optimization procedure developed in this work. The evaluation of the objective functions required by the procedure, namely the total power loss from the gap and the parameter for defining the non-uniformities in the gap (discussed in detail in CHAPTER 4) is performed with the help of the outputs obtained from the FSI model. The FSI model has been developed and validated with experimental capacitive film thickness measurements in the lateral gap [1]. In the same research work, thermal deformation effects have also been added to the lateral lubricating gap mode. However, it was also shown that these effects in the considered reference cases did not significantly change the results. Thus, for the purposes of developing this optimization tool in the present work, the thermal deformation effects have not been considered.

The FSI-EHD model of the lateral lubricating gaps in EGMs has been developed as an independent application using the programming language C++ and was linked with open source libraries like OpenFOAM [41] for FV discretization of PDEs and linear system solving, GSL [42] for multidimensional root-finding and spline interpolation.

There are various submodels which are part of the lateral gap model which are listed below.

Automatic rotating mesh generator/ Solid mesh generation: Finite volume meshing of the fluid film geometry and the solid components.

Interface with HYGESim Fluid Dynamic Model: Setting of boundary faces on the fluid film mesh.

Gap Flow Model: Finite volume solver for the main constitutive equations for the fluid.

Structural Model: Finite volume solver for the main constitutive equations for the solids i.e. the gears and the lateral bushes.

Force Balance Model: Accounts for the balance of forces acting on the lateral bushes and the gears.

The submodels can be classified into two broad categories namely, Preprocessors and Solvers. A schematic illustration of the lubricating gap model along with its submodels are shown in Figure 10. In this section, the details of various submodels that comprise the FSI gap model are discussed.

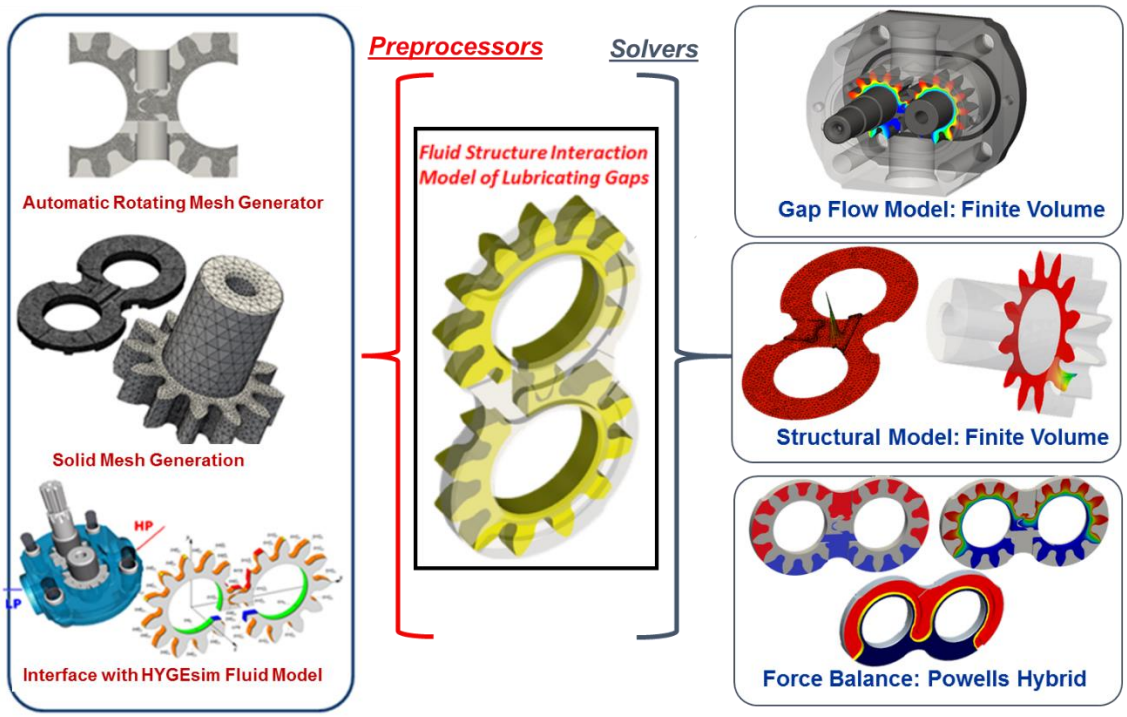

Figure 10: Figure showing the various submodels, divided into two categories, which are part the FSI_EHD

3.2.1 Mesh Generation

3.2.1.1 Generation of Fluid Mesh

A mesh generation module for creating the mesh for the fluid domain was developed in C++ as part of the preprocessing for the FSI model. This module offers a lot of flexibility by possessing the ability to create FV fluid mesh for a wide variety of gear geometries starting from the CAD drawings of the EGM as an input. Stereo Lithography (STL) CAD

files of half a tooth of the gears (as shown in Figure 11(A)) and the profiles of the high pressure and the low pressure grooves (as shown in Figure 11(B) and Figure 11(C)) are the inputs required by this module.

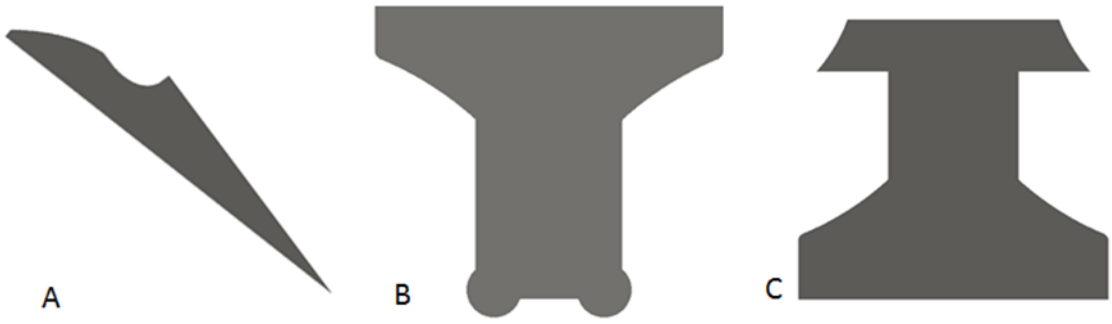

Figure 11: CAD inputs used in the mesh generation module A) Gear tooth profile B) HP relief groove C) LP relief groove.

The definition of the fluid domain for the lubricating gap must take fully into account the rotation of the gears and the intersection of the lateral gap domain with the high pressure (HP) and low pressure (LP) relief grooves. The gap area that is directly under the relief grooves has the uniform instantaneous pressure from the inlet or the outlet port – thus, this region is excluded from the gap flow computation. Thus, a two dimensional (with a single cell in the third dimension) FV mesh consisting of 6 node prism elements of the gears are created using the open source GMSH libraries. Then the mesh created is rotated by the appropriate step in order to create the base FV domain. The intersection of the relief groove geometry with this base domain is performed, where all cells of the finite volume mesh that are either inside or cut by the relief grooves are removed and the boundaries of this cut region is smoothened. The same procedure is performed for each angle of rotation of the gears. Two representative meshes for different angles of rotation is shown in Figure 12.

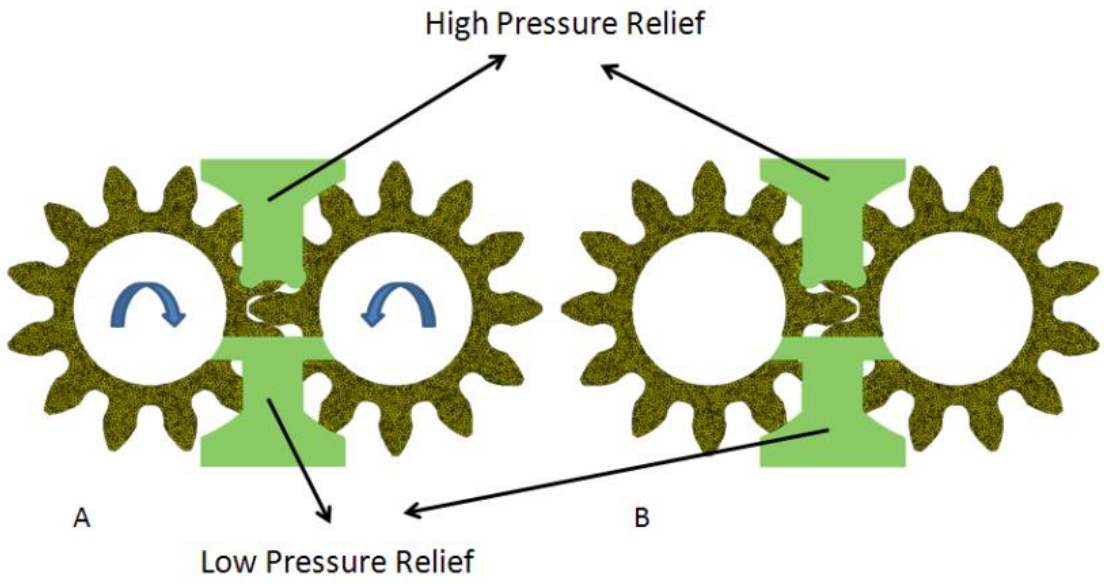

Figure 12: Dynamic 2D meshes for an angle of rotation (in degrees) A) 0˚ B) 15˚. Average size of the dynamic mesh is ~44500 elements for the case represented.

3.2.1.2 Generation of Solid Meshes

The 3 Dimensional FV meshes (shown in Figure 13) for the solids were generated using the commercial code ANSYS [43]. Tetrahedral meshes for the solid components were chosen since this allowed for the most automated and fastest meshing solution, with the meshes conforming to the geometry very accurately. The mesh generation for the solids is comparatively simple, since the geometry of the meshes remains constant. Of the 3D solid meshes, the mesh of the bushing is static, while the mesh of the gears is rotated at the specified angular velocity of the pump using a simple rotational coordinate transformation for all the cells in the gear mesh,

$$x_{new,i} = x_{old,i}\, cos(\theta) - y_{old,i}\, sin(\theta), \tag{3.4}$$

$$y_{new,i} = x_{old,i}\, sin(\theta) + y_{old,i} cos(\theta). \tag{3.5}$$

The coupling of the solid and the fluid domains is one of the key aspects of the FSI model and this requires transferring of information between the fluid mesh and the two solid meshes. This is accomplished by numerically linking the three meshes by using an inverse distance weighted interpolation method.

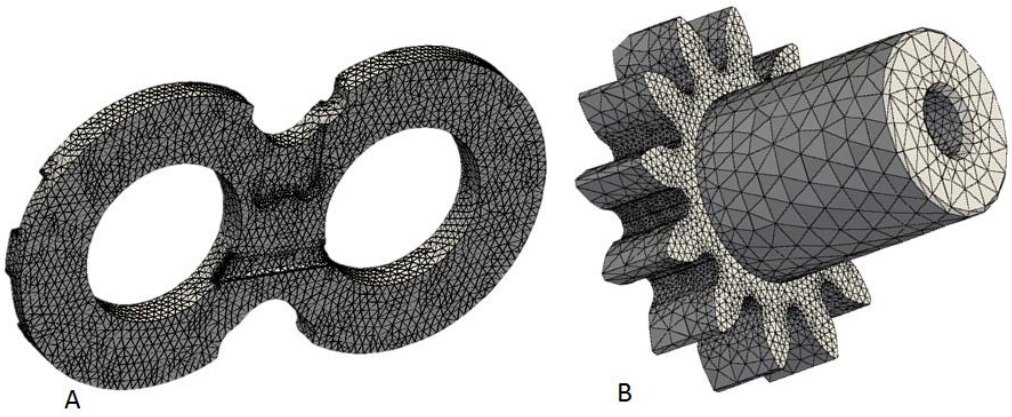

Figure 13: Figure showing the solid meshes of A) Lateral bushing – Pressure plate type design (~12000 cells) and B) Gears (~54000 cells).

3.2.2 Interface with HYGESim

The interaction of the lateral gap model with the fluid dynamic model of HYGESim was outlined earlier in 3.1. There is a two way interaction between the two models while they exchange pressure-leakage information to set the boundary conditions at the various interfaces of the gap domain which include those in the meshing region and those outside this region, as shown in Figure 14.

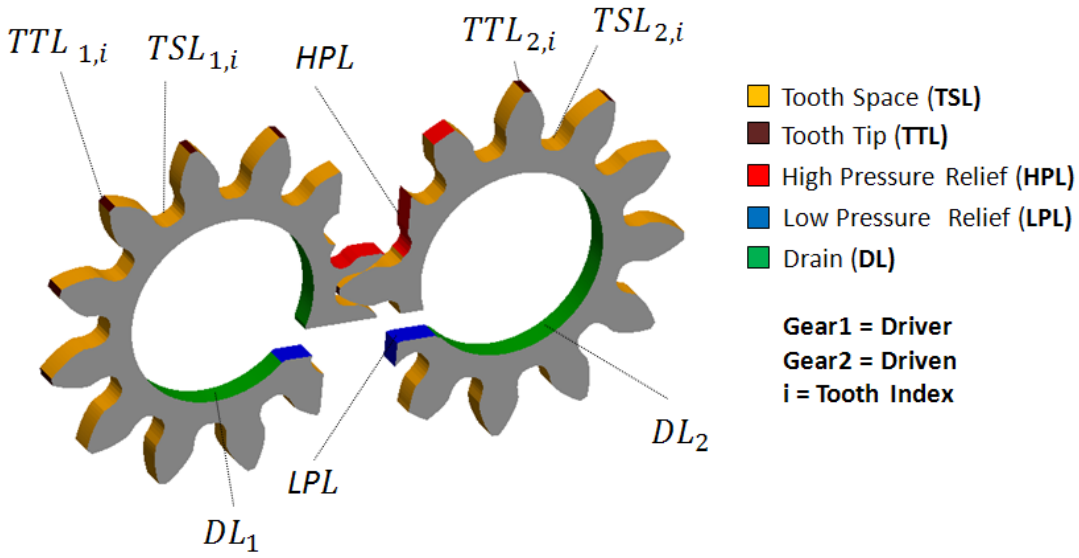

Figure 14: The lateral gap and interfaces along which the FSI and the HYGESim fluid dynamic model interact.

Apart from setting the pressure boundary conditions, the FSI model is also provided by the variable areas and center of mass of the TSVs as the gear rotates over the entire revolution.

3.2.3 Gap Flow Model

The pressures and the flow field in the lateral lubricating gap is solved with the help of the Reynolds equation which is derived from the well-known Navier Stokes' equations using certain simplified assumptions which are suitable for this case [44]. However, the most common form of the Reynolds equation has the limitation of being able to model surface features on only one boundary, with the other required to be flat. In the lubricating gap both the gears and the bushing are expected to deform. Thus, an appropriate form of the Reynolds equation was derived for the geometry of the lateral gap in EGMs. The detailed derivation of this form of Reynolds equation can be found in [1].

$$\nabla.\left(\left(\frac{-\rho h^3}{12\mu}\right)\nabla p\right)+\frac{\rho \mathbf{v_b}}{2}.\nabla h+\rho \mathbf{v_b}.\nabla(h_b)+\rho\left(\frac{\partial h_t}{\partial t}-\frac{\partial h_b}{\partial t}\right)=0, \tag{3.6}$$

where $h = h_t - h_b$, is the lubricating gap height.

In the geometry being used in the current case (shown in Figure 15) the velocity of the upper surface $\mathbf{v}_t = 0$ since the lateral bushes are stationary. The lower surface corresponds to the lateral surface of the gears and rotates with a velocity $\mathbf{v}_b = \mathbf{v}_g$.

Each term in the Reynolds equation captures different effects. In brief,

- $\nabla.\left(\frac{-\rho h^3}{12\mu}\nabla p\right)$: Diffusion of the pressure ("Poiseuille effects") from the boundaries into the domain.
- $\frac{\rho \mathbf{v_b}}{2}.\nabla h$, $\rho \mathbf{v_b}.\nabla(h_b)$: Hydrodynamic ("wedge effects") generation of pressure due to surface features on the top and bottom surfaces.
- $\rho\left(\frac{\partial h_t}{\partial t}-\frac{\partial h_b}{\partial t}\right)$: Hydrodynamic ("squeeze effects") generation of pressure due to micro motion of the top and bottom surfaces.

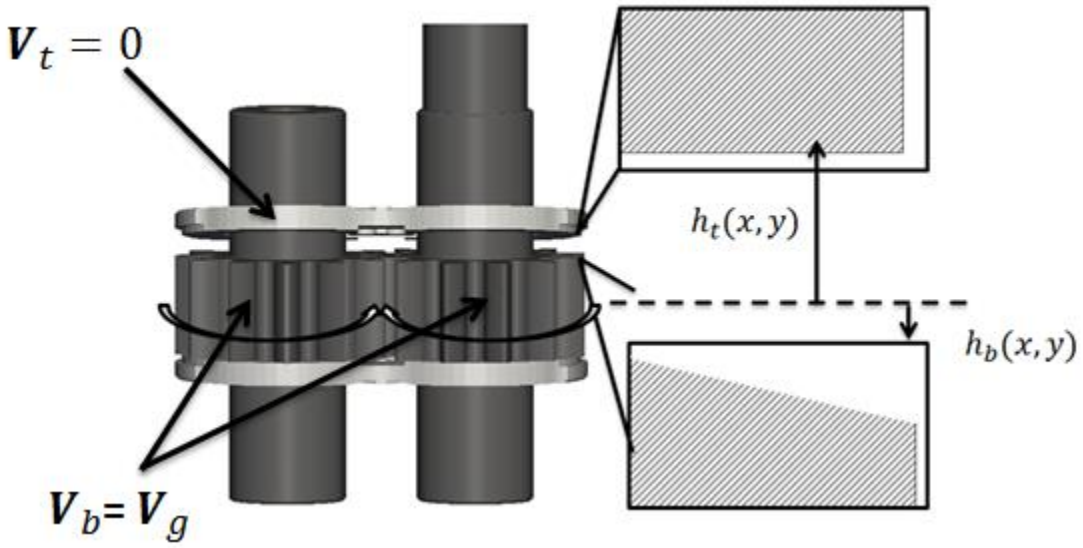

Figure 15: Figure depicting the terms in the Reynolds equation for the current case with height of the top surface as $\boldsymbol{h_t}$ and bottom surface as $\boldsymbol{h_b}$ where $\boldsymbol{h = h_t - h_b}$. The rotational speed of the gears is $\boldsymbol{v_b}$ and the lateral bushing is fixed with $\boldsymbol{v_t}$.[1].

A finite volume solver for the Reynolds equation was implemented in an application developed in C++. The pressure is solved for using a Preconditioned Conjugate Gradient algorithm, with a Diagonalized Incomplete Cholesky preconditioner.

The dependence of the density and viscosity of the fluid on pressure are modeled using the relations for fluid properties found in [19].

$$\rho = \rho_0(1 + \beta_p(p - p_0)), \tag{3.7}$$

$$\mu = \mu_0 e^{\alpha_p p}. \tag{3.8}$$

3.2.4 Determination of Gap Heights and Squeeze Velocities

The geometry of the lateral gap is a plane when solid deformations are not considered, and therefore can be fully determined considering the 3 points that are shown in Figure 16. Using the gap height information stored at the points T0, T1 and T2 the gap height for an arbitrary point in the domain can be calculated using the following,

$$h_{UD}(x,y) = x\frac{2h_{T2} - h_{T1} - h_{T0}}{2(d+R)} + y\frac{h_{T1} - h_{T0}}{2R} + \frac{h_{T0} - h_{T1}}{2}. \tag{3.9}$$

The information about the squeeze velocities are also stored at the three points as shown in the Figure 16, and the resultant squeeze velocity at an arbitrary point is given by,

$$\frac{\partial h(x,y)}{\partial t} = x\frac{2\frac{\partial h_{T2}}{\partial t} - \frac{\partial h_{T1}}{\partial t} - \frac{\partial h_{T0}}{\partial t}}{2(d+R)} + y\frac{\frac{\partial h_{T1}}{\partial t} - \frac{\partial h_{T0}}{\partial t}}{2R} + \frac{\frac{\partial h_{T0}}{\partial t} - \frac{\partial h_{T1}}{\partial t}}{2}. \quad (3.10)$$

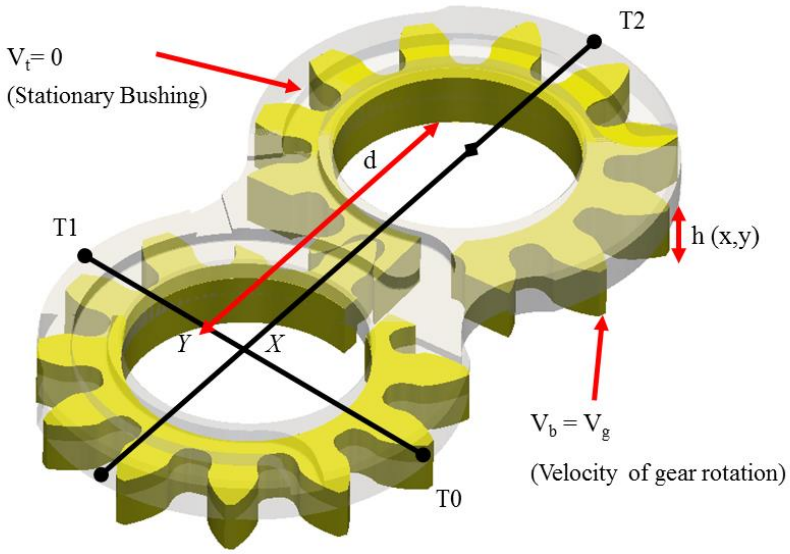

Figure 16: Figure showing the lubricating gap (in yellow) between the lateral bushing (transparent view) and the gears.

3.2.5 Structural Model

The structural components of the lubricating interface: gears and the lateral bushes experience high pressure loads and deformation which is expected to be in the EHD lubrication regime. Thus, the deformation of the solid components is modeled using a finite volume stress/deformation solver and the gap model fully coupled the effects of the solid and the fluid domains. Using the formulation described in [45], the elasticity equation may be written in a form amenable to segregated FVM solution (shown in Eq. (3.11)) and the resulting discretized linear system was solved using a geometric multi-grid solver.

$$\nabla.\,[(2\xi+\lambda)\nabla\mathbf{u}] + \nabla.\,[\xi(\nabla\mathbf{u})^{T} + \lambda\mathbf{I}\mathrm{tr}(\nabla\mathbf{u}) - [(\xi+\lambda)\nabla\mathbf{u}] = -\rho\mathbf{f}\,. \quad (3.11)$$

Detailed discussion of the different criteria behind developing and formulating this FV deformation solver have been validated and published in [1], [12]. In the same works, different constraints applied on the lateral bushing for calculating its deformation have been discussed. For all the results presented in this paper, a LP constraint on the lateral

bushing has been used wherein the lateral bushing is assumed to be pressed against the casing in the low pressure side. Further details pertaining to the evaluation of the deformation of the lateral bushes and the gears using an offline technique is also explained in [1].

3.2.6 Coupled Fluid Structure Interaction – Axial Balance Algorithm

The numerical scheme implemented for solving the FSI-EHD regime in the lubricating interfaces of EGMs is shown in Figure 17.

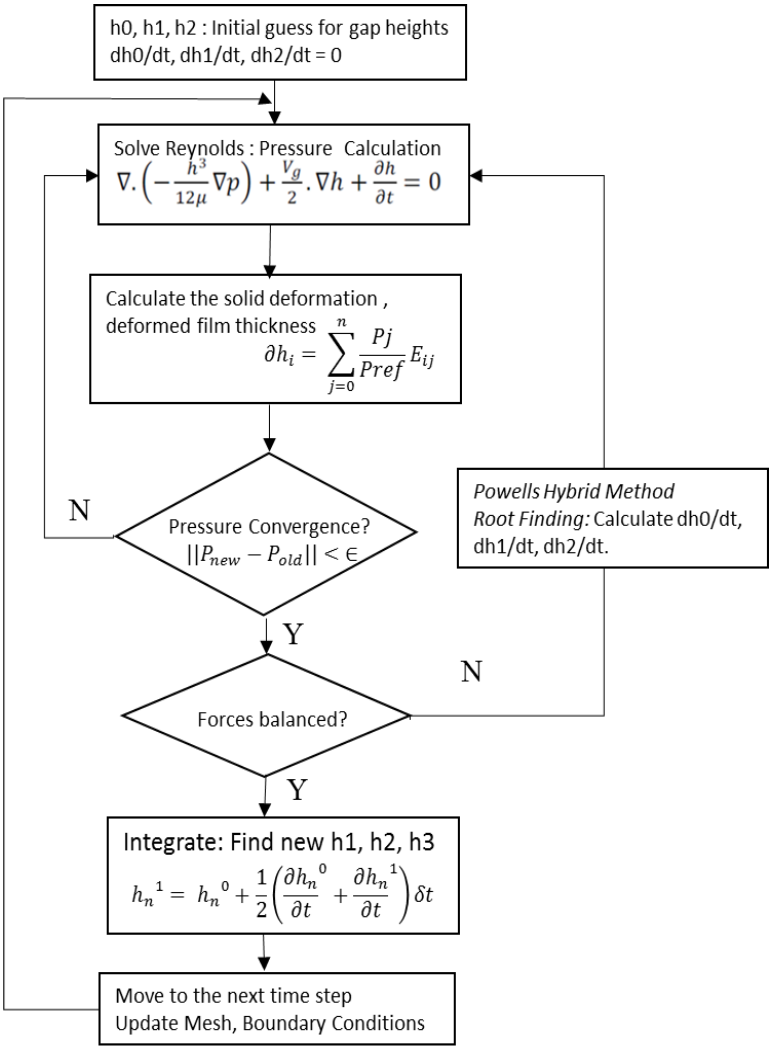

Figure 17: Coupled numerical scheme for the FSI-EHD lateral gap model ([11]).

Starting with an initial guess for the film thickness, the pressure in the gap is solved using the Reynolds equation. Subsequently, using this information, solid deformation is used to

calculate the new film thickness and this loop continues until the pressure values in the gap are converged. The force balance system in the lateral bushing is then solved till the equilibrium condition is reached. Subsequently after achieving this force equilibrium, the squeeze velocities are then integrated to find the instantaneous gap heights at 3 selected points. Similar procedure is carried out for different time steps in the mesh until an overall convergence in film thickness is observed. Further details of the coupled FSI numerical scheme can be found in [11] and [12].

CHAPTER 4. AUTOMATIC NUMERICAL PROCEDURE FOR FINDING OPTIMAL AXIAL BALANCE

In this section, the numerical procedure developed for optimizing the axial balance in EGMs by finding the corresponding optimal balance area on the rear side of the lateral bushing (side not facing the gears) as shown in Figure 4(B). This numerical optimization procedure is one of the chief original contributions of the present research study.

4.1 Forces Acting on the Solid Components of the Lateral Lubricating Interfaces

The modeling of the force balance on the lateral bushing to achieve steady state operation of the EGM and the 'axial balance' condition is presented in this subsection. Accurate evaluation of the forces acting on the solid components is important for both the structural solver to determine the deformation of the components, as well as the axial force balance solver. The following has been cited from [1] and detailed discussion of these forces can be obtained from the same. The main forces acting on the lateral bushes are:

- *Forces acting on the Balancing Areas of the Lateral Bushes:* As introduced briefly in chapter 1 the balancing areas of the lateral bushes have a high pressure and a low pressure area separated by a seal (which is assumed to be at high pressure). These are highlighted in Figure 17(B). The individual forces and the resultant is calculated accordingly,

  $$F_{HP,Bal} = p_{HP} A_{HP,Bal} \,, \tag{4.1}$$

  $$F_{LP,Bal} = p_{LP} A_{LP,Bal} \,, \tag{4.2}$$

  $$F_{Bal} = F_{HP,Bal} + F_{LP,Bal} \,. \tag{4.3}$$

  The point of application of the resultant balance force is calculated using the centers of mass of the high and low pressure balance areas,

$$X_{Bal} = \frac{F_{HP,Bal}X_{HP} + F_{LP,Bal}X_{LP}}{F_{Bal}} \quad , \tag{4.4}$$

$$Y_{Bal} = \frac{F_{HP,Bal}Y_{HP} + F_{LP,Bal}Y_{LP}}{F_{Bal}} \quad . \tag{4.5}$$

- *Forces acting on the Relief Grooves:* At a particular angle of rotation the pressures acting on the relief grooves can be assumed to be uniform at the high pressure or the low pressure, according to the values provided by the fluid dynamic model. The relief grooves are shown in Figure 18(A). The resultant force acting on the lateral bushes due to the high pressure relief grooves is given by,

  $$F_{HP} = p_{HP}A_{HP,Rel}, \tag{4.6}$$

  and the resultant force due to the low pressure relief groove is given by

  $$F_{LP} = p_{LP}A_{LP,Rel}. \tag{4.7}$$

  It will also be of importance in upcoming analysis to calculate the resultant forces as well as the point of application of these resultants. Thus, the resultant force due to the pressures in the relief grooves is given by,

  $$F_{Rel} = F_{HP} + F_{LP}. \tag{4.8}$$

- *Forces acting on the areas corresponding to the TSVs:* The pressures in the TSVs of the two gears are calculated using the fluid dynamic model of HYGESim. A typical distribution of the pressures from the TSV acting on the lateral bushing is shown in Figure 18(C). The force acting on the lateral bushes due to these pressures can be calculated using the information of the pressures in the TSVs introduced previously as an input. The information regarding the areas of the TSVs are provided by the geometric model of HYGESim (as discussed in 3.1).

  $$F_{TSV} = \sum_{i}^{n_t} p_i A_i. \tag{4.9}$$

- *Force arising out the solution of the Reynolds Equation from the Gap:* The final force that is necessary of the calculation of axial balance of the lateral bushes is force arising out of the pressure solution that is calculated in the lubricating gap, solving the Reynolds equation. Since the gap domain is discretized using an FV

mesh the resultant force must be calculated using the pressures in the individual cells and also the areas of the individual cells,

$$F_{Gap} = \sum_{i}^{nFaces} p_i A_i. \quad (4.10)$$

A typical distribution of pressure in the gap is shown in Figure 18(D).

On the other hand, the forces acting on the gears is primarily due to the pressures in the lubricating gap. However, the pressures in the relief grooves are taken to be acting on the parts of the gears that are inside the relief grooves for a particular angle of rotation.

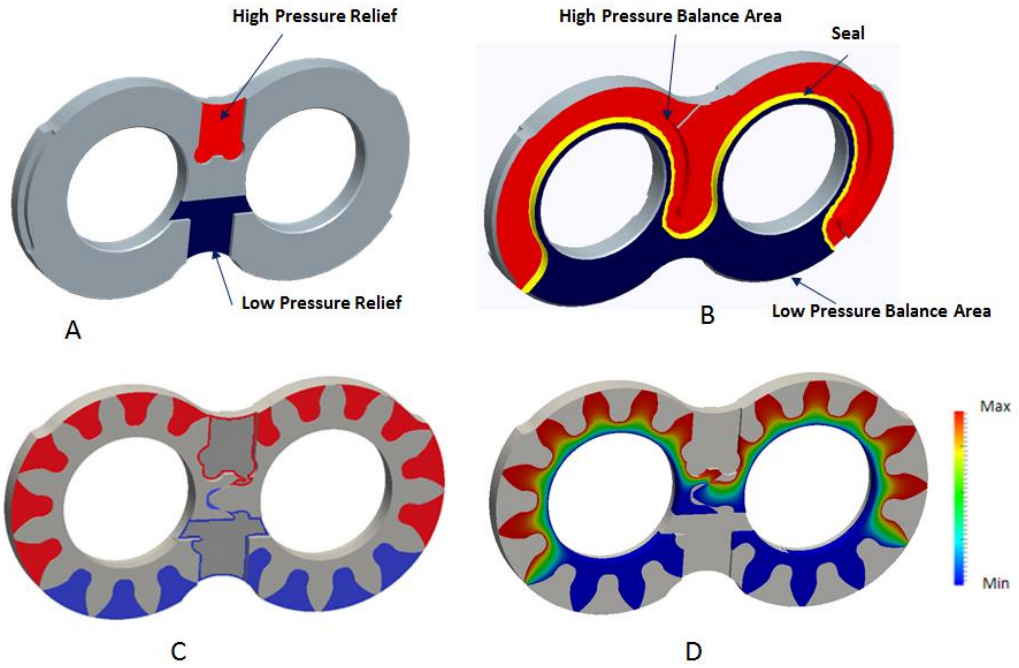

Figure 18: The pressures acting on the lateral bushing from the A) Relief grooves and B) the pressure compensating balance areas C) TSVs and D) the lateral lubricating gap.

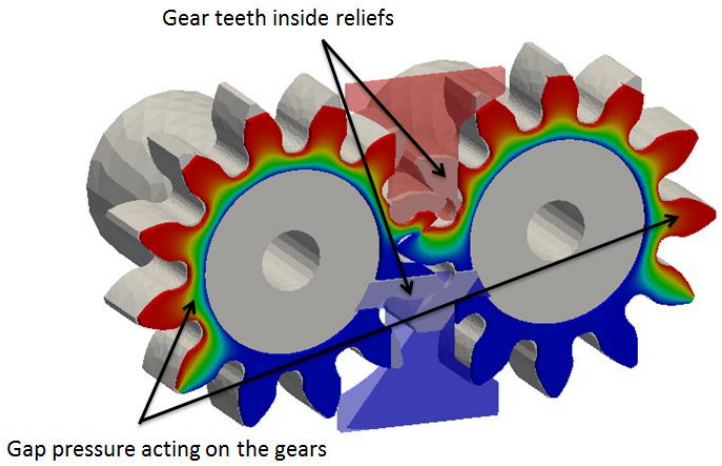

Figure 19 : Gap pressure shown acting on the gears (section view).

4.2 Force Balance of the Lateral Bushing

In a steady state operation of an EGM, the forces arising from the lubricating film will have to balance out all external forces acting on the lateral bushing. Thus, to achieve this steady state operation, the forces acting on the lateral bushing described in previous section can be used in setting up the static force balance algorithm for the lateral bushing.

The forces acting on the lateral bushing can be primarily classified in to two broad categories ([1]): Clamping force (F_c) which is the force that tends to push the lateral bushing towards the gears and lifting force (F_{li}) which lifts the lateral bushing away from the gears. Hence, the forces are classified into the following equations,

$$F_c = F_{Bal}\,, \tag{4.11}$$

and,

$$F_{li} = F_{Rel} + F_{TSV} + F_{Gap}. \tag{4.12}$$

The force balance algorithm (as developed in [1]) proceeds by considering that the lateral bushing achieves static equilibrium at every instantaneous position of the gears. The balance of the lifting forces and the clamping forces is what determines the condition 'axial balance' in EGMs. An illustration of this system of forces acting on the lateral bushing (pressure plate type design) is shown in Figure 20.

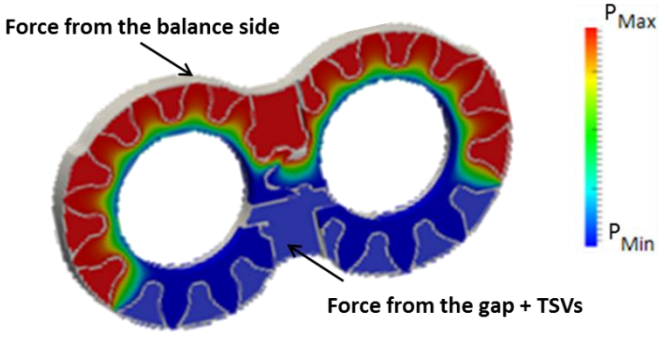

Figure 20: System of forces acting on the lateral bushing (which constitute the axial balance condition).

Since for a particular iteration the values of F_{Bal}, F_{Rel} and F_{TSV} are based on inputs to the FSI model, the above conditions of static equilibrium are fulfilled by the solution of the pressure in the gap. For every iteration in the progress of the algorithm a value of the resultant force from the lubricating gap - F_{Gap} , therefore, must be found which fulfills the necessary conditions for static equilibrium of the lateral bushing. This is achieved in particular by the use of the hydrodynamic squeeze effect, i.e. the generation of pressure due to the squeeze velocities $\frac{\partial h_t}{\partial t}$ ([1]) in the gap domain.

Of all the forces constituting this force balance system, the force F_{bal} acting on the balance areas of the lateral bushes is of particular interest. This force, particularly the force acting on the high pressure balance area can be varied by varying the balance area itself for a given operating condition. Thus, such a numerical variation of the balance area can be used to alter the value of F_{bal} in the force system and thus determine an optimal axial balance. Although both the forces acting on both high pressure and low pressure balance area constitute F_{bal} , design of the high pressure balance area is focused in this study owing to its sheer magnitude over the low pressure balance area.

To determine the optimal axial balance, first, a closer look at the total power losses from the lateral lubricating gap is needed and it represents one of the main objective function of the optimization procedure developed in this work. Minimizing the total power loss from the lateral gap is thus one of the chief goals of this procedure. There are two primary sources of power losses in the lateral gap, which are:

- *Power losses due to the fluid friction in the gap* - These losses are of mechanical nature and arise from the shear stresses due to fluid viscosity. Typically, these losses are high when the values of fluid film thickness in the gap are low.
- *Power losses due to the lateral leakages from the gap* – These losses represent the volumetric losses occurring due to leakages from the lateral lubricating gap. These losses are typically high when the gap heights in the lubricating interfaces increases to slightly higher values.

It can be observed from the above description of the power losses in the lateral lubricating gap that the two sources of power losses have opposing effects with respect to the fluid film thickness in the gap, which makes the design of an optimal axial balance configuration a very delicate procedure by achieving a reasonable compromise in the gap heights. A good axial balance therefore, contributes to an improved reliability and reduced chances of wear in the machine. Thus, the total power losses from the lubricating interfaces can be considered as an objective function for the numerical optimization procedure.

A second objective function is considered for developing the numerical optimization procedure with a goal of avoiding sharp contacts between the gears and the lateral bushes which are associated with excessive relative tilt between these mechanical elements. The necessity of this second objective function in addition to minimizing power losses, was propelled by the fact that the optimization procedure uses the FSI-EHD lateral gap model assumes a full film lubrication regime in the gap and very low gap heights are numerically saturated to a minimum value. These occurrence of these very low gap heights correspond regions of contact which are not addressed properly by the gap model. Such regions of contact might arise in some of the designs simulated in the optimization procedure. These designs are undesirable although their power losses may be comparable to some other designs without any such sharp contact regions. Thus, a factor Gap Non-uniformity Index (GNI) is defined in this study to account for the non-uniformities and sharp contacts in the gap between gears and lateral bush, which may occur in some designs.

Figure 21 shows the flowchart illustrating a step by step account of the developed automatic procedure for finding the optimal balance area. It can be observed from this figure that input operating conditions are needed for this iterative procedure. Hence, the final optimal balance area determined will have an axial balance configuration which will serve as a compromise of both the objective functions between all these operating conditions at input. A set of designs are generated and their objective functions are evaluated using their corresponding output fields generated by the FSI-EHD lateral gap model. A direct search method is used to generate a new set of designs based on the information obtained from the current evaluation. The procedure continues iteratively until a preset convergence criterion is reached. Each step in the flowchart will be discussed in detail in the order in which they appear in the flowchart.

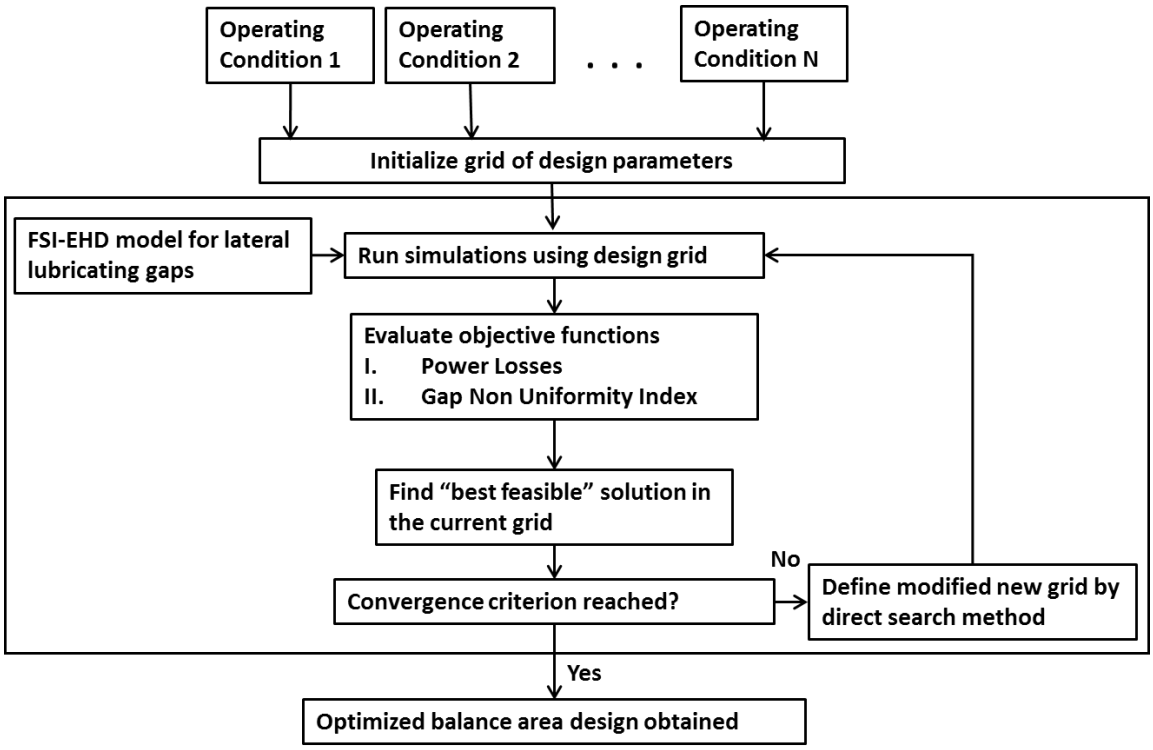

Figure 21: Flowchart for designing the optimal axial balance of EGMs.

4.3 Design Parameters for the Optimization Procedure

The aim of this optimization procedure is to design the high pressure balance area as discussed earlier in this chapter. The balance area on the lateral bushing can be sufficiently defined with the help of two design parameters: the area A (highlighted in red as shown in

Figure 22(A)) and the Y coordinate of the point of application of the resultant force which acts on the high pressure balance area. It is assumed that the X coordinate of this resultant force is used to define the symmetry of the design area and thus does not change with different configurations of the balance area. This assumption appears to be reasonable for the current reference case where the two gear profiles are identical.

In all the results presented in this study, the various lateral bushings were chosen to be constrained in its LP side when the deformation was evaluated in the FSI gap model. Several different constraints for calculating the bushing deformation are possible as outlined in [1]. But, constraining the LP side was found to perform the best by validating with corresponding experimental measurements as published in [12].

Figure 22 shows the high pressure that acts on the balance area of the lateral bush. This high pressure force can be reduced to a single equivalent resultant force which has a single point of application (point P shown in Figure 22). Therefore, the balancing force and moment arising from rear side of the lateral bushing can be fully defined by the point of application of the resultant force and the value of the balance area A. By varying A and Y (Y coordinate of point P), the forces and moments acting on the lateral bushing also varies. The optimization procedure is used to find the parameters A and Y corresponding to the best feasible design for optimal axial balance evaluated according to the flow chart shown in Figure 21.

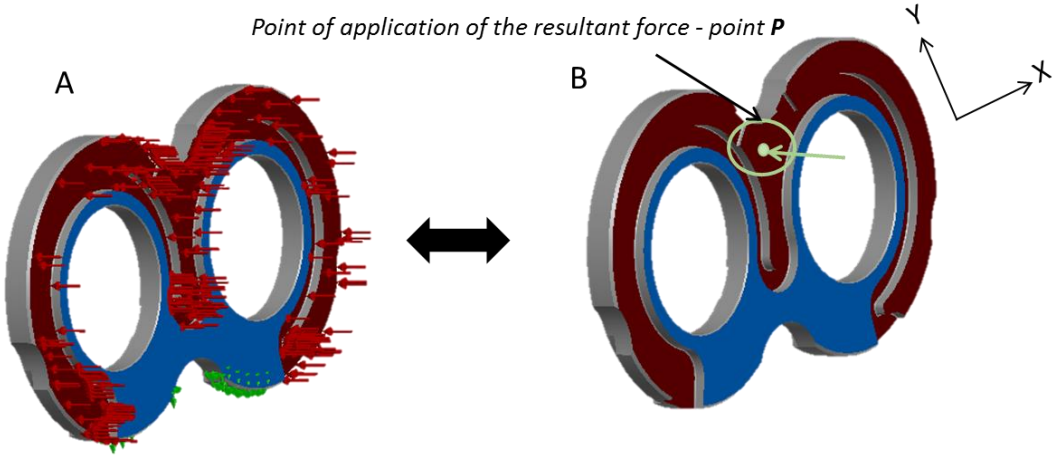

Figure 22: A) Uniform pressure force acting on the balance area of the lateral bushing (shown here is the pressure plate type design) subject to the constraint on the LP side (shown in green). B) Equivalent resultant force and its point of application on the lateral bush.

4.4 Objective Functions

The optimization procedure developed in the present study considers two objective functions namely the total power loss from the lateral gap and the gap non-uniformity index for the evaluation of each design considered, as outlined earlier in this chapter. The evaluation of the two objective functions for each design is explained as follows:

4.4.1 Evaluation of Power Losses from the Lateral Lubricating Gap

There are two main sources of power losses from the lateral gap as outlined earlier in this section: volumetric losses due to lateral leakages and mechanical losses due to viscous friction. The outputs obtained from converged simulations run with the FSI model for each design are used to calculate these losses. The equations used for evaluating these losses ([1]) are explained below,

4.4.1.1 Calculation of Power Losses Due to the Lateral Leakages from the Gap

The velocity field in the lubricating gap is obtained from the FSI model and the details of the derivation for the following equations can be found in [1].

$$u = \frac{1}{2\mu}\frac{\partial p}{\partial x}(z^2 - z(h_t + h_b) + h_t h_b) - \frac{z u_g}{h_t - h_b} + \frac{h_t u_g}{h_t - h_b}, \tag{4.13}$$

$$v = \frac{1}{2\mu}\frac{\partial p}{\partial y}(z^2 - z(h_t + h_b) + h_t h_b) - \frac{z v_g}{h_t - h_b} + \frac{h_t v_g}{h_t - h_b}. \tag{4.14}$$

The velocity field obtained from the above expressions can be integrated to give the leakage flow rate (Eqn. 4.3) and the power losses due to leakages from the lubricating gap can thus be found using (Eqn. 4.4).

$$Q_{leak} = \sum_i \iint_{A_i} v_i . n_i dA, \tag{4.15}$$

$$P_{loss,leak} = Q_{leak} \boldsymbol{\Delta P}. \tag{4.16}$$

4.4.1.2 Calculation of Power Losses Due to Shear Stress on the Gear Surface

The shear stresses due to fluid viscosity are calculated on the surface of the gears and represent a form of power loss from the lubricating gap for the EGM. Considering the gears to be aligned along the XY plane with the Z axis being normal to the gear lateral surfaces the shear stresses on the gear surface are given by,

$$\tau_{zx} = \mu \frac{\partial u}{\partial z}, \tag{4.17}$$

$$\tau_{zy} = \mu \frac{\partial v}{\partial z}, \tag{4.18}$$

From the assumptions detailed in [1], the shear stresses on the surface of a gear can be found to be described as a function of the pressure field and the gear velocity.

$$\tau_{zx} = -\frac{h}{2}\frac{\partial p}{\partial x} - \frac{\mu u_g}{h}, \tag{4.19}$$

$$\tau_{zy} = -\frac{h}{2}\frac{\partial p}{\partial y} - \frac{\mu v_g}{h}. \tag{4.20}$$

In the above equations u_g and v_g are two components of the velocity vector obtained from the angular speed of the gear. This results in a torque that opposes the motion of the gears (Eqn. 4.9).

$$\mathbf{T} = \sum_i 2A_i(\mathbf{r_i} \times \boldsymbol{\tau_i}). \tag{4.21}$$

where *i* is summed over the cells in the FV domain.

Thus the power loss associated with fluid viscous friction may be calculated.

$$P_{loss,shear} = T.\omega. \tag{4.22}$$

4.4.2 Evaluation of Gap Non-Uniformity Index (GNI)

The orientation of the lubricating gap also needs to be taken into account, in addition to the minimizing the power losses in the gap while designing the axial balance in EGMs, owing to the reasons outlined earlier in this section. It has been observed that sharp contacts and undesirable tilts leading to regions of contact between the gears and the lateral bushes occur even in designs with comparable values of power losses. An example of this is illustrated with the help of some very simplified designs for the sake of explanation in Figure 23. Both the designs shown in Figure 23 have comparable values of the total power loss. But, the design in Figure 23(A) has a tendency to approach sharp contacts owing to the low minimum film thickness and the number of non-uniformities are high and thus a design like the one shown in Figure 23(B) is more desirable than the former.

Thus, a factor Gap Non-uniformity Index (GNI) has been defined in this study to limit the number of non-uniformities in the gap and to promote a desirable orientation of the lubricating gap.

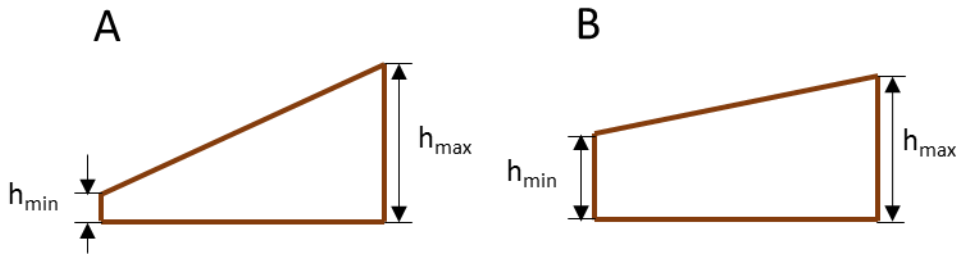

Figure 23: Figure showing the necessity for introducing the factor GNI to differentiate two designs with comparable total power losses A) Design with undesirable sharp contacts B) Design with desirable lesser.

Tilt of the lateral bushes has been defined previously in [40] and [46] using a rigid body model for solving the pressure field in the lubricating gaps of EGMs. However, a more rigorous measure of the orientation of the gap is required when the elastic deformations of the solid components are involved. This arises the need for a parameter which ensures that the relative gradients of deformation of the lateral bushes and the gears are not too steep and thus promoting designs with smoother non-uniformities in the gap while the procedure selects an optimal design from a pool of possible designs. Thus, we define the factor gap non-uniformity index as a measure of the relative orientation of the lubricating gap between

two extreme points of maximum and minimum film thickness to the average film thickness across the lubricating gap. The Gap Non-uniformity Index (GNI) for the lubricating interface of a design in the reference EGM is calculated with the help of the following equation.

$$GNI = \frac{h_{max} - h_{min}}{2h_{avg}}. \tag{4.23}$$

It can be observed that if the GNI for a design under consideration is high, it translates to the fact that the lubricating interface between the lateral bushing and the gears in this design has a higher number of non-uniformities and may have undesirable regions of contact. Thus, evaluating the GNI as an objective function of the optimization procedure gives a satisfactory measure of the orientation and uniformity of the lubricating gap for a given design of balancing areas in the lateral bush.

4.4.3 Evaluation of the Objective Functions for Each Design

The numerical optimization procedure developed in this work formulates this multiobjective design problem as an equivalent single objective one and an approach similar to that described in [47] is followed. For every design, each of the objective functions namely, the two sources of power loss and the GNI are normalized with respect to their corresponding reference design. Following this, all the normalized values of the objective functions are added for each operating condition using the following equations,

$$f_N = \frac{P_{loss,shear,ocN}}{P_{loss,shear,Ref,ocN}} + \frac{P_{loss,leakages,ocN}}{P_{loss,leakages,Ref,ocN}} + \frac{GNI_{ocN}}{GNI_{Ref,ocN}}, \tag{4.24}$$

Where N corresponds to the nth operating condition (oc). The reference design is usually chosen as original design (nominal) of the balance area on the lateral bushing which is being optimized. Therefore, for every design considered in the procedure, a value of f is computed for each operating condition. These values for each design are then further combined according to the formulation defined in [47] by using the following equation,

$$\boldsymbol{F} = \sqrt{f_1^2 + f_2^2 + \cdots f_N^2}. \tag{4.25}$$

Thus, all the designs studied in this procedure will have a corresponding value of **F** which is used to find the 'best compromise' design in the current grid and also to use the

information in the current grid to progress into the next iteration using the methods which will be described in 4.7.

4.5 Reference Operating Conditions

The inputs to the numerical procedure include the values of the objective functions for the original design and operating conditions amongst which an optimal axial balance needs to be determined. Extreme operating conditions between pressure and speed are used as input operating conditions which can help to reasonably ensure that the balance area design obtained from the procedure will provide a fairly good axial balance at all operating conditions varying in terms of shaft speed, operating pressure and fluid temperature.

Typically, the procedure has been made flexible to handle any number of operating conditions as input. Four operating conditions involving all the possible combinations of high and low pressures and speeds have been used in one of the results which will be presented later in this paper (6.1). It will be shown later that very little difference in results were obtained between two and four operating conditions as input. Hence, for the sake of saving computational time, two input operating conditions have been used in producing all other results presented in this paper.

It must be noted that choosing the input operating conditions is very specific and largely dependent on the reference EGM under consideration. A preliminary investigation was made to verify that the most significant variations in the objective function values for a given bearing block design can be observed for the selected operating conditions. Since a variety of EGMs have been used for the results presented in this study, the input operating conditions for each case has been discussed prior to presenting each of those results.

4.6 Design Variables Initialization and Constraints

The design variables A and Y (as chosen for this study and explained in 4.3) needs to be initialized and constraint limits need to be placed on these variables prior to starting the optimization procedure. By initializing and placing limits on the variables using educated guesses, the time taken by the optimization procedure can be minimized and the efficiency of the procedure itself can be improved. Thus, the design variables are initialized using the

pressure field in the lateral as predicted by the FSI model and the TSV's pressures (as shown in Figure 8).

Considering only the dominant hydrostatic component of forces acting on the lateral bushing solely for the purposes of initializing the design parameters, the magnitude of the resulting system of forces acting on the lateral bushing from the lateral gap and the TSVs and their point of application are plotted in Figure 24. The evaluation of these forces and their point of application has been detailed in 4.1. Since the hydrodynamic components of these forces 'balance' the system with respect to the fixed point of application of the resultant balance area force, such an analysis provides a starting point for initializing the design parameters. Further detailed analysis on this study can be found in [10].

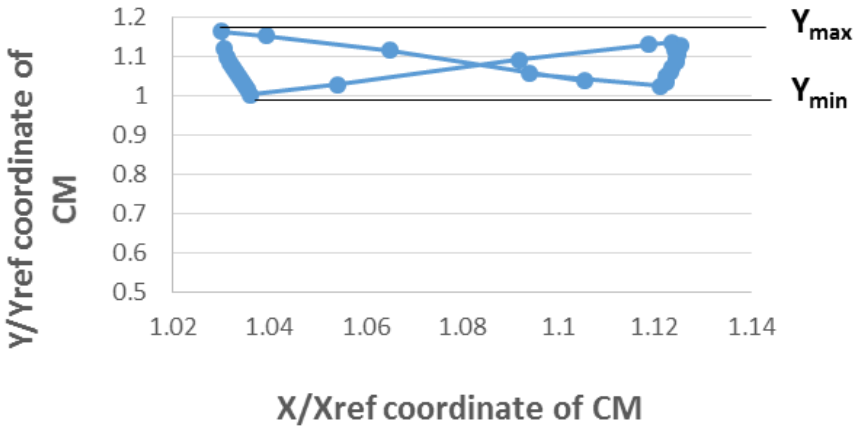

Figure 24: Point of application of the resultant forces acting on the lateral bushing considering only the hydrostatic components of the force system on the lateral bush.

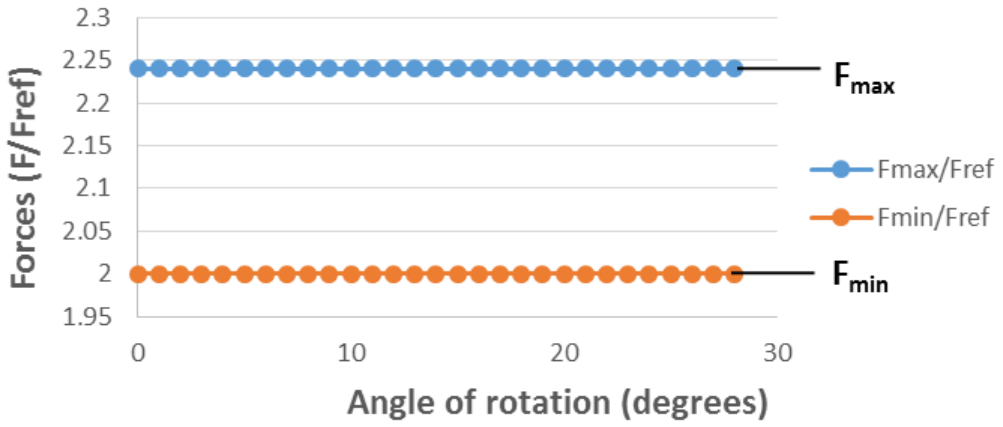

Figure 25: Magnitude of the resultant forces acting on the lateral bushing considering only the hydrostatic components of the force system on the lateral bush.

The range of values of the design parameters A and Y used in the optimization procedure is obtained from the limits of the two graphs shown in Figure 24 and Figure 25. The maximum and minimum values of Y and F are obtained as shown in Figure 24 and Figure 25. The values of A_{max} and A_{min} can be obtained from the corresponding values of F_{max} and F_{min} by using the value of pressure for each of the operating conditions under study. The coordinates of the point of application of the resultant force is normalized with the help of X_{ref} (of **O** (20 mm)) and Y_{ref} (of **O** (5 mm)) and CM in the figure refers to the point of application. It is noted that since the reference pump used for this particular study shown in the figure has 13 teeth per gear and thus the pattern described in the figure repeats itself for every 28 degrees of rotation of the shaft.

With the limits for the design parameters obtained, step sizes for each of the parameters: Δ_A and Δ_Y are initialized and varying values of A and Y are obtained which can be perceived as forming a grid of design variables as represented in Figure 26.

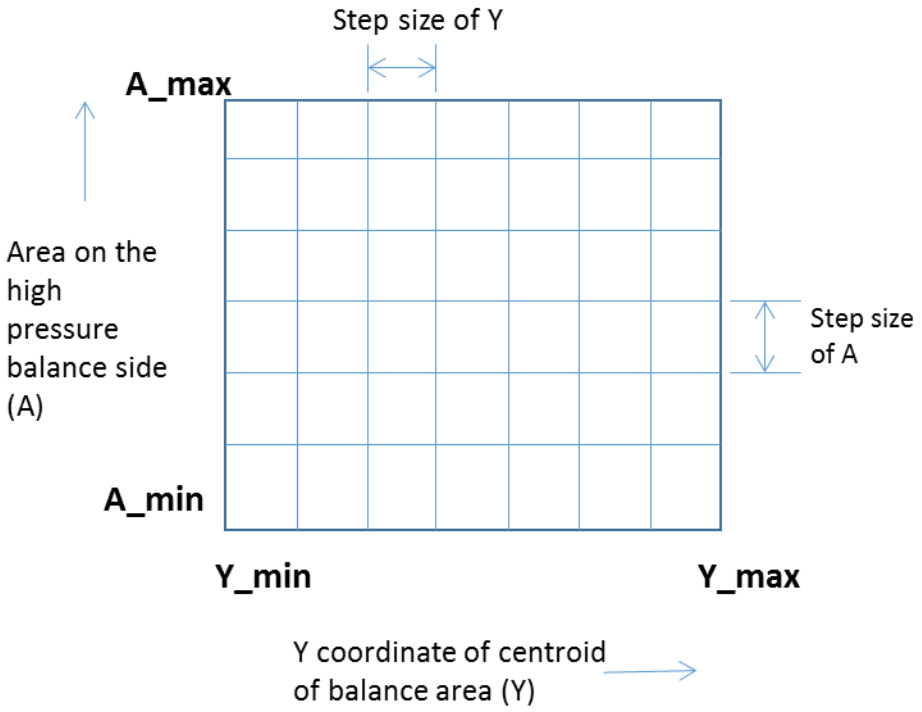

Figure 26: Representative grid of the design parameters A and Y used in the optimization procedure.

4.7 Search Methods and Design Grid Selection

A direct search method has been used in the iterative procedure developed in this study to obtain information from the current iteration to progress across successive iterations. The primary advantage of choosing this method is that it does not require evaluating derivatives of objective functions which could be a computationally expensive and difficult exercise in this case.

Direct search methods for multiobjective functions have been extensively studied and developed in numerous works, especially in [47-50]. An approach similar to [47] and [50] have been implemented in this procedure where the method aims at improving the "best feasible objective function found" [50] by evaluating the function at the current mesh points. The equivalent single objective function **F** comprising of all the objective functions and operating conditions used in the optimization procedure for each of the designs under study can be obtained from the formulation discussed in 4.4.3. This formulation aids in finding a well-balanced compromise for the final design solution of the balance area on the lateral bush.

The minimum value of **F** across the grid size is estimated and with this corresponding grid point as the focal point, a new mesh of trial points is established for the next iteration by invoking a 'search step' [50] without changing the current step size Δ_A and Δ_Y. Simulations are performed with the new mesh points and objective functions are similarly evaluated again.

If there is an improvement to the best estimate of the objective function in this succeeding iteration, the search step is performed again in a similar manner with a new focal point. However, if no such improvement is observed, the step sizes Δ_A and Δ_Y are halved by invoking a 'poll step' [50] and a new mesh of trial points are generated for the next iteration with the focal grid point in the current iteration. Simulations are performed again for the current mesh points and depending on the outcome of evaluating the objective functions, the decision is made to invoke the 'search step' or the 'poll step'.

The procedure continues until the step sizes Δ_A and Δ_Y decrease and reach a certain preset value which is the convergence criterion signaling the end of the optimization procedure. This convergence criterion for the step sizes for each of the design parameters is set before the start of the procedure and this criterion is heavily dependent on the geometric dimensions of the lateral bushing of the reference EGM under consideration. Thus, this criterion varies for the different types of EGMs considered in this study. Thus, the final solution presents the closest balance area design which offers a best feasible solution considering power losses in the lubricating gap and gap orientation between the different operating conditions.

CHAPTER 5. OPTIMAL BALANCE AREA FOR TWO DIFFERENT AXIAL BALANCE CONFIGURATIONS

The numerical procedure developed in this research work has been formulated in a versatile and flexible manner to optimize a wide range and variety of lateral bushes and EGM designs. In the present section, the application of the developed optimization tool has been used to find the optimal axial balance for two varied axial balance configurations of the EGM, namely symmetric and asymmetric.

In symmetric axial balance configuration of an EGM, the two lateral bushes in the machine are identical to each other in terms of the geometry, the relief grooves machined on them and the balance area design on the side of each of the lateral bushes facing away from the gears. Hence, the two lateral lubricating interfaces on either side of the gears are identical to each other and the axial balance of these kind of EGMs is defined to be symmetric. This axial balance configuration is the most commonly found design in currently available pressure compensated EGM designs in the market, for high pressure application (up to 250 bar). An example of a symmetric axial balance configuration with a pressure plate type design of the lateral bushing is shown in Figure 27. The lateral bushes in a symmetric balance can be any one of the pressure plate type or the bearing block design.

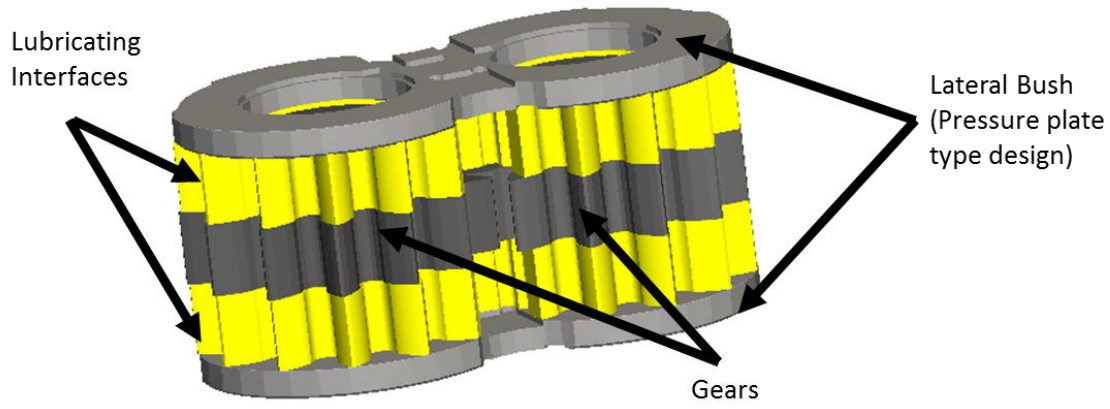

Figure 27: Figure showing the lubricating interfaces (exaggerated for clarity) with lateral bushes and gears in a symmetric axial balance configuration.

The approach for modeling the lateral lubricating interfaces in this symmetric axial balance configuration is the same as the one outlined in 3.2 where a boundary condition of symmetry is assumed at the gears.

On the other hand, there are certain kind of EGM designs where the two lateral bushes present in the machine have distinct geometric designs and balance area configuration. Thus, the two lateral lubricating interfaces found on either side of the gears and their corresponding gap flow are not identical to each other. Thus, asymmetric conditions are established for the two gap flows and the term ‘asymmetric axial balance’ is assigned to such EGM designs. However, to design an optimal axial balance in these kind of EGM designs, designing the balance area on only one of the lateral bushes is sufficient since there is no balance area on the bearing block which is considered to be pushed against the casing. Thus, the only fluctuating element for the axial balance design is the lateral bush. An illustration of the lateral lubricating interfaces in these EGMs is shown in Figure 28.

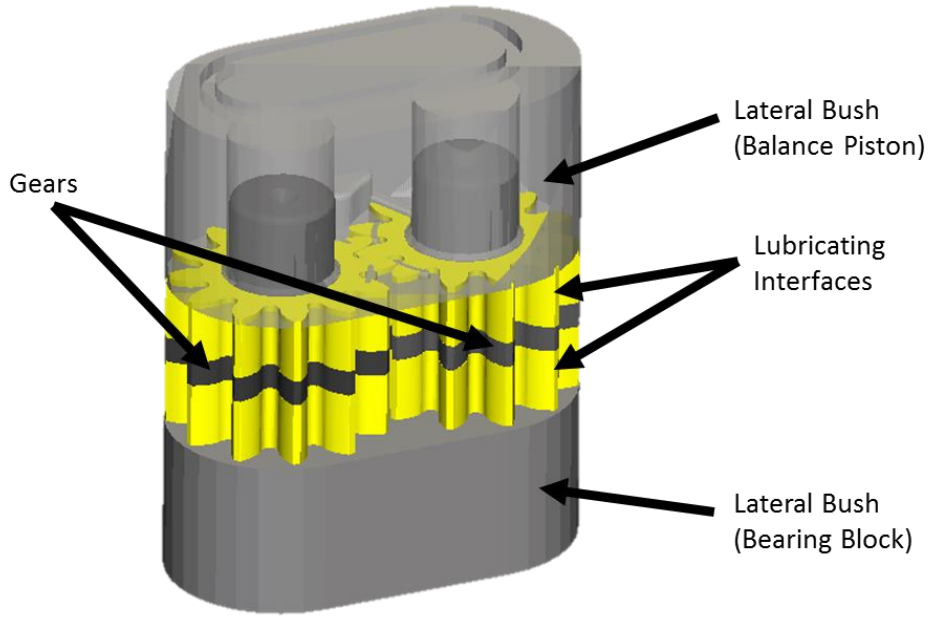

Figure 28: Figure showing the two asymmetrical lateral lubricating interfaces between the lateral bushes and the gears.

It can be observed from Figure 28 that the two lateral bushes are different from each other, and are referred to as balance piston and bearing block for the reference EGM considered for this study. Since the two lubricating interfaces are different from each other, the two interfaces need to be modelled separately and the FSI phenomenon needs to be fully coupled between them. Additionally, due to the absence of symmetry, the gears now have lateral forces acting on them. The modelling of the lateral lubricating interfaces needs to be modified from the approach presented in 3.2 and the formulation of the modified FSI-EHD model for asymmetric axial balance has been developed in the work of [1]. This modified FSI model has been used to develop the optimization procedure for an asymmetrically balanced EGM in the present study.

Results from the numerical optimization procedure for each of the reference EGMs considered for symmetric and asymmetric axial balance configurations will now be presented in this section.

5.1 EGM with Symmetric Axial Balance Configuration

In this section, optimal axial balance is determined for a reference EGM with a symmetric axial balance configuration. The reference EGM with a pressure plate type design of the

lateral bushing which is chosen for this study, has a displacement **O** (30 cm^3), typically used in mobile fluid power applications. The speed range of the pump is 500-3500 rpm and the max pressure rating is 280 bar. It must be noted that the notation **O** refers to the order of magnitude of the quantity specified in the brackets. Some of the values specified in this paper are given in terms of the order of magnitude rather than the actual value for reasons of confidentiality.

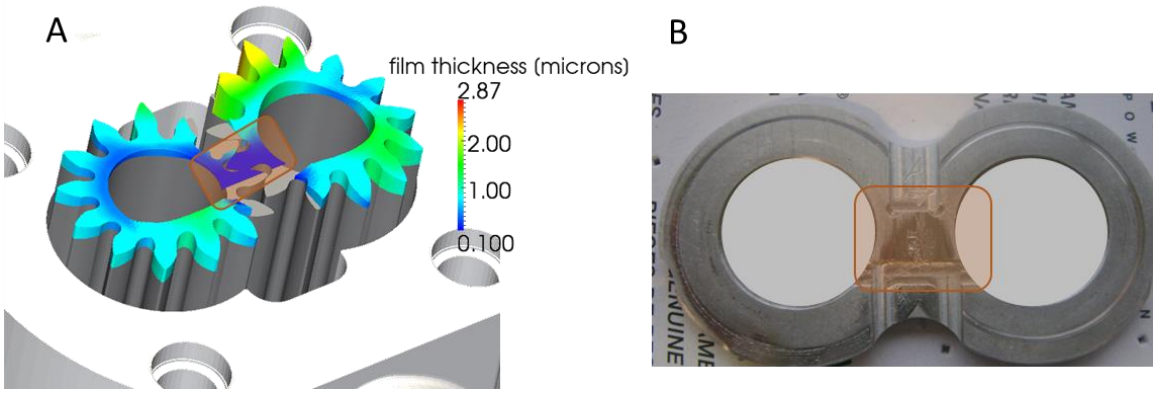

Figure 29: A) Film thickness results from simulation of the reference pump with symmetric axial balance configuration with the FSI model. Low gap heights observed near the meshing zone. B) Wear pictures of the lateral plate from the same reference EGM after several hours of operation. Wear is observed in the meshing zone.

For the reference pump chosen for this particular study, it has been observed that at conditions of higher pressure, there is a tendency of excessive wear near the meshing zone of the gears. This observation as shown in Figure 29 was made from both simulation using the FSI model (described in 3.2) and qualitative comparison with the wear pictures of the same reference EGM after several hours of operation. The simulation of the reference EGM using the FSI model was carried out at an operating condition of 1000 rpm shaft speed and $\frac{p}{p_{ref}} = 0.7$ delivery pressure, where p_{ref} is in the **O** (300 bar). Thus, finding the optimal axial balance using the numerical procedure developed in this study could promote lesser wear and reduced power losses in the reference EGM.

5.1.1 Reference Operating Conditions

As outlined earlier, only two input operating conditions were chosen for this particular study to limit simulation time although a case with four extreme operating conditions

between shaft speed and delivery pressure is performed in the following chapter of this thesis. The selected conditions are $\frac{p}{p_{ref}} = 0.32$ pressure, 1000 rpm speed for Operating Condition 1 and $\frac{p}{p_{ref}} = 0.7$ pressure, 1000 rpm speed for Operating Condition 2. The value of p_{ref} is in the **O** (300 bar) and corresponds to the maximum operating pressure of the reference EGM. A preliminary investigation was made to verify that the most significant variations in the objective function values for a given bearing block design can be observed for the two selected operating conditions.

5.1.2 Results from the Optimization Procedure

The optimized results for the balance area obtained from the numerical procedure along with the comparisons with the original design of the balance area of the reference EGM chosen for this study are presented and discussed in this section. Baseline simulations were performed on the original design of the balance area on the lateral bushing of the reference EGM using the FSI-EHD model for the lateral lubricating gaps for the purposes of comparison with the optimized design. The baseline design was evaluated at the two operating conditions: Operating Condition 1 as $\frac{\mathrm{p}}{\mathrm{p_{ref}}} = 0.32$ pressure, 1000 rpm speed and $\frac{\mathrm{p}}{\mathrm{p_{ref}}} = 0.7$ pressure, 1000 rpm speed as Operating Condition 2 which were outlined earlier as the input conditions to the numerical optimization procedure. It was observed that larger regions of contact were noticed in operating contact were found in Operating Condition 2 (as shown in Figure 32). Thus, a higher weight was given to this operating condition while optimizing the axial balance.

The optimization procedure was carried out with initial step sizes of $\frac{\Delta A}{A_{ref}} = 0.017$ and $\frac{\Delta Y}{Y_{ref}} = 0.9$ and with the convergence criteria set at $\frac{\Delta A}{A_{ref}} = 0.0023$ and $\frac{\Delta Y}{Y_{ref}} = 0048$. It must be noted that the values of A_{ref}(**O** (1400 mm2)) and Y_{ref} (**O** (5 mm) used here correspond to the design parameters of the original balance area design in the reference EGM under study. The final converged results were obtained after 4 iterations in the procedure which included 2 poll steps and 2 search steps. The focal point of the design grid

obtained at the end of the first poll step was $\frac{A}{A_{ref}} = 1.004$ and $\frac{Y}{Y_{ref}} = 1.146$. In the next poll step with altered search directions, the design variables with minimum objective functions were $\frac{A}{A_{ref}} = 1.004$ and $\frac{Y}{Y_{ref}} = 1.366$. The additional two search steps performed until convergence with refined design grids and successively halving the step sizes resulted in no further improvement in the final design solution.

The plots of the objective functions at the end of poll step 1 and poll step 2 are shown in Figure 30 and Figure 31 respectively. The focal point at the end of each of these iterations is represented in the figures as a point highlighted in red. The black colored point shown in Figure 30 represents the original design of the balance area in the reference EGM and illustrates the fact that the optimization algorithm aims to minimize the objective functions considered in the study. It is observed that since two different objective functions are considered for each of the two operating conditions, the best feasible design point at the end of each iteration is a compromise among all these functions and the weights assigned to each of them. Thus, the design solution obtained at the end of the optimization procedure was a balance area with design parameters $\frac{A}{A_{ref}} = 1.004$ and $\frac{Y}{Y_{ref}} = 1.366$.

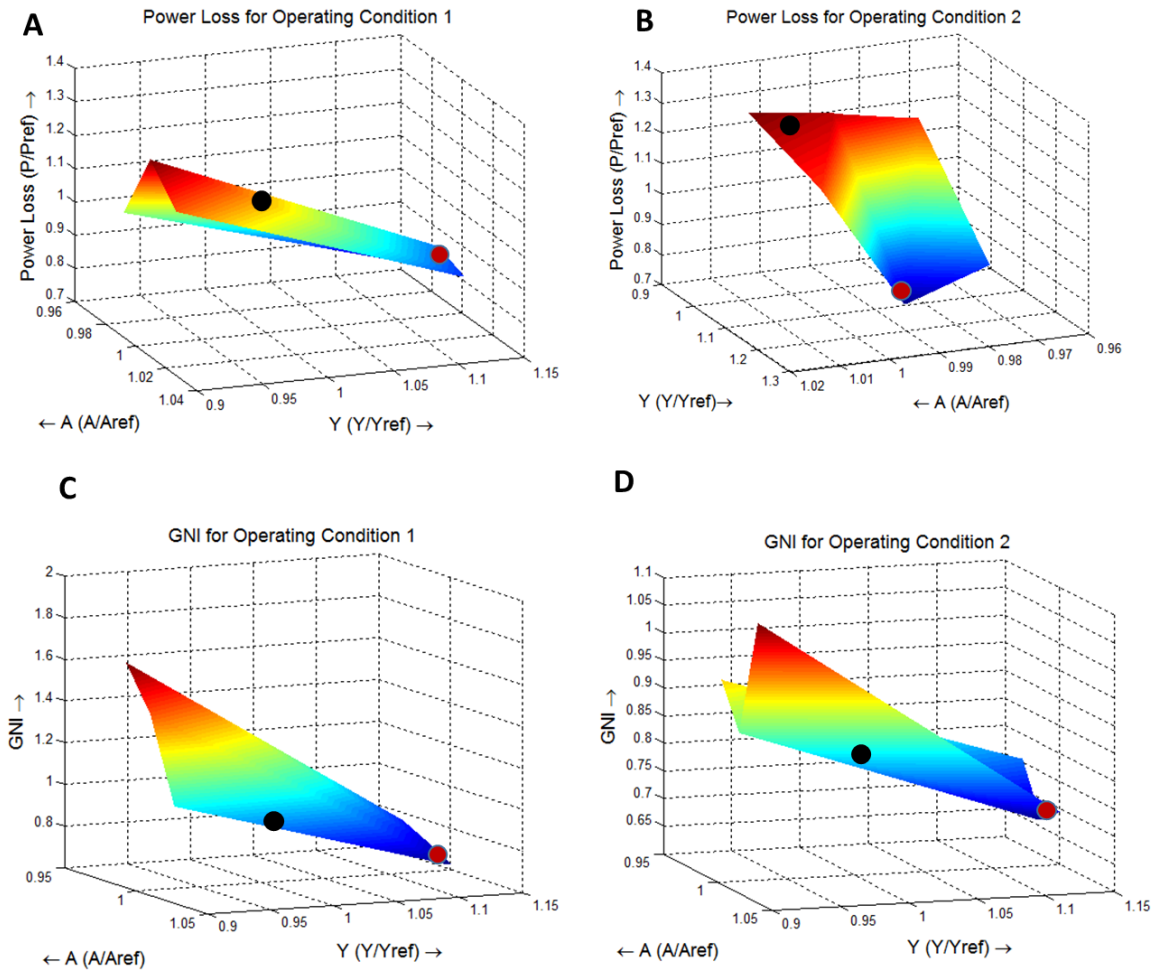

Figure 30: Objective function plots after poll step 1. A) Power loss in Operating Condition 1 B) Power loss in Operating Condition 2 C) GNI for Operating Condition 1 D) GNI for Operating Condition 2. The point highlighted in red represents the design with the minimum value of the objective functions in the current design grid and the black point represents the value of the objective functions for the reference original balance design.

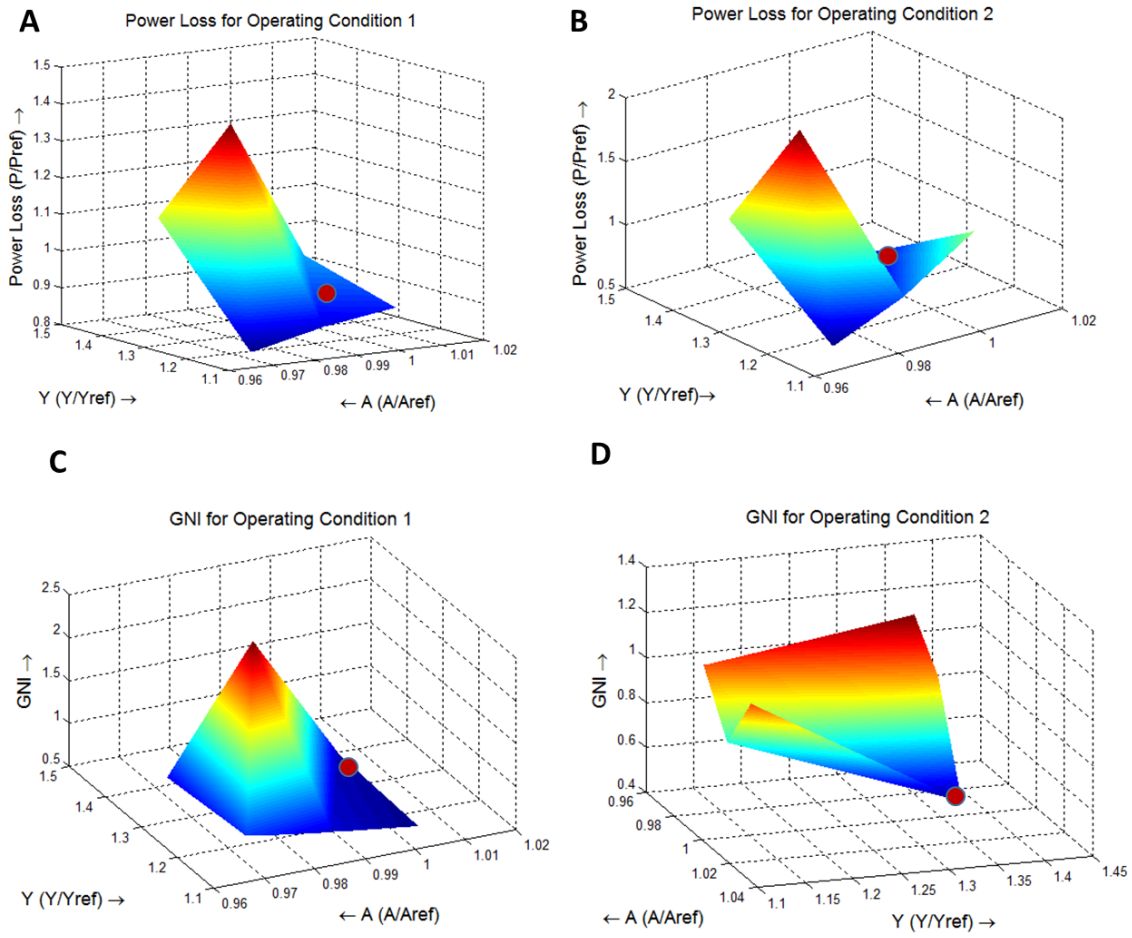

Figure 31: Objective function plots after poll step 2. A) Power loss in Operating Condition 1 B) Power loss in Operating Condition 2 C) GNI for Operating Condition 1 D) GNI for Operating Condition 2. The red point marks the focal point in the current design grid.

The lubricating gap film thickness plots of this optimized balance area design obtained from the procedure are compared to the reference balance area design on the lateral bushing for operating condition 1 are shown in Figure 33. For this operating condition, a total reduction of 2.9 % in power loss was observed along with a reduction of 37.87 % in the GNI of the lubricating interface. It is observed that a reduced GNI is more favorable due to the fact that it represents reduced non uniformities in the orientation of the lubricating interface. The gap heights in the interface are normalized with the help of the factor h_{ref} which is in the **O** (3 μm). The film thickness plots of the optimized design simulated for the operating condition 2 is compared with those from the reference design in Figure 32. A total of 36.72 % reduction in the power losses from the lubricating gap and a reduction

of 51.2 % in its GNI were observed. It must be noted that a higher weight was assigned to this operating condition during the procedure and hence, more favorable values of the objective function are observed at operating condition 2 as against those obtained from operating condition 1.

The final optimized design parameters obtained from the optimization procedure are $\frac{A}{A_{ref}} = 1.004$ and $\frac{Y}{Y_{ref}} = 1.366$ for the reference EGM with symmetric axial balance configuration chosen for this study.

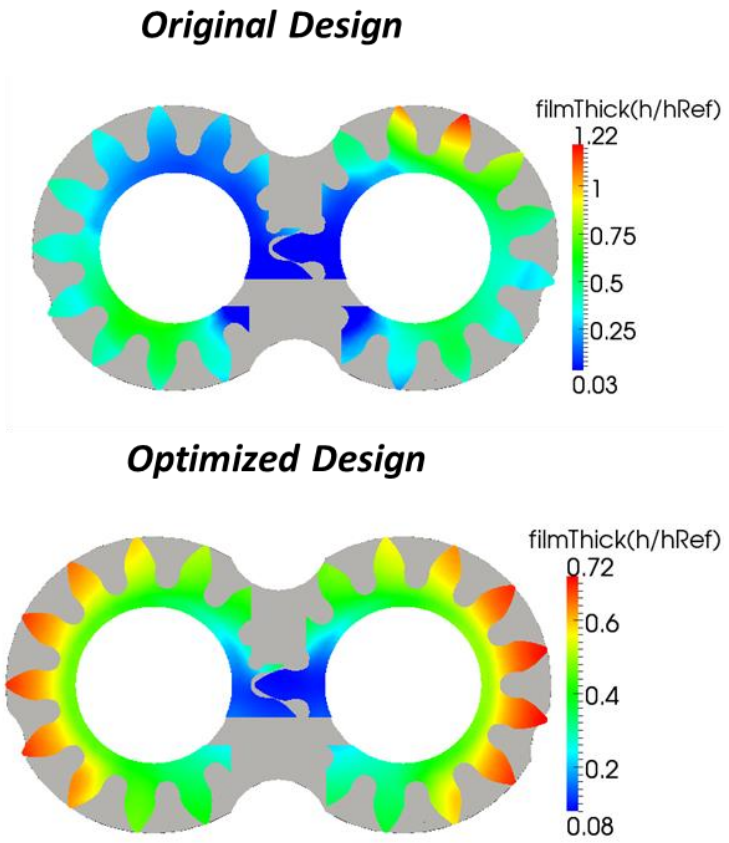

Figure 32: Figure comparing profiles of film thickness in the lubricating gap between the original balance area design (top) with the optimized design from the procedure (bottom) at Operating condition 2. The legends used for each design is selected to obtain the best representation of the gap heights profile in each case and thus, they are different.

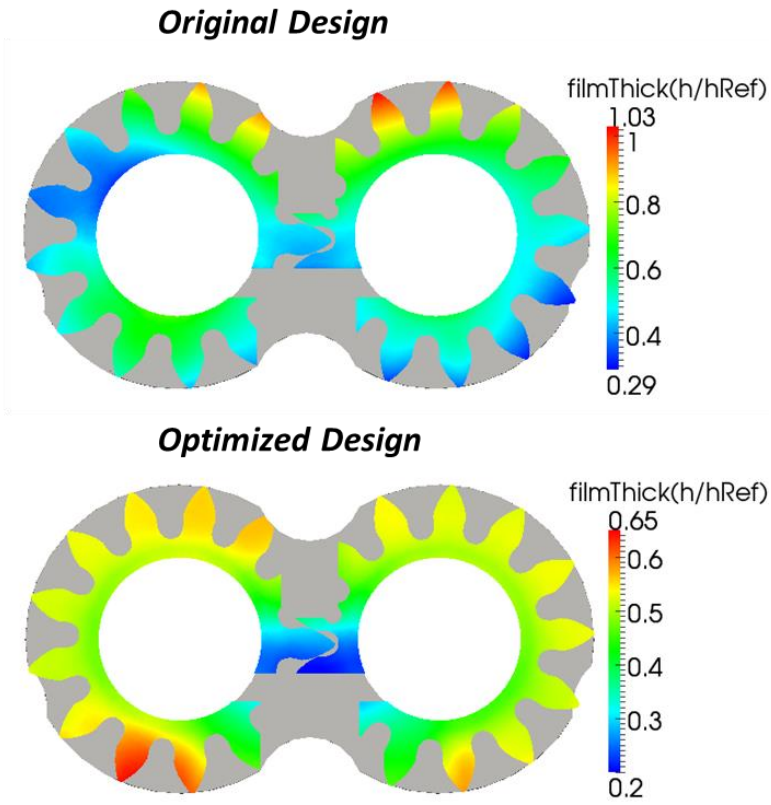

Figure 33: Figure comparing profiles of film thickness in the lubricating gap between the original balance area design (top) with the optimized design from the procedure (bottom) at Operating Condition 1.

5.2 EGM with Asymmetric Axial Balance Configuration

A brief discussion of EGMs with asymmetric lateral lubricating interfaces and axial balance was presented in the introduction to this chapter. The significant details of the reference EGM with asymmetric axial balance along with its working fluid and solid component materials is shown in Table 1.

The detail of the lubricating gap geometry of this EGM is shown in Figure 28, and consists of three main parts

1. Balance Piston: The lateral bushing which has a high pressure compensating area as shown in Figure 34(A).
2. Bearing Block: The lateral bushing with no high pressure compensating area.
3. Gears: Free to move axially.

The two lubricating interfaces designated as the piston/gears interface and the block/gears interface are illustrated in Figure 34(B) since the lubricating interfaces are different from each other due to the symmetric axial balance. The goal of the optimization procedure when applied to the asymmetrically balanced reference EGM under study is to design the high pressure area on the side of the balance piston facing away from the gears. Thus, only the balance piston is responsible for balancing the axial forces and moments arising from the pressures in the TSVs and lateral gap, as shown in Figure 34(A). A LP constraint for used for the balance piston to evaluate its deformation in the FSI model. The bearing block is assumed to be pressed against the casing due to the high pressure in the TSVs and the lateral gap. Thus, it does not have a role to play in the axial balance of the EGM and the boundary faces on this side which is pressed against the casing are constrained in the lubricating gap model.

Table 1: Relevant details of the reference asymmetrically compensated EGM, working fluid and solid component materials.

Details of EGM	
Displacement of EGM	0.26 cc/rev
Number of gear teeth	12
Operating speed	1000 rpm
Maximum operating pressure	170 bar
Working Fluid	Skydrol 500B-4
Density @ 20˚C, atmospheric pressure	1057 kg/m^3
Viscosity @ 20˚C, atmospheric pressure	0.022 Pa-s
Lateral Bushes	Aluminum alloy
Young's Modulus	69 GPa
Poisson's Ratio	0.33
Density	2700 kg/m^3
Coefft. of thermal expansion	23.6 µm/m-K
Thermal Conductivity	167 (W/mK)
Gears	Steel
Young's Modulus	200 GPa
Poisson's Ratio	0.3
Density	7850 kg/m^3
Coefft. of thermal expansion	11 µm/m-K
Thermal Conductivity	60.5 (W/mK)

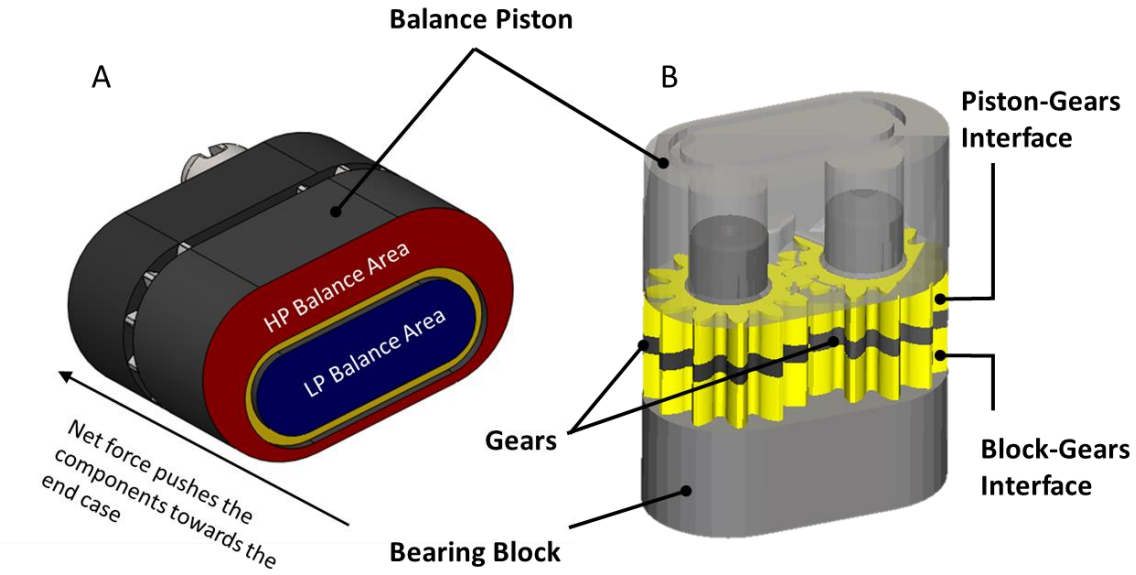

Figure 34: A) The lateral bushing (balance piston) used in the present EGM with specially designed high pressure (HP) and low pressure (LP) balance areas. The areas are separated by an elastomeric seal placed in the yellow area of the figure. Being the bearing block not pressure balanced (the surface opposite to the gears is at low pressure), a net force (F_{net}) pushes the components towards the end case as indicated in figure. B) The piston/gears interface and block/gears interface are both shown in yellow.

The symmetry boundary condition that was used for the gears in the standard EGM design (5) is no longer applicable for this EGM, since the gear deformation will be dictated by the difference in the pressure fields from the two interfaces. Thus, not only can gears exhibit surface deformations (as was the case in the standard EGM design), the gear teeth can also exhibit deflection, i.e. bend toward either the bearing block or the balance piston depending on the pressure fields. In order to capture this behavior the gear shaft was constrained for the structural solver, since this part will be encased by the lateral bushings, and is not expected to effect the deformation of the gears lateral surfaces.

The FSI model previously discussed in 3.2 needed to be modified to accommodate all the features listed above and to enable the prediction of the lubricating gap heights in the piston/gears interface and the block/gears interface. The algorithm of the extended FSI model is shown in Figure 35. Further development of the FSI model along with the details of the modeling efforts can be found in [1].

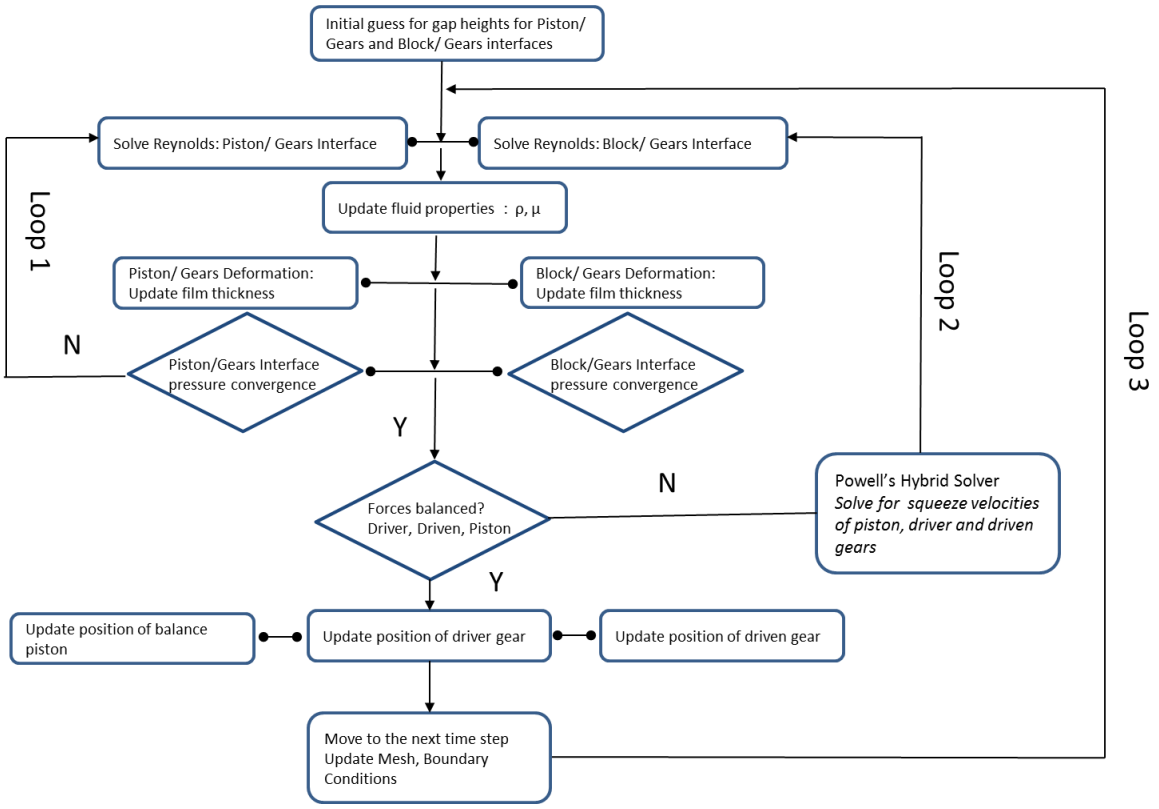

Figure 35: FSI-Axial Balance coupled algorithm for the EGM with asymmetric balancing.

The initial design of the asymmetrically balanced EGM was simulated for a wide range of operating conditions: $\frac{p}{p_{Ref}} = 0.33\ ,\ 0.66; n = 1000\ RPM$ and T=20°C, 70°C and -10°C based on the expected operating range of the EGM [1]. The film thickness predictions provided by the asymmetric FSI model for the above operating conditions are shown in Figure 36. It is generally seen that the film thicknesses on the piston/gears interface are lower than on the block/gears interface.

In addition it was also noted that the regions of lowest film thickness on the piston/gears interface was observed near the delivery (HP) port while the regions of low film thickness on the block side were on the suction (LP) side. A further qualitative check was performed for the results with the asymmetric EGM with the help of wear pictures obtained for the lateral bushes. The wear on the balance piston and the bearing block for two prototype EGMs after many hours of operation are shown in Figure 37. As can be seen the correlation

between the regions of low film thickness **O** (0.1μm) predicted by the FSI model and the wear regions observed experimentally are excellent: the wear on the balance piston being near the HP port while the wear on the bearing block was near the LP port.

The results for the baseline simulations at various operating conditions along with the qualitative comparison with wear pictures were presented to demonstrate that predictions of film thicknesses on both interfaces enable design improvements focused on each interface specifically. Results from the optimization procedure aimed at improving the performance of the lubricating interfaces will be described in the following section.

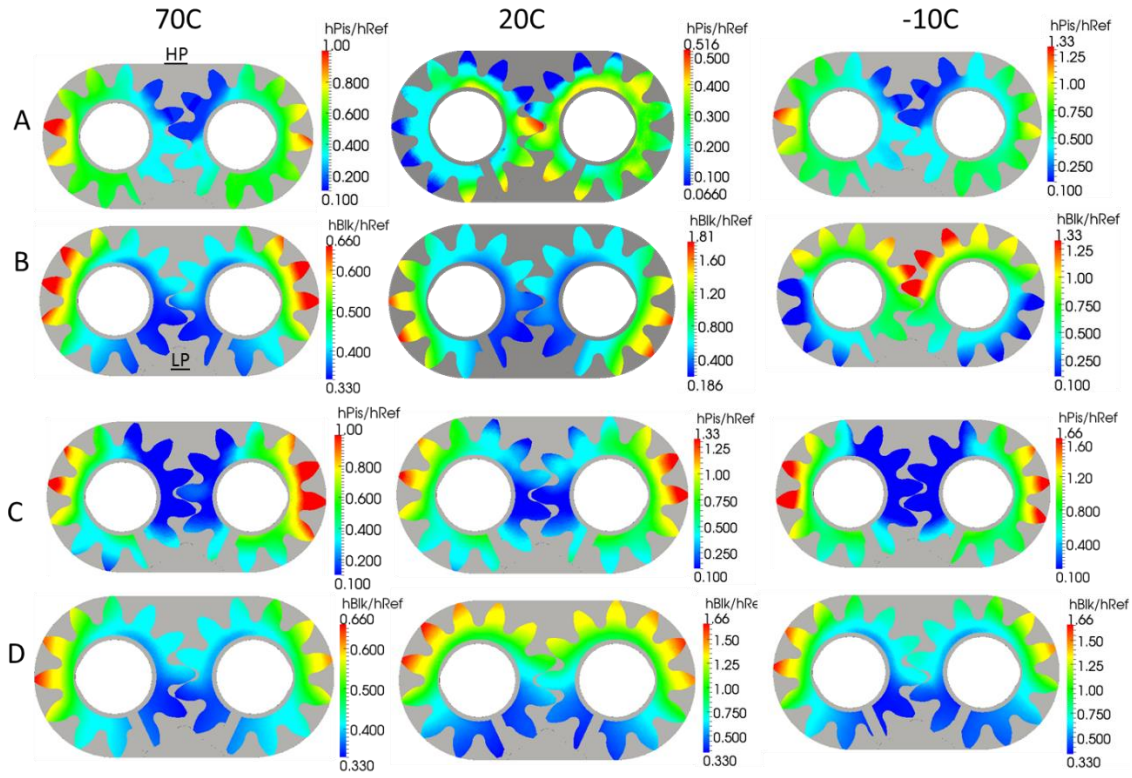

Figure 36: Film thickness prediction for $\frac{p}{p_{Ref}} = 0.33$ on the A) Block/Gears interface and B) Piston/Gears interface. Film thickness prediction for $\frac{p}{p_{Ref}} = 0.66$ on the C) Block/Gears interface and D) Piston/Gears interface.

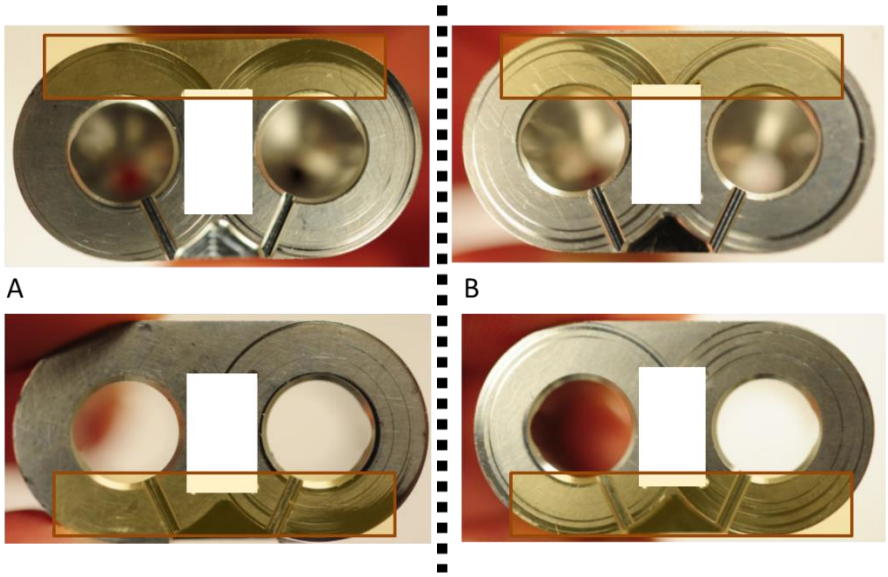

Figure 37: Wear patterns observed on the balance piston (top) and bearing block (bottom) for A) first prototype EGM and B) second prototype EGM after hours of operation. The regions of wear observed are highlighted in yellow. The white boxes are placed to reasons of confidentiality.

5.2.1 Reference Operating Conditions

Two significantly different operating conditions involving different delivery pressure and fluid temperature were chosen to optimize the axial balance of the reference asymmetrically compensated EGM. The selected conditions are $\frac{p}{p_{ref}} = 0.33$ pressure, 20 °C temperature, 1000 rpm speed for Operating Condition 1 and $\frac{p}{p_{ref}} = 0.66$ pressure, -10 °C temperature, 1000 rpm speed for Operating Condition 2. A preliminary investigation was made to verify that the most significant variations in the objective function values for a given bearing block design, which can be observed for the two selected operating conditions.

5.2.2 Results from the Optimization Procedure

The results from evaluating the objective functions and from the final balance area design obtained from the optimization procedure are presented and discussed in this section. When the preset convergence criterion is met, it results in a set of very close designs of the balance area, from where the best feasible solution is chosen. For the two input operating conditions considered (Operating Condition 1 and 2), the most feasible solution obtained from the

procedure had the design variables set at $\frac{A}{A_{ref}} = 0.933$ and $\frac{Y}{Y_{ref}} = 1.071$ where the parameters A_{ref} and Y_{ref} are the design parameters of the original balance area of the lateral bushing before the optimization procedure and the value of A_{ref} is **O** (250 mm^2). The design solution was obtained after 5 iterations of the procedure which included 2 poll steps and 4 search steps with the convergence criterion as $\frac{\Delta_A}{A_{ref}} = 0.0163$ and $\frac{\Delta_Y}{Y_{ref}} = 0.067$.

The plots showing film thickness for the new design are compared against the original design of the balance area on the lateral bushing and shown in Figure 38 for operating condition 1 and in Figure 39 for operating condition 2. For operating condition 1, the new design showed improved results with a reduction of 51 % in total power losses from the lateral gaps from both the lubricating interfaces and an improvement in GNI of 51 % in the block/gears interface and an increase of 26 % in GNI in the piston/gears interface.

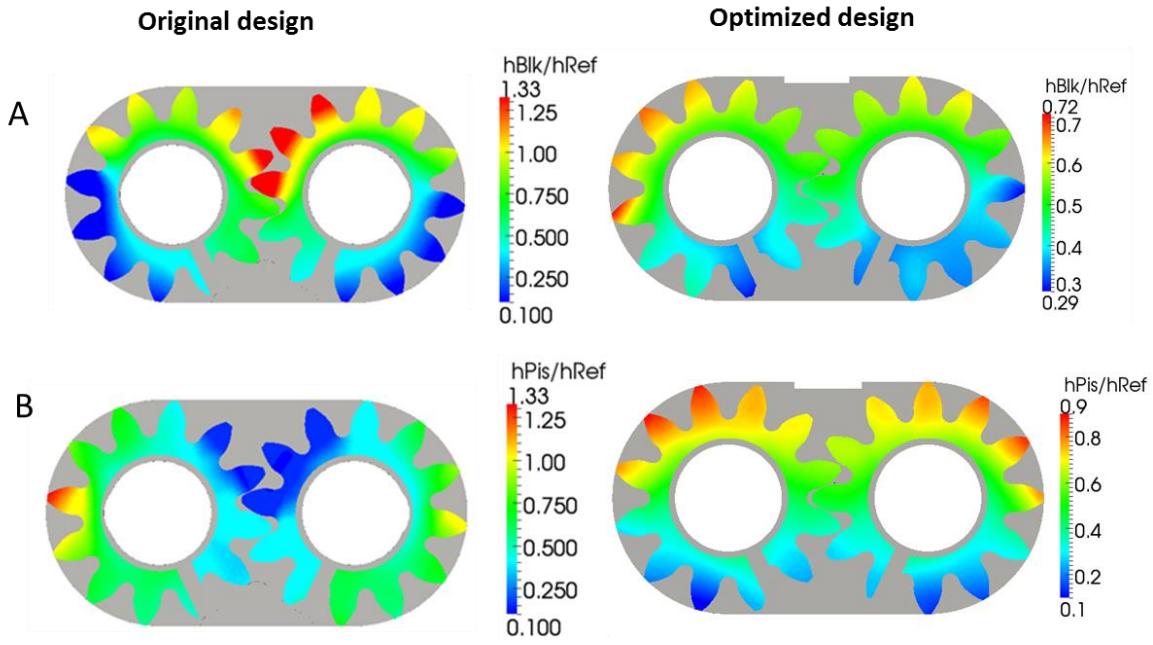

Figure 38: Figure comparing film thickness profiles between original and optimized designs in operating condition 1 for A) Block/Gears interface and B) Piston/Gears interface. Legends for each film thickness profile has been chosen to best represent that particular gap and thus, differs across every plot.

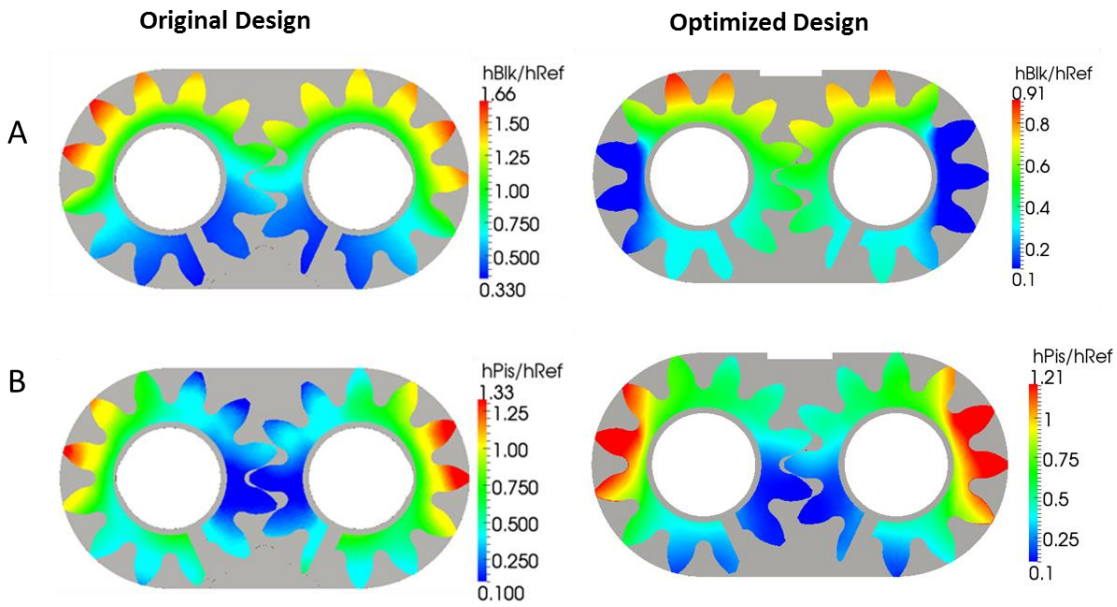

Figure 39: Figure comparing the film thickness profiles between original and optimized designs in operating condition 2 for A) Block/Gears interface and B) Piston/Gears interface.

On the other hand, for operating condition 2, the new design showed a reduction of 51 % in total power losses from the lateral gap. But, since the current case represents a multi objective problem with two very different operating conditions, a compromise needs to be made in the final optimized solution and thus an increase in GNI of both the lubricating interfaces is observed in operating condition 2. The GNI in the piston/gears interface increased by 29 % in the block/gears interface and by 8 % in the piston/gears interface.

The objective functions in iteration 1 and iteration 4 of the procedure are illustrated since these were the successful steps which led to locating the required focal point of optimization. The objective functions in iteration 1 are shown in Figure 40. The focal point from this iteration is marked as a red dot.

The procedure was initiated with a step sizes $\frac{\Delta_A}{A_{ref}} = 0.065$ and $\frac{\Delta_Y}{Y_{ref}} = 0.267$. At the end of iteration 1, some very strong trends directed towards a minimum were noticed in the power loss plots as shown in Figure 40 and with the help of the factor GNI in both the lubricating interfaces in the two operating conditions, the focal point which finds a good compromise between all the objective functions were found at $\frac{A}{A_{ref}} = 0.868$ and $\frac{Y}{Y_{ref}} = 1.205$.

Consequently, a search step was invoked in iteration 2 which was unsuccessful and the global focal point remained the same.

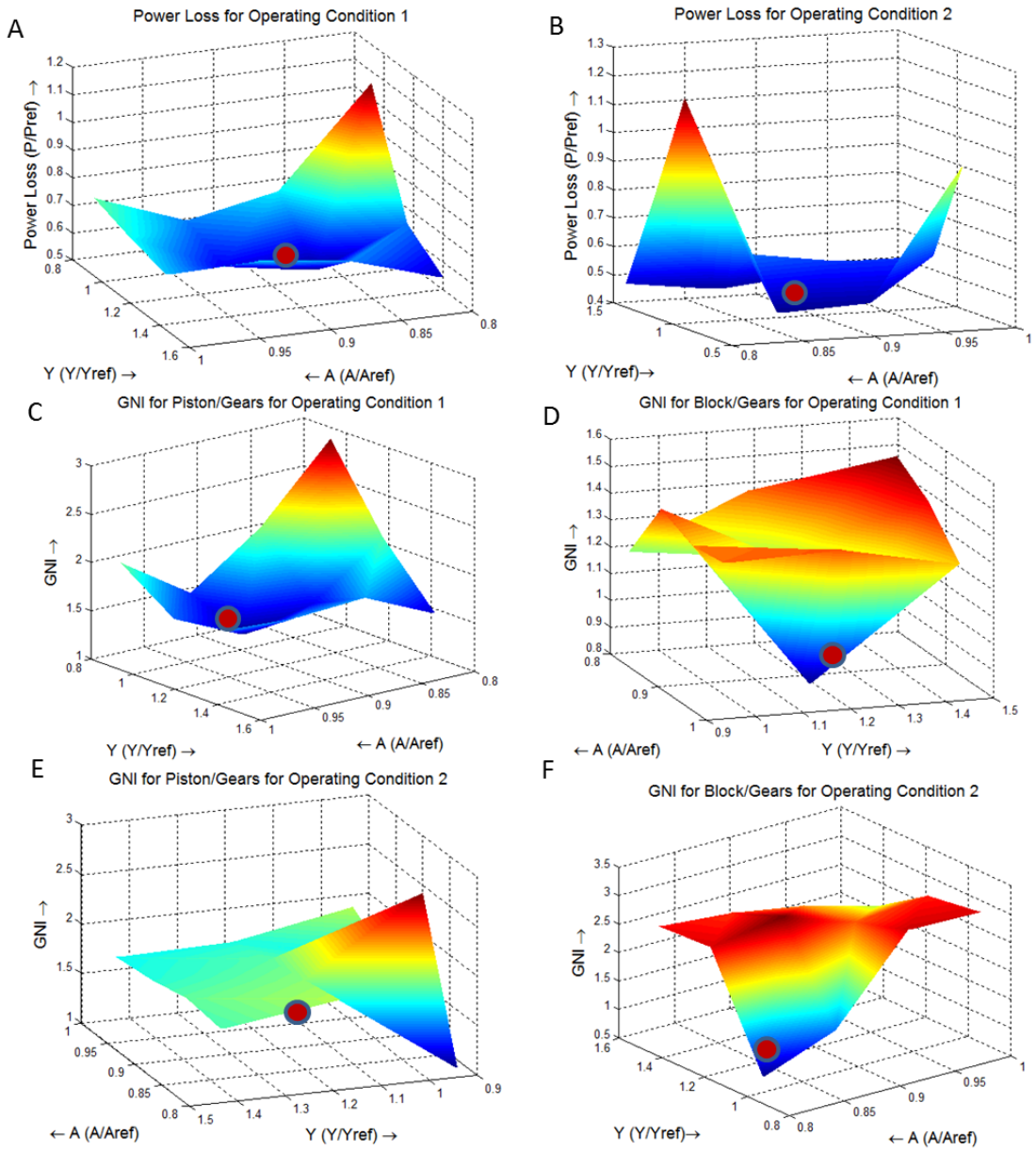

Figure 40: Objective function plots after iteration 1. A) Power loss in operating condition 1 B) Power loss in operating condition 2 C) GNI for Piston/Gears interface in operating condition 1 D) GNI for Block/Gears interface in operating condition 1 E) GNI for Piston/Gears interface in operating condition 2 F) GNI for Block/Gears interface in operating condition 2. The focal point at the end of the iteration is marked in red in all the plots.

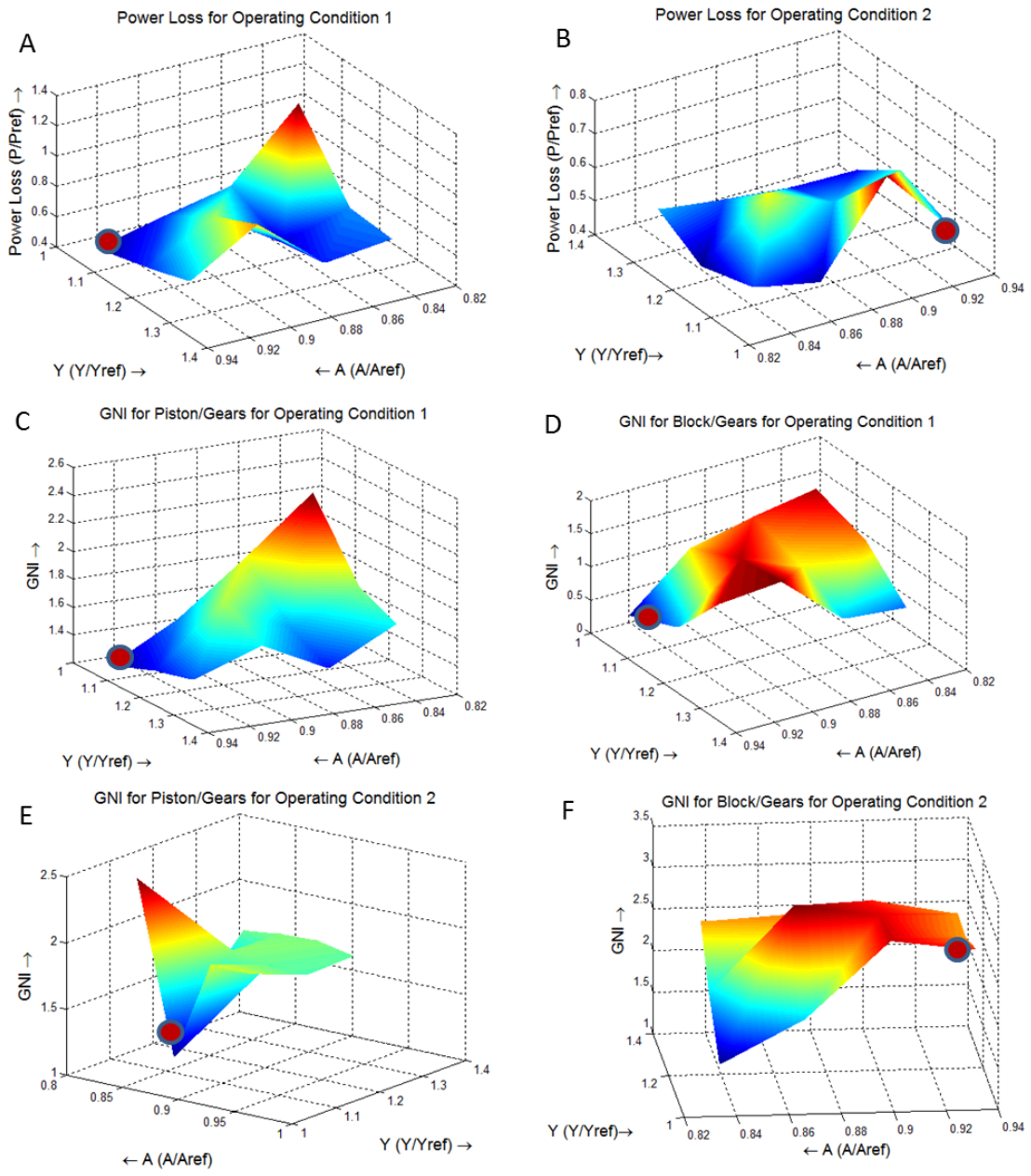

Figure 41: Objective function plots after iteration 3. A) Power loss in operating condition 1 B) Power loss in operating condition 2 C) GNI for Piston/Gears interface in operating condition 1 D) GNI for Block/Gears interface in operating condition 1 E) GNI for Piston/Gears interface in operating condition 2 F) GNI for Block/Gears interface in operating condition 2. The focal point at the end of the iteration is marked in red in all the plots.

In the subsequent iteration 3, a poll step was invoked with the step size halved and this poll step was successful and led to an improved focal point at $\frac{A}{A_{ref}} = 0.933$ and $\frac{Y}{Y_{ref}} = 1.071$. The trends in objective function values observed in this iteration are shown in Figure 41.

In iteration 4, a search step resulted in no further improvement in the focal point and after a subsequent poll step in iteration 5 which resulted in halving the step size and a search step following that did not improve the best feasible solution. Further reduction in the step sizes in the subsequent iteration resulted in meeting the convergence criterion set prior to the procedure.

Thus, the final design parameters for the optimized balance area design for the balance piston was found at $\frac{A}{A_{ref}} = 0.868$ and $\frac{Y}{Y_{ref}} = 1.205$ which presents a well-balanced compromise solution between the various objective functions and operating conditions for the asymmetrically balanced EGM. Thus, although asymmetrically compensated EGMs add complexity to the design of axial balance due to the presence to two distinct lateral lubricating interfaces, the optimization procedure was able to accommodate all the aspects and provide an optimal balance area design for the reference EGM under consideration.

CHAPTER 6. POTENTIAL OF THE OPTIMIZATION PROCEDURE IN INVESTIGATING NOVEL DESIGNS FOR IMPROVED LUBRICATION PERFORMANCE

The capability of the optimization tool developed in the present research work to design the optimal axial balance in traditional EGM designs with both symmetric and asymmetric pressure compensations were demonstrated in the previous sections. However, the ability of this design tool can be extended easily to improve the efficiency of novel EGM designs which include adding a linear sloping wedge on gear teeth, shot peening on the surface of the gears and the lateral bushes, waved gears and many more. Micro-surface patterns such as those, are used with the purpose of modifying the hydrodynamic pressure generation in the gap, thus achieving different balance features. This can permit to have more stable balance, with respect to the variation of the operating condition or to design units for non-traditional operating conditions, such as very low or very high speed. Thus, the developed optimization tool has a potential to design an optimal balance for such varied features. The possibilities of improving the lubrication performance using such novel designs have been shown in the work of [1]. Significant reduction of power losses in the lateral lubricating interface has been observed in some of these designs like wedged gears, by analyzing these designs with an advanced FSI lateral lubricating gap model.

Since it has been demonstrated in the previous sections that the optimization procedure can achieve an optimal axial balance and thus improve the lubrication performance, implementation of the procedure to design the optimal axial balance in these novel designs can help in achieving a stable axial balance for the variety of design features added.

The reference EGM for this study is a pump with displacement **O** (20 cm3) and speed range of the pump is 500-3500 rpm and the max pressure rating is 280 bar. Thus, in this section, efforts have been made to demonstrate the potential of the procedure to improve the

lubrication performance to the maximum possible extent by considering the micro-shaping effect of adding a wedge profile to the surface of the gears.

6.1 Past Effort in Investigating Effects of Wedged Gears in EGMs

The novel design of the wedged gears has been shown to have improved lubricating gap heights reduced losses in the gap especially in the losses due to viscous friction by using the FSI-EHD model for lateral gaps in [1]. A linear sloping wedge was added on each of the gear tooth with maximum wedge depth being 0.9 μm with a slope of 0.1 μm/mm. A representation of adding the wedge depth to the gear teeth to a gear along with the representation of the lateral gap by adding wedge profile to the surface of the gears is shown in Figure 42. It must be noted that wedges on the surface are greatly exaggerated (scaled by ~10000) in order to be visible.

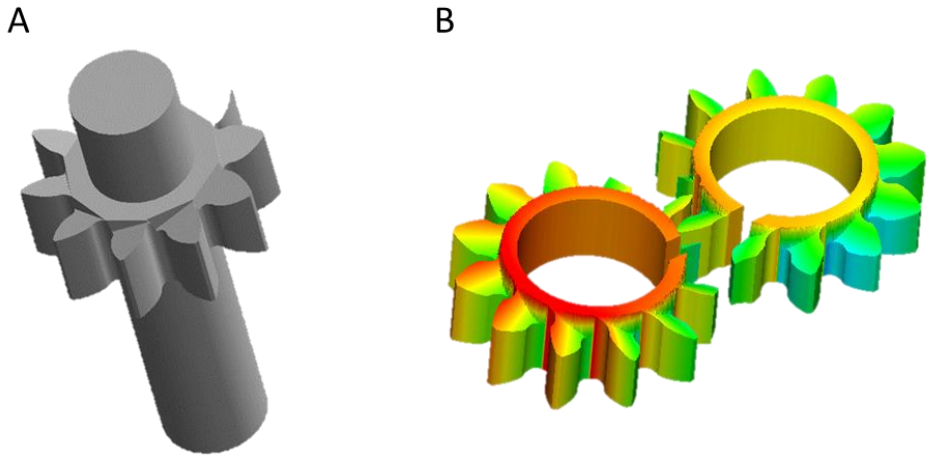

Figure 42: A) Representation of adding a linear sloping wedge to each of the gear teeth in a 10 teeth gear. B) Representation of the lateral gap by adding a wedged profile to the surface of the gears in an EGM with 12 teeth gears.

From the results of this work, the total losses were seen to have reduced for all the operating conditions tested, with the maximum improvement being by 66% at $\frac{p}{p_{Ref}} = 0.2$. This improvement is particularly driven by the hydrodynamic wedge effects that were created by the direction of the wedge on the gear teeth. A sample prediction of the lubricating gap heights and resultant pressures obtained for $n = 2000\ RPM$, $\frac{p}{p_{Ref}} = 0.6$ in the reference EGM with wedged gear surfaces is shown in Figure 43.

Figure 44 shows that by using the wedged gears solution, both the minimum gap heights and the total losses from the lateral gap showed large improvements at a range of operating conditions, particularly at low pressures. Aside from improving the performance of the lubricating interface in EGMs as evidenced from the reasons stated above, the design with wedged gears is also expected to be relatively feasible as regards manufacturing and cost.

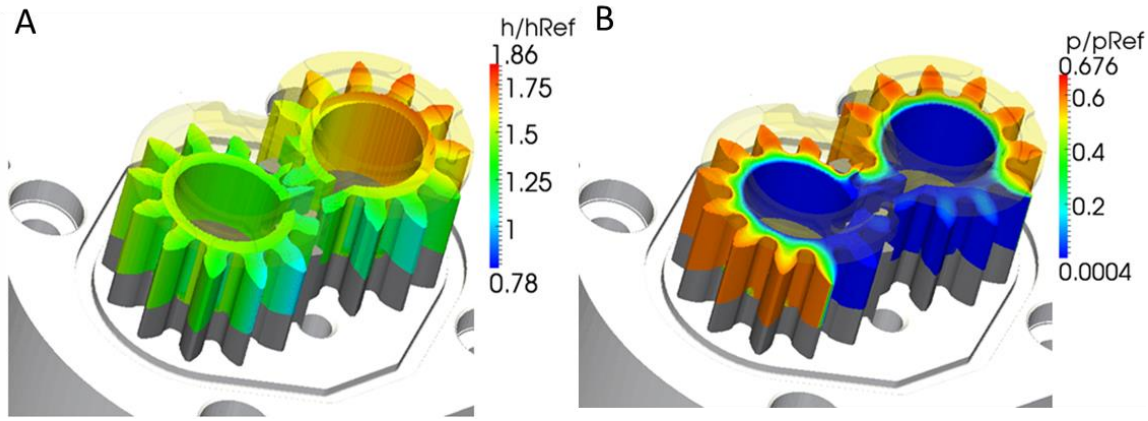

Figure 43: Lateral gap results from the FSI model by adding the wedged gear effects A) Prediction of film thickness in the gap B) Prediction of resultant pressures in the gap [1].

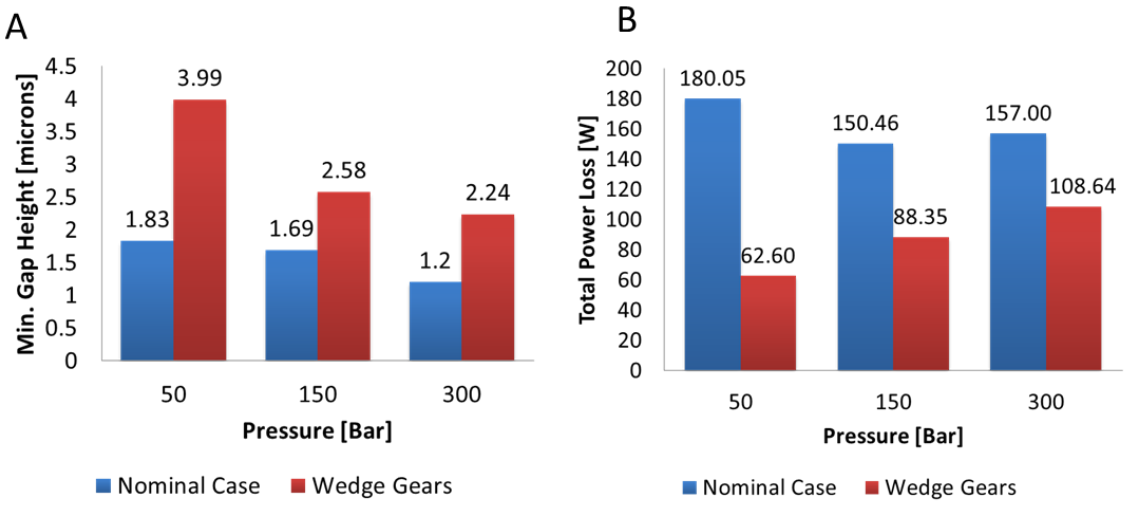

Figure 44: Comparison of the lubrication performance between wedged gears and the nominal case at different operating conditions A) Plot of minimim gap heights in the gap B) Plot of total power losses in the gap [1].

Although the results from the above work established the potential of wedged gears to improve the lubrication performance of lateral gaps in EGMs, such a study was performed with only one particular value of the wedge depth (0.9 µm). The optimization tool

developed in the present research can be used to investigate more designs of the wedged gears by varying the wedge depths since an optimal axial balance configuration can be obtained for each design. Since the axial balance varies for each of the wedged designs, the same balance area cannot be assumed for each wedged design. Thus, the same fixed balance area cannot be assumed to give a stable axial balance for the variations in the design features. The developed optimization tool has the advantages of ensuring an optimal axial balance configuration each design of the wedged gears and thus can be a useful tool in the investigation of such novel designs.

6.2 Investigation of Varying Designs of Wedged Gears

The design concept in wedged gears includes adding a linear sloping wedge profile to the surface of the gears on its either side, as outlined earlier. In this section, efforts have been made to analyze the effect of varying the maximum wedge depth when adding the linear wedge profile to the surface of the gears. This maximum wedge depth has been varied from 0.5 μm to 7 μm to understand the effect of this parameter on the total power losses in the lubricating gap as well as the factor GNI. This effort can also help in guiding the direction of using the numerical procedure developed in this research to design the optimal axial balance for a given wedge depth of the gears.

Baseline simulations using the original balance of the reference EGM were performed using the extended FSI model with capabilities to include the effects of wedged gears in the lateral gap (model details published in [1], with varying values of the maximum wedge depths for different operating conditions. The two operating conditions chosen for this purpose were: $^{p}/_{p_{ref}} = 0.32$, 1000 rpm which will be designated as Operating Condition 1 (OC 1) and $^{p}/_{p_{ref}} = 0.64$, 2000 rpm which will be designated as Operating Condition 2 (OC 2). In this case, the value of p_{ref} is **O** (300 bar) corresponding to the maximum pressure rating of the pump.

The film thickness results from the FSI model for the various wedge depths in the gear surfaces at the two operating conditions OC 1 and OC 2 are presented from Figure 45 to Figure 53. It can be observed from these plots that as the wedge depths increase, the axial

balance of the EGM is affected since the same balance area on the lateral plate has been used for simulating all the designs. At the higher values of wedge depth (4 - 7 µm) simulated, maximum gap height increases to high values indicating that the EGM with this design of wedged gears is not well balanced and results in high power losses in the gap. This promotes the necessity of applying the optimization procedure developed to design the optimal axial balance for each of the designs of wedged gears since each design has a unique balance feature associated with it.

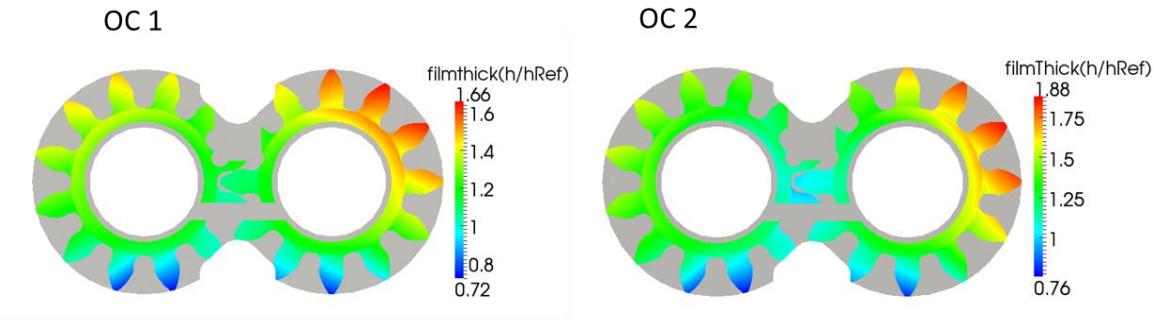

Figure 45: Film thickness results from the FSI model for wedged gear design of **0.5 micron** wedge depth at operating conditions OC 1 (left) and OC 2 (right).

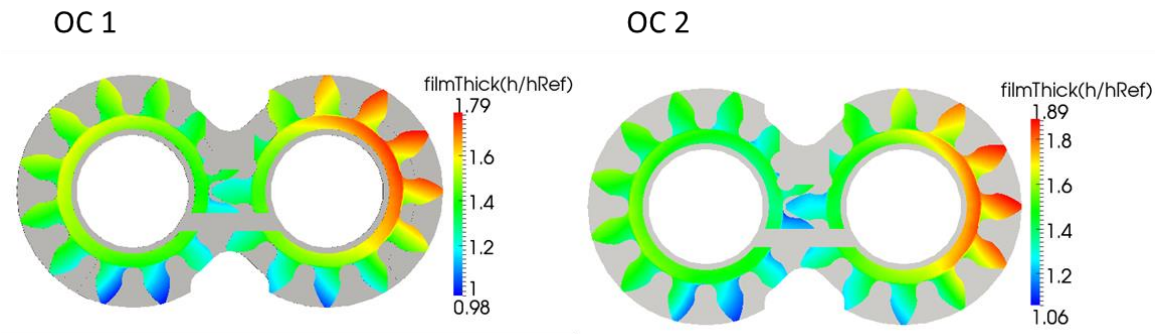

Figure 46: Film thickness results from the FSI model for wedged gear design of **1 micron** wedge depth at operating conditions OC 1 (left) and OC 2 (right).

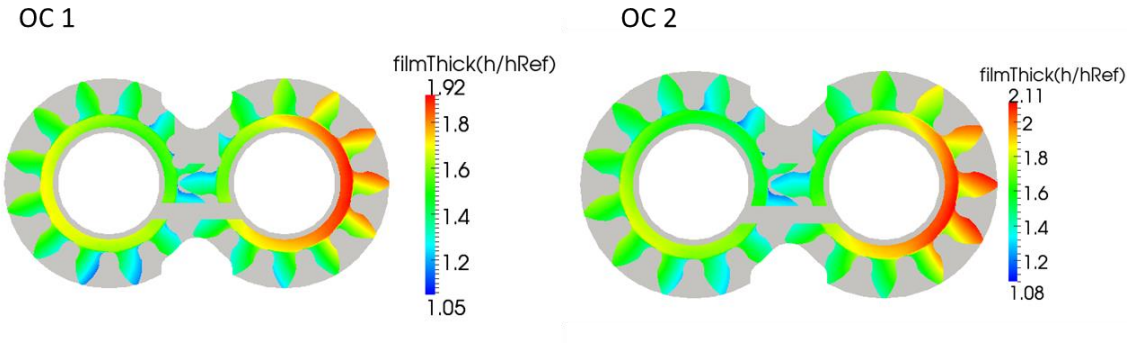

Figure 47: Film thickness results from the FSI model for wedged gear design of **1.5 micron** wedge depth at operating conditions OC 1 (left) and OC 2 (right).

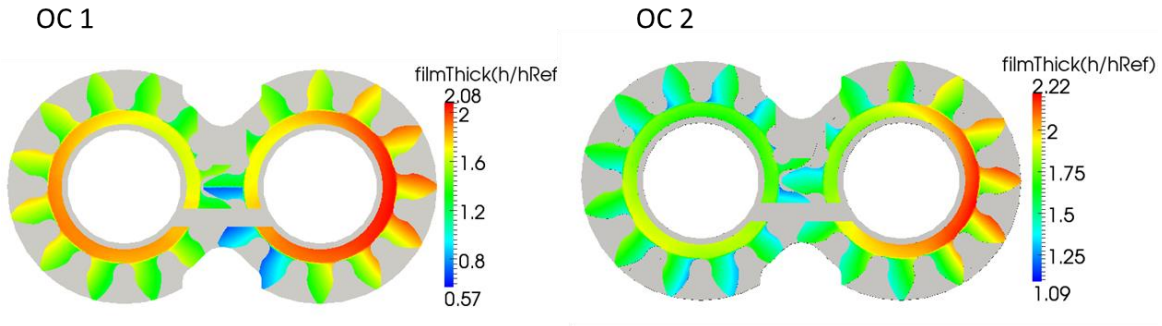

Figure 48: Film thickness results from the FSI model for wedged gear design of **2 micron** wedge depth at operating conditions OC 1 (left) and OC 2 (right).

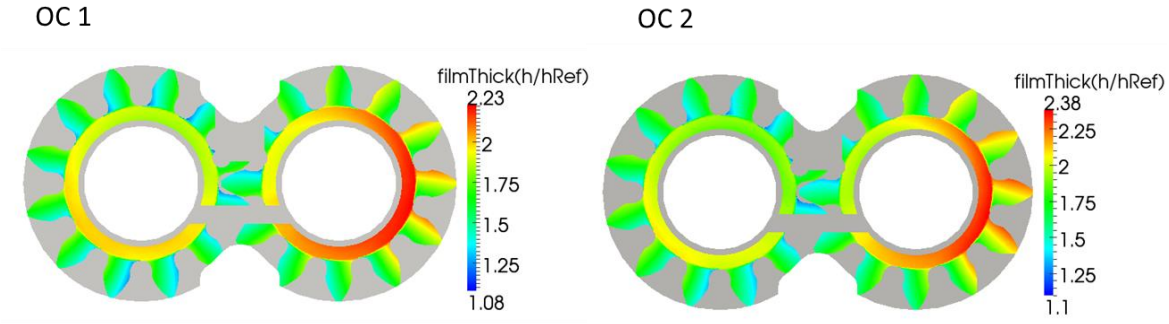

Figure 49: Film thickness results from the FSI model for wedged gear design of **2.5 micron** wedge depth at operating conditions OC 1 (left) and OC 2 (right).

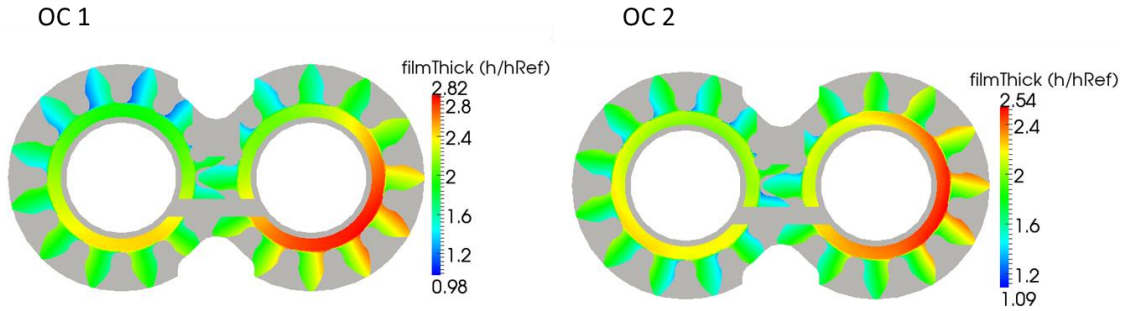

Figure 50: Film thickness results from the FSI model for wedged gear design of **3 micron** wedge depth at operating conditions OC 1 (left) and OC 2 (right).

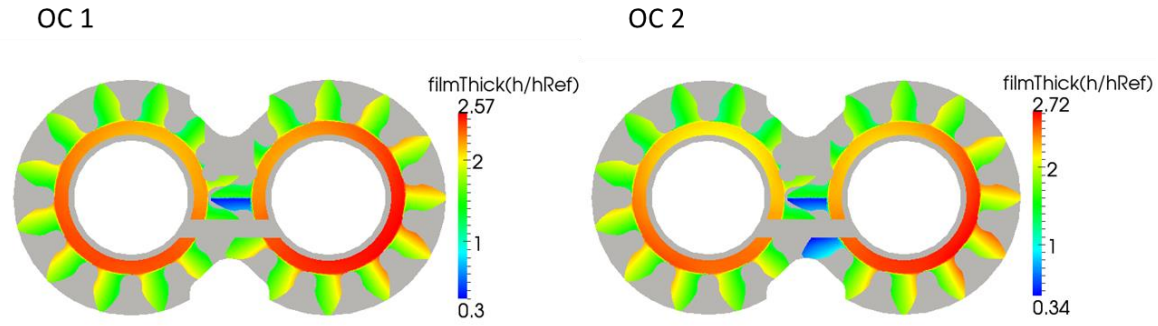

Figure 51: Film thickness results from the FSI model for wedged gear design of **4 micron** wedge depth at operating conditions OC 1 (left) and OC 2 (right).

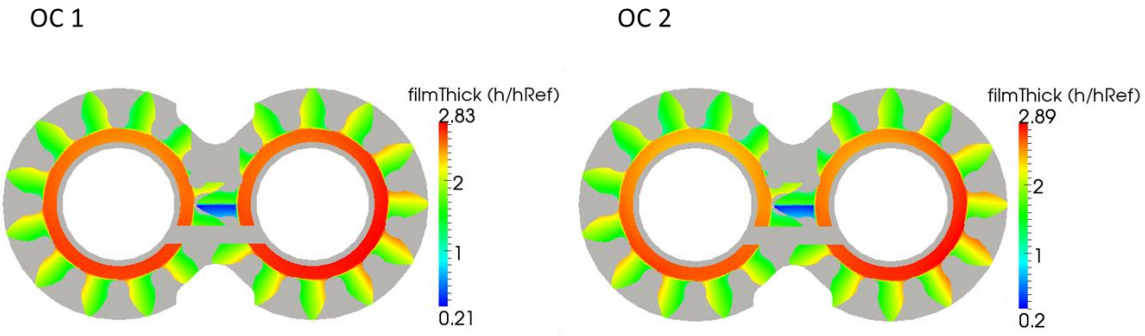

Figure 52: Film thickness results from the FSI model for wedged gear design of **5 micron** wedge depth at operating conditions OC 1 (left) and OC 2 (right).

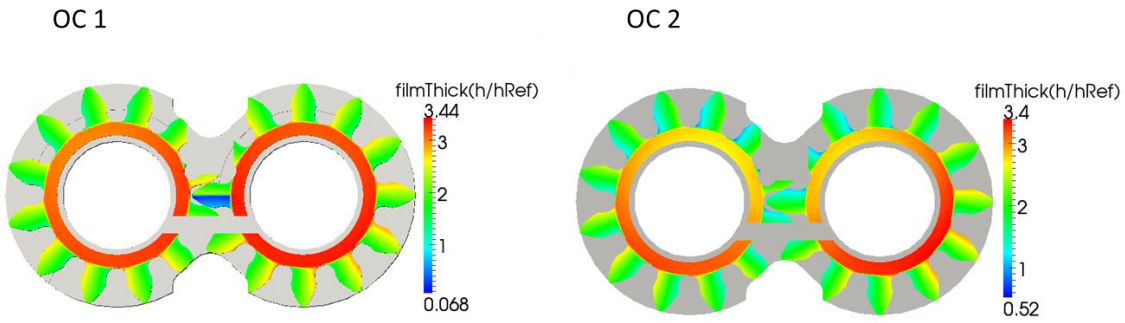

Figure 53: Film thickness results from the FSI model for wedged gear design of **7 micron** wedge depth at operating conditions OC 1 (left) and OC 2 (right).

The total power losses from the lubricating gap across varying maximum wedge depths on the surface of the wedged gears from the baseline simulations at two selected operating conditions is shown in Figure 54. It is observed that the total power losses from the lateral gap gradually decreases before marginally increasing to higher values for increasing values of wedge depths. This is due to the fact that the hydrodynamic effect of the physical wedge promotes higher gap heights in the lateral gap and at higher wedge depths, due to increased gap heights, the lateral leakages increases and the power loss due to the leakage source increases although the power loss due to viscous friction will decrease in these cases. However, at lower wedge depths where this hydrodynamic effect is not so prominent, the power losses due to fluid shear are high. This explains the trend of marginally decreasing total power loss values before increasing at higher wedge depths owing to the fact that the two sources of power loss (due to leakages and viscous friction) oppose each other. At higher wedge depths, the power losses due to leakages dominate and EGM might lose its axial balance.

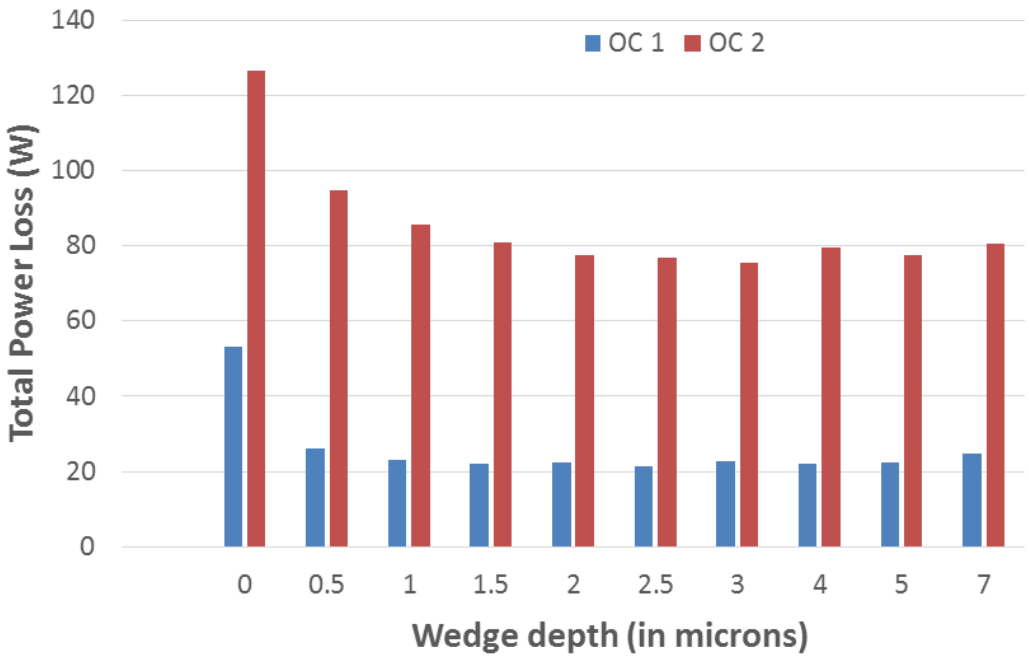

Figure 54: Variation of total power losses from the lateral lubricating gap at two operating conditions for varying wedge depths on the surface of the wedged gears.

Another interesting analysis can also be obtained by plotting the values of the parameter Gap Non-uniformity Index (GNI) (earlier defined in 4.4.2) at the two chosen operating conditions for varying wedge depths as shown in Figure 55. Higher values of GNI are observed at increased values of wedge depths which attributes to increased number of non-uniformities in the lateral gap. This can be directly related to the fact mentioned earlier that the axial balance of the EGM is expected to get affected by using the same design of the balance area on the lateral plate. Thus, an automatic numerical procedure to design the optimal axial balance would serve as a valuable design tool in investigating novel efficient designs such as wedged gears as demonstrated by this particular study.

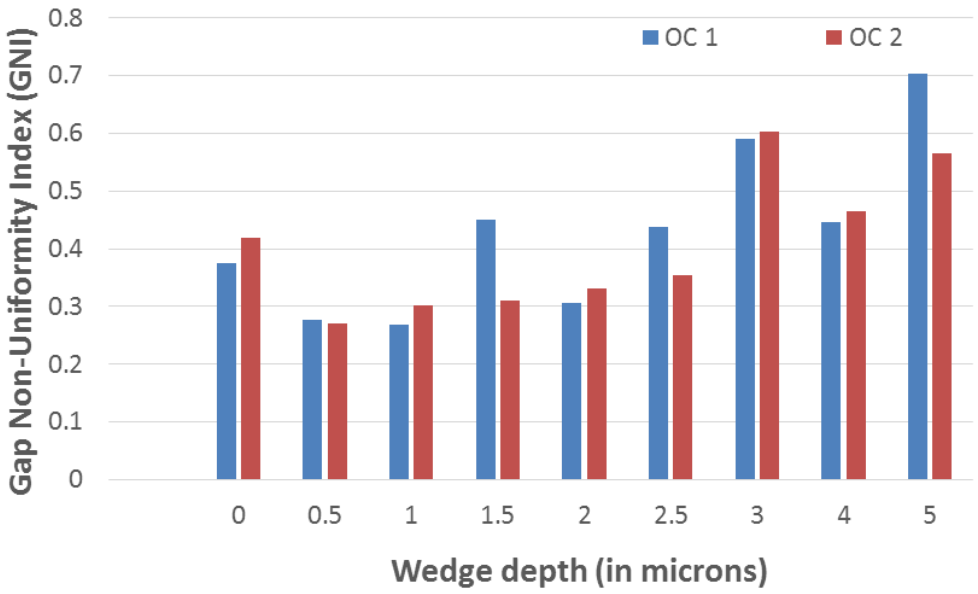

Figure 55: Variation of the parameter GNI of the lateral lubricating gap at two operating conditions for varying wedge depths on the surface of the wedged gears.

6.3 Optimization of Axial Balance for Wedged Gears Design

As outlined in the previous section, there is a need for using the numerical optimization procedure developed in this research to design the optimal axial balance for exploring novel efficient EGM designs. Therefore, to demonstrate this potential of such the optimization procedure, it has been applied to design the optimal axial balance for two maximum wedge depths on the surface of the wedged gears: 3 µm and 5 µm and the results from this effort has been presented in this section. The reasons for choosing these values of maximum wedge depth are that the case with 1 µm was shown to perform well in [1] and the potential of the rest of the wedge depths were not fully investigated owing to the fact that lack of optimal axial balance at these conditions can result in high losses and GNI as demonstrated in 6.2. Thus, two wedge depths 3 µm and 5 µm were selected to demonstrate the potential of the optimization tool. First, four selected operating conditions involving all combinations of high and low shaft speeds and delivery pressure has been used as input to design the optimal axial balance of wedged gears design with maximum wedge depth as 3 µm. These results are shown to match very closely with those obtained by considering two

input operating conditions (also used for the results presented in CHAPTER 5) for the same design. This also indicates that two input operating conditions which can save computational cost and time, are sufficient to design the optimal axial balance of an EGM. Thus following this inference, two input operating conditions are also used for designing the optimal axial balance for the case of the wedged gear design with maximum wedge depth of 5 μm.

Extending the range of operation of EGMs with a fairly good axial balance for a wide range of operating conditions can be achieved with the help of the optimization procedure developed in this work. The balance of an EGM is especially found to be critical at high pressures and between high and low speeds. The application of optimization procedure to find an optimal axial balance between such extreme operating conditions for the reference EGM with wedged gears has been discussed in the last section of this chapter.

6.3.1 3 Micron Wedge Depth with Four Reference Operating Conditions

In this subsection, axial balance of an EGM with a linear sloping wedged profile on the gear surface with a maximum wedge depth of 3 micron is optimized between four operating conditions which was provided as an input to the numerical procedure developed in the present research.

6.3.1.1 Reference Operating Conditions

The input operating conditions for the optimization procedure applied to the reference EGM case has been chosen to include all possible combinations of a given set of high and low values of shaft speed and output delivery pressure. Thus, the four operating conditions chosen here correspond to low pressure-low speed, high pressure-high speed, high pressure-low speed and low pressure-high speed conditions. The selected operating conditions along with the designated terms are listed in Table 2.

Table 2 : Four input operating conditions used for optimizing the axial balance for 3 micron wedge depth.

Operating Condition	Delivery Pressure	Shaft speed
OC 1	$^{p}/_{p_{Ref}} = 0.32$	1000 rpm
OC 2	$^{p}/_{p_{Ref}} = 0.64$	2000 rpm
OC 3	$^{p}/_{p_{Ref}} = 0.64$	1000 rpm
OC 4	$^{p}/_{p_{Ref}} = 0.32$	2000 rpm

6.3.1.2 Results from the Optimization Procedure

The optimization procedure was carried out with initial step sizes starting from $\frac{\Delta A}{A_{ref}} = 0.00673$ and $\frac{\Delta Y}{Y_{ref}} = 0.0625$ where A_{ref} is **O** (1000 mm^2), Y_{ref} is **O** (10 mm), ΔA is **O** (10 mm) and ΔY is **O** (1 mm). It must be noted here that the reference values of the design parameters A and Y used for normalizing the values refer to the corresponding values of the original balance area design in the reference EGM under study. The final converged results were obtained 4 iterations of the optimization procedure which included 2 poll steps and 2 search steps as a part of the direct search method (described in 4.7). In the first two iterations, two poll steps were performed with varying search directions which was followed by two successive search steps in the next two iterations. Each of the search steps reduced the step size of the previous iteration by half.

The plots of the objective functions, power loss and GNI for each of the operating conditions in iteration 1 are shown in Figure 56 and Figure 57 respectively. The focal point in this iteration which was found by using the relation described in Eqn. 4.13 represents the best compromise solution found from the current grid of designs. The values of the various objective functions at this point is represented by a red dot in the corresponding graphs shown in Figure 56 and Figure 57.

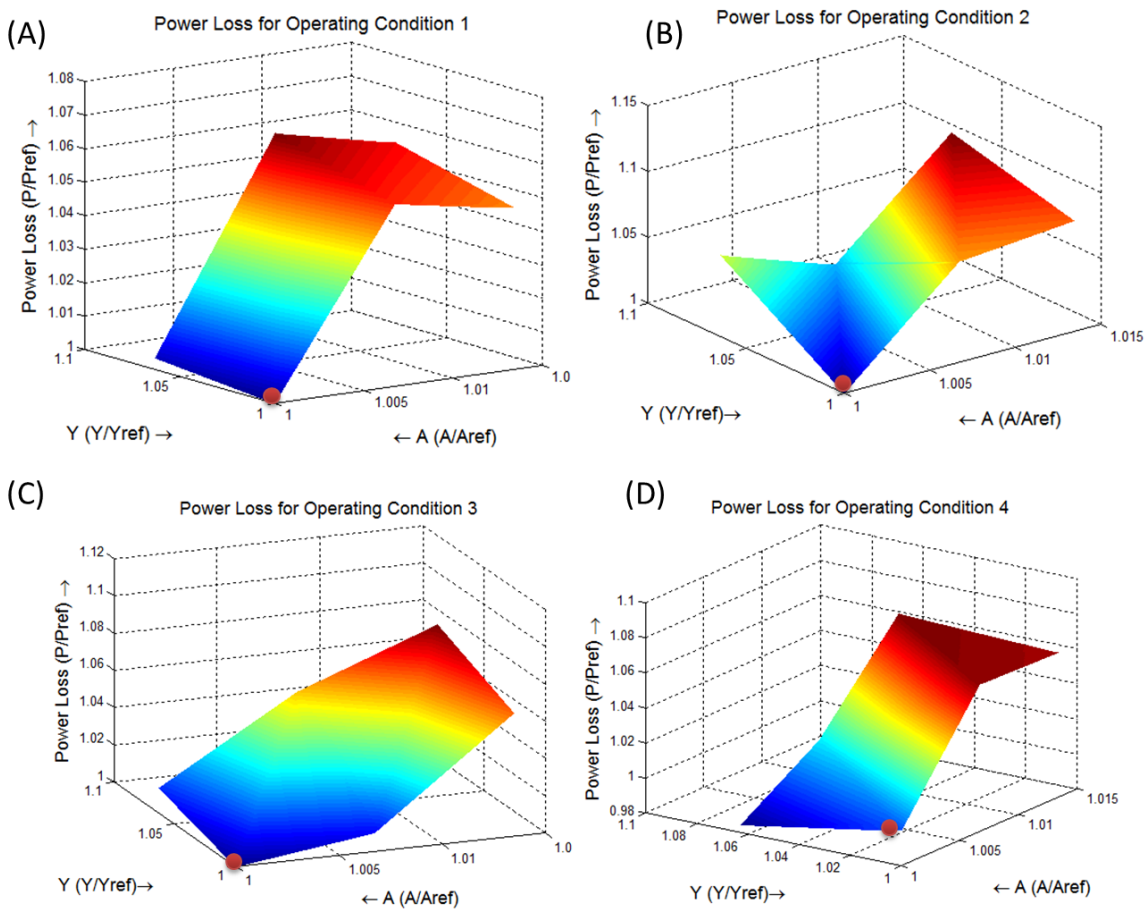

Figure 56: Plots of total power loss from the lateral lubricating gap for the four input operating conditions in Iteration 1 (A) Operating condition 1 (B) Operating Condition 2 (C) Operating Condition 3 (D) Operating Condition 4. The focal point of the iteration is highlighted as a red mark.

The search directions are now changed in the second iteration to focus on the grid points closer to the focal point found in the previous iteration. The plots of the total power losses from the lateral lubricating gap and the GNI of the gap for the design grid in the second iteration is shown in Figure 58 and Figure 59. The focal point in this iteration was found to be the same point as the previous iteration. Hence, for the iteration succeeding the current one, the step size is halved and attempts are made to find if a better solution exists in the region close to the current focal point by refining the grid further by half.

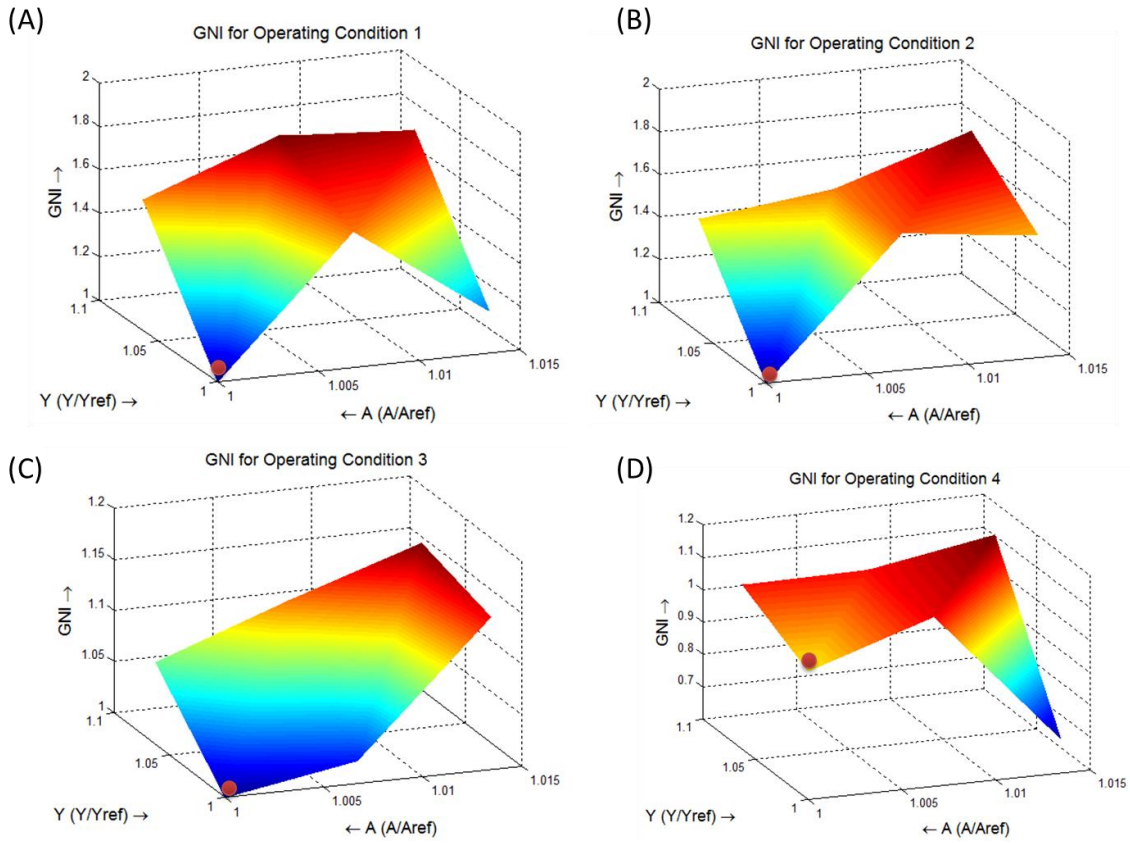

Figure 57: Plots of GNI in the lateral lubricating gap for the four input operating conditions in Iteration 1 (A) Operating condition 1 (B) Operating Condition 2 (C) Operating Condition 3 (D) Operating Condition 4. The focal point of the iteration is highlighted as a red mark.

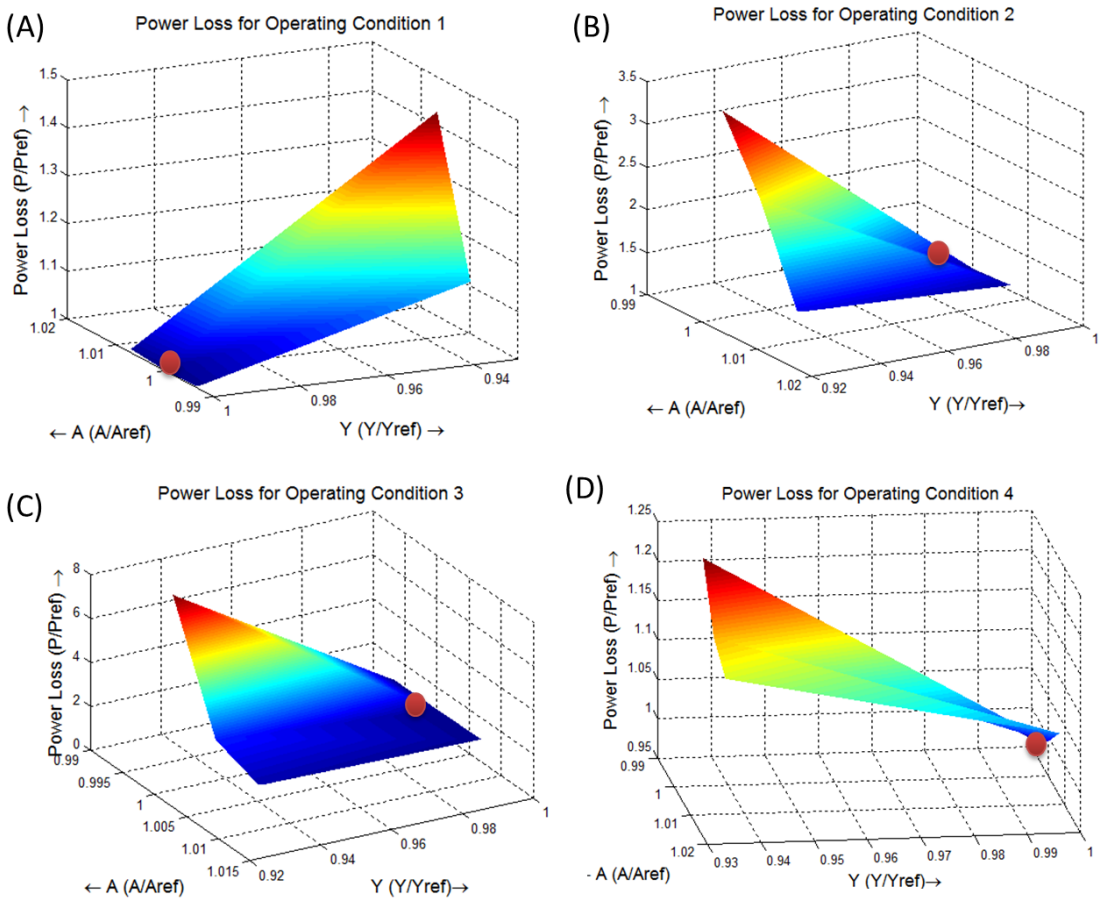

Figure 58: Plots of total power loss from the lateral lubricating gap for the four input operating conditions in Iteration 2 (A) Operating condition 1 (B) Operating Condition 2 (C) Operating Condition 3 (D) Operating Condition 4. The focal point of the iteration is marked as a red point.

In the third iteration which was a search step (part of the direct search method discussed in 4.7), the step size is halved to produce a refined design grid near the previous focal point. The plots of the total power loss in the lateral gap and the GNI of the gap at the end of the third iteration are shown in Figure 60 and Figure 61 respectively. This search step was successful in finding a new focal point which was ${}^{A}/_{A_{Ref}} = 1.0034$ and ${}^{Y}/_{Y_{Ref}} = 1$. This focal point is marked in red in the Figure 60 and Figure 61. Further iterations of the procedure by successive reduction of the step size of the design grid until the convergence criterion was reached, did not yield a better design point. Thus, this design point yielded the best possible solution for the reference EGM design with four input operating conditions.

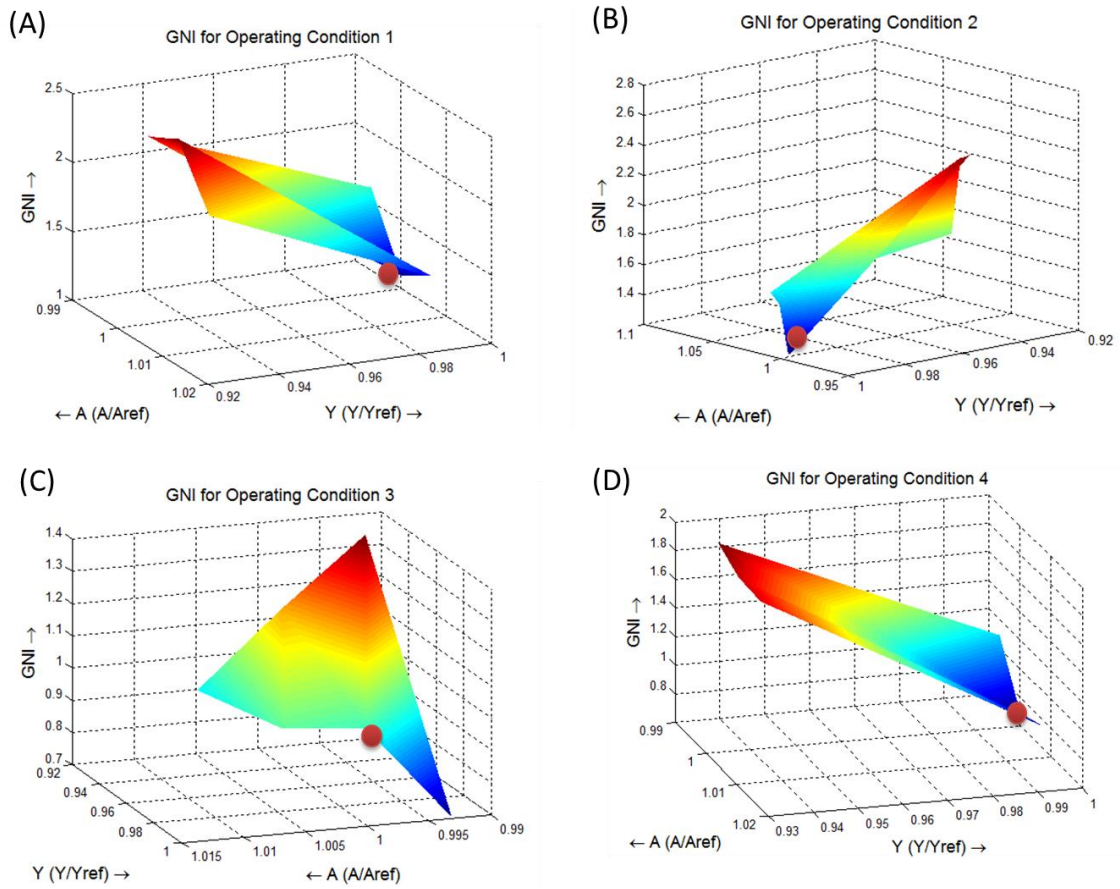

Figure 59: Plots of GNI from the lateral lubricating gap for the four input operating conditions in Iteration 2 (A) Operating condition 1 (B) Operating Condition 2 (C) Operating Condition 3 (D) Operating Condition 4. The focal point of the iteration is marked as a red point.

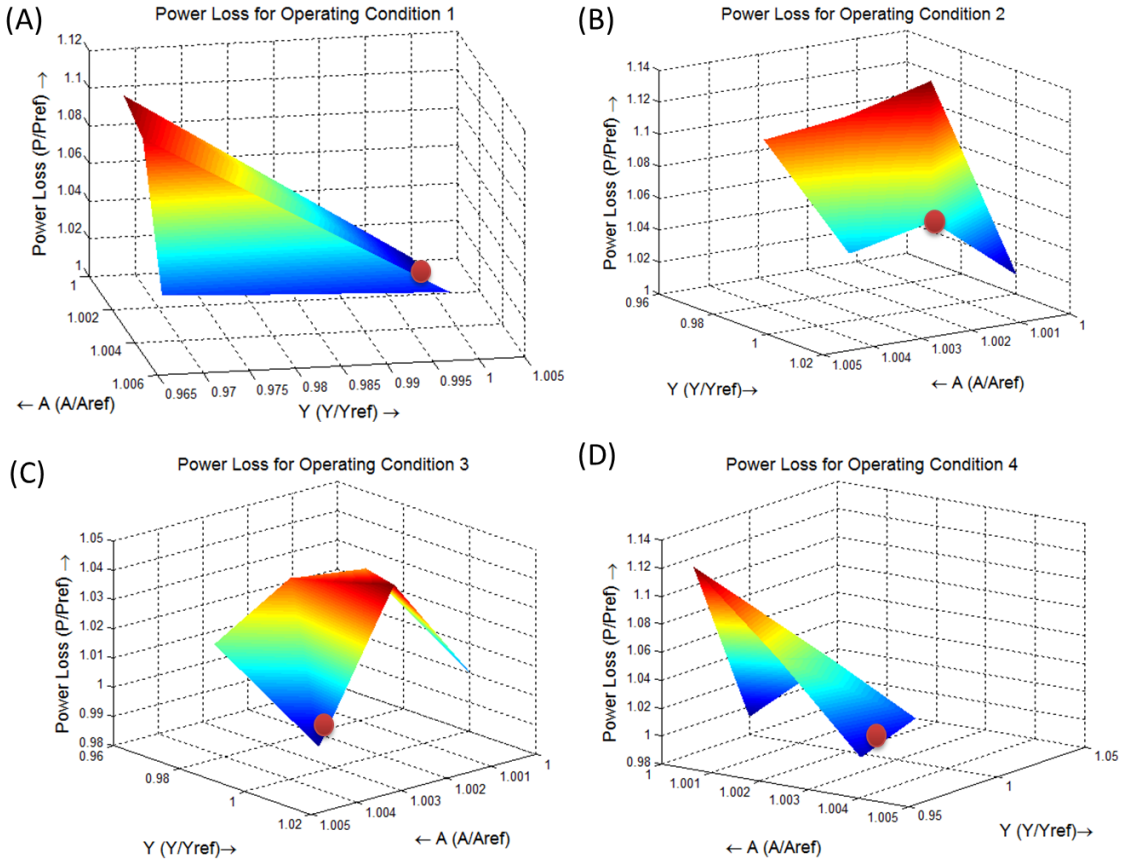

Figure 60: Plots of total power loss from the lateral lubricating gap for the four input operating conditions in Iteration 3 (A) Operating condition 1 (B) Operating Condition 2 (C) Operating Condition 3 (D) Operating Condition 4. The focal point of the iteration is marked as a red point.

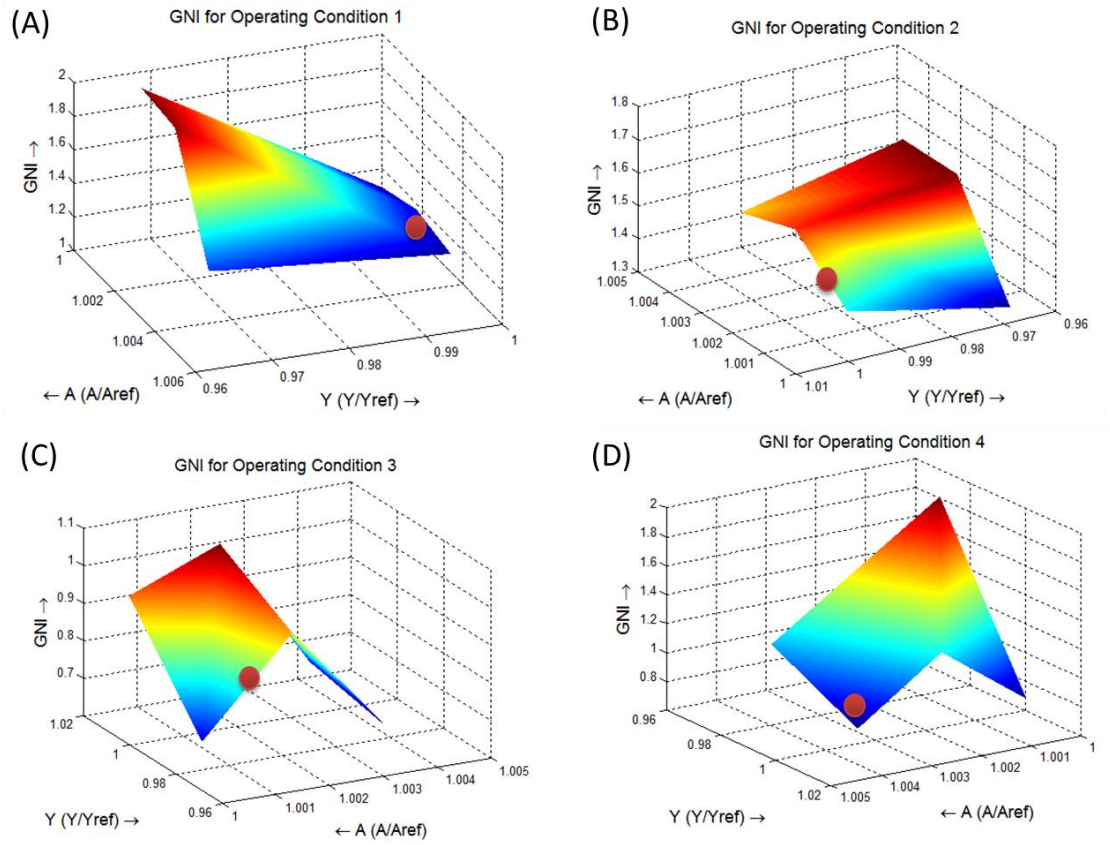

Figure 61: Plots of GNI from the lateral lubricating gap for the four input operating conditions in Iteration 2 (A) Operating condition 1 (B) Operating Condition 2 (C) Operating Condition 3 (D) Operating Condition 4. The focal point of the iteration is marked as a red point.

The gap film thickness results for the nominal reference design without the wedged gear profile for the four selected operating conditions is shown in Figure 62. All the film thickness results have been normalized with respect to the value of h_{Ref} in the **O** (5 µm). These results shown in Figure 62 were obtained using the FSI-EHD model for lateral gaps using the original balance area of the reference EGM. It can be seen that the minimum gap height obtained in the high pressure low speed condition (OC 3) is significantly lower than the others and thus this operating condition remains one of the most critical OC of all the selected OCs.

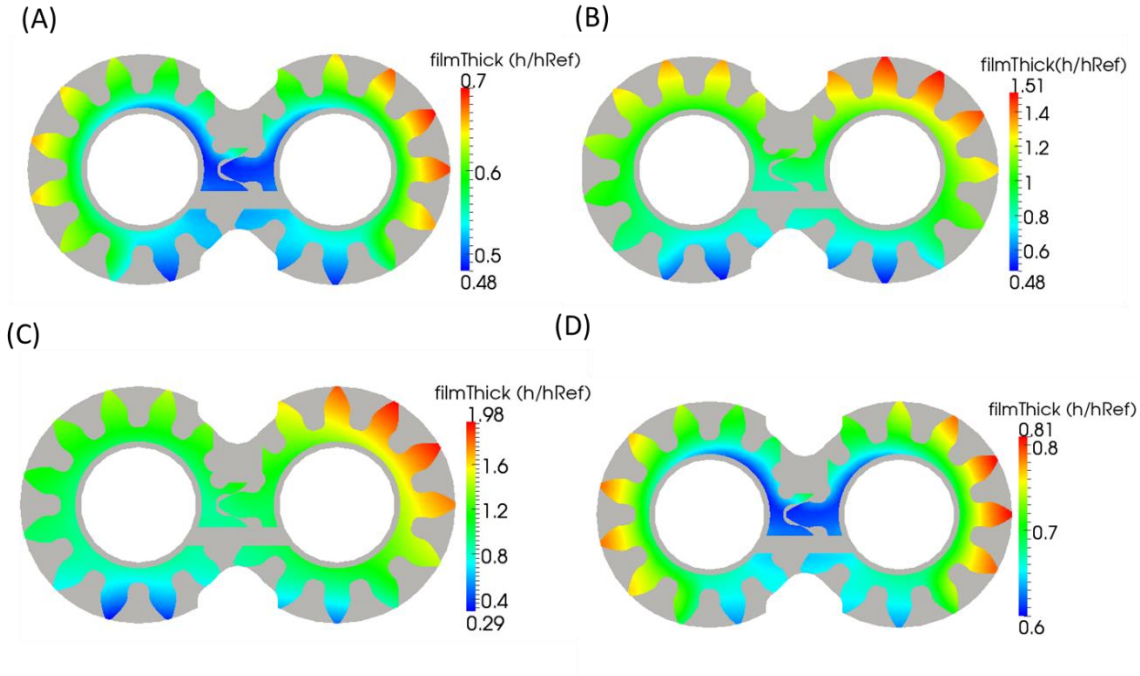

Figure 62: Gap film thickness results for the nominal reference design without the wedge profile on the gears (A) Operating Condition 1 (B) Operating Condition 2 (C) Operating Condition 3 (D) Operating Condition 4.

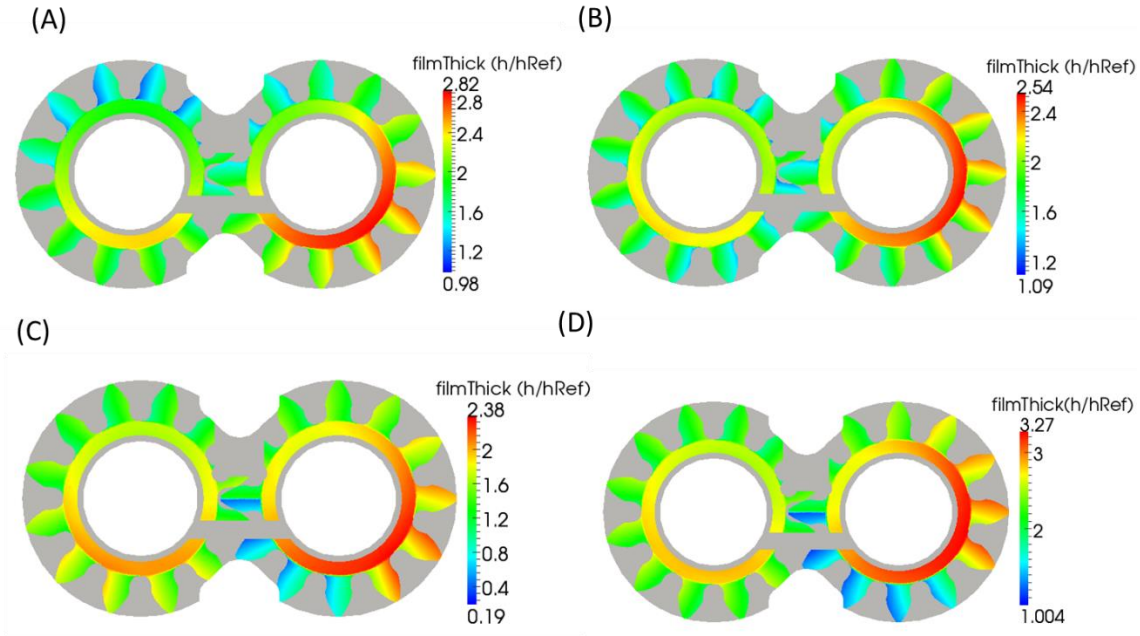

Figure 63: Gap film thickness results for nominal reference design (original balance area design) with wedged profile on the gears (maximum wedge depth 3 µm (A) Operating Condition 1 (B) Operating Condition 2 (C) Operating Condition 3 (D) Operating Condition 4.

The lubricating gap film thickness for the wedged gear profile in the reference EGM design with original balance area at the four selected operating conditions (described in Table 2) are shown in Figure 63. It can be observed that just by adding the wedged profile to the surface of the gears, some noticeable improvements in the minimum gap heights can be observed in Figure 63 and Figure 64 at most of the operating conditions. The gap film thickness for the optimized balance area for a 3 micron wedge depth on the gears surface for the same four operating conditions are shown in Figure 64.

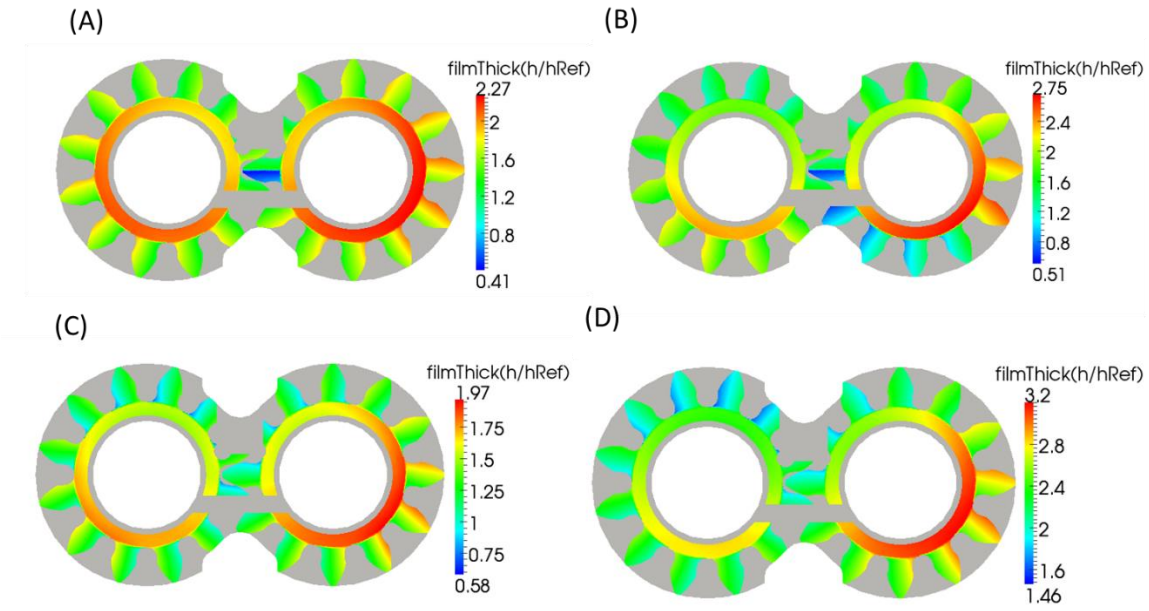

Figure 64: Gap film thickness results for optimal balance area design with wedged profile on the gears (maximum wedge depth 3 μm (A) Operating Condition 1 (B) Operating Condition 2 (C) Operating Condition 3 (D) Operating Condition 4.

It can be observed from both figures Figure 63 and Figure 64 when compared to Figure 62 that adding a linear wedged profile to the gears surface provides the hydrodynamic effect which increases the minimum film thickness and helps in reducing regions of contact. Further improvement in the power losses was achieved by optimizing the balance area design for the reference EGM configuration under study. A quantitative comparison of all the three results presented in Figure 62, Figure 63 and Figure 64 in terms of the objective functions power losses and GNI used in this study has been made in Table 3.

Table 3: Quantitative comparison of total power loss and GNI of the lateral gap between wedged gears (3 micron maximum wedge depth) with original balance area and optimized balance area design with respect to the reference design without wedged gears.

Operating condition	**Power loss (wrt reference EGM design)**		**GNI (wrt reference EGM design)**	
	Wedged gears with original balance area	*Wedged gears with optimized balance area*	*Wedged gears with original balance area*	*Wedged gears with optimized balance area*
OC1	Reduced by 57.50 %	Reduced by 58.93 %	Increased by 56.77 %	Increased by 64.73 %
OC2	Reduced by 40.28 %	Reduced by 34.679 %	Reduced by 31.37 %	Increased by 11.79 %
OC3	Reduced by 7.27 %	Reduced by 11.28 %	Reduced by 13.21 %	Reduced by 38.43 %
OC4	Reduced by 63.46 %	Reduced by 65.12 %	Reduced by 67.86 %	Increased by 56.04 %

It can be observed from the table that significant improvements in the lubrication performance of the EGM in terms of the total power loss from the gap and the GNI of the lateral gap can be seen by adding a wedged profile to the surface of the gears. Some further improvements in the objective function values can be seen with the optimized balance area on the wedged gear surface although in the case of OC2, the original balance area design is marginally better. This can be attributed to the fact that the current optimization is a multi-objective problem and a well-balanced balance area solution which offers a good performance at all the operating conditions considered in this study. Hence, the optimized balance results from other operating conditions, especially from OC3 are quite significantly better than the original design. Thus, the optimized balance area solution for the wedged gears offers the best compromise design which combines the advantages offered by wedged gears and the optimization procedure developed in this work.

6.3.2 3 Micron Wedge Depth with Two Reference Operating Conditions

In the previous subsection, the optimization of axial balance for a wedged gear surface with a 3 micron wedge depth was evaluated with four input operating conditions. The optimization procedure with four input operating conditions was a computationally expensive and a time consuming exercise owing to the number of objective function values involved. However, the same exercise was carried out with two input operating conditions (as shown in Table 4) in this section and it was found that it was sufficient for the reference EGM considered for this study.

6.3.2.1 Reference Operating Conditions

Two input operating conditions corresponding to a low pressure low speed (OC 1) and high pressure high speed (OC 2) condition were chosen for the present study. The selected operating conditions are specified in Table 4.

Table 4: Two input operating conditions used for optimizing the axial balance for 3 micron wedge depth.

Operating Condition	Delivery Pressure	Shaft speed
OC 1	$p/p_{Ref} = 0.32$	1000 rpm
OC 2	$p/p_{Ref} = 0.64$	2000 rpm

6.3.2.2 Results from the Optimization Procedure

The optimization procedure was carried out with initial step sizes starting from $\frac{\Delta A}{A_{ref}} = 0.00673$ and $\frac{\Delta Y}{Y_{ref}} = 0.0625$ where A_{ref} is **O** (1000 mm^2), Y_{ref} is **O** (10 mm), ΔA is **O** (10 mm) and ΔY is **O** (1 mm). The final converged results were obtained 5 iterations of the optimization procedure which included 3 poll steps and 2 search steps as a part of the direct search method (described in 4.7). In the first two iterations, two poll steps were performed with varying search directions which was followed by a search steps, a poll step and a search step in the next three iterations. Each of the search steps reduced the step size of the previous iteration by half.

The plots of the objective functions power loss and GNI at the end of the first iteration (a poll step) are shown in Figure 65. The focal point of this iteration (defined previously in Eqn. 4.13) is highlighted with the help of a red circle in each of the objective function plots at the selected two operating conditions.

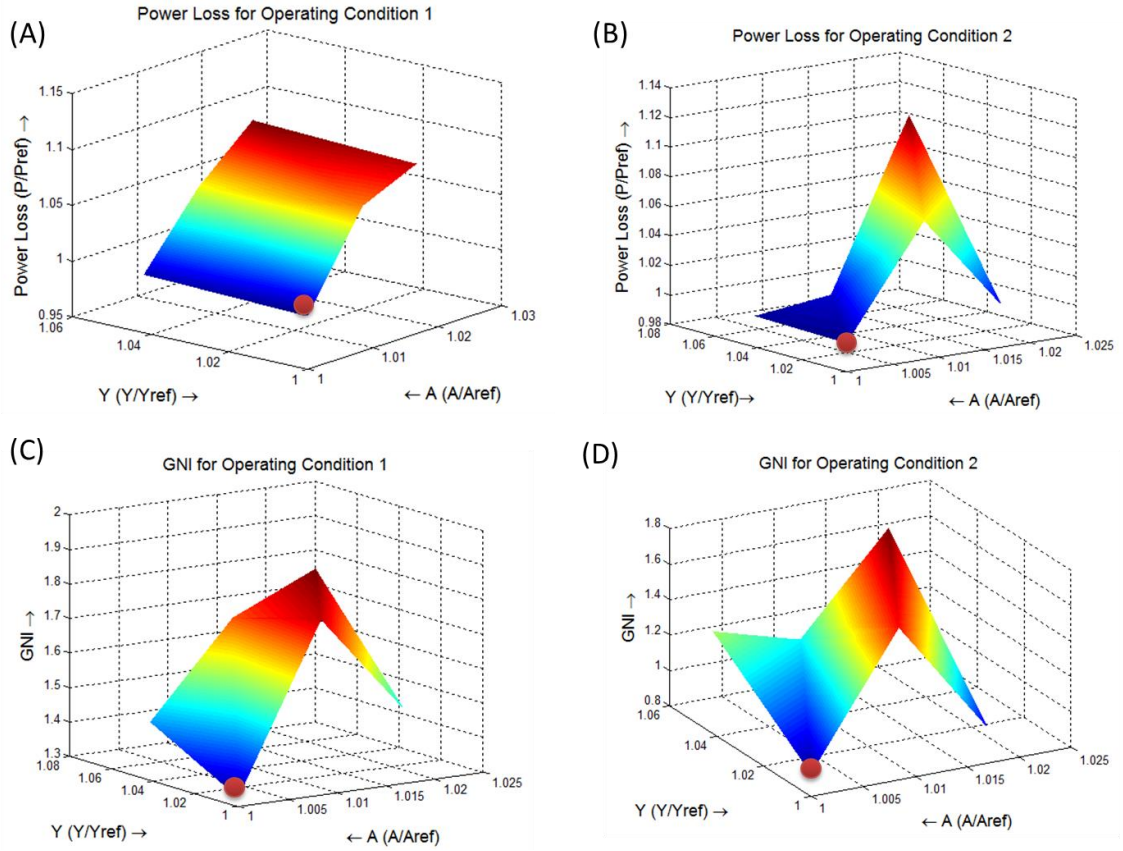

Figure 65: Plots of objective function values at the end of iteration 1. (A) Power loss for OC 1 (B) Power loss for OC 2 (C) GNI for OC 1 (D) GNI for OC 2. The focal point of the iteration is highlighted as a red circle.

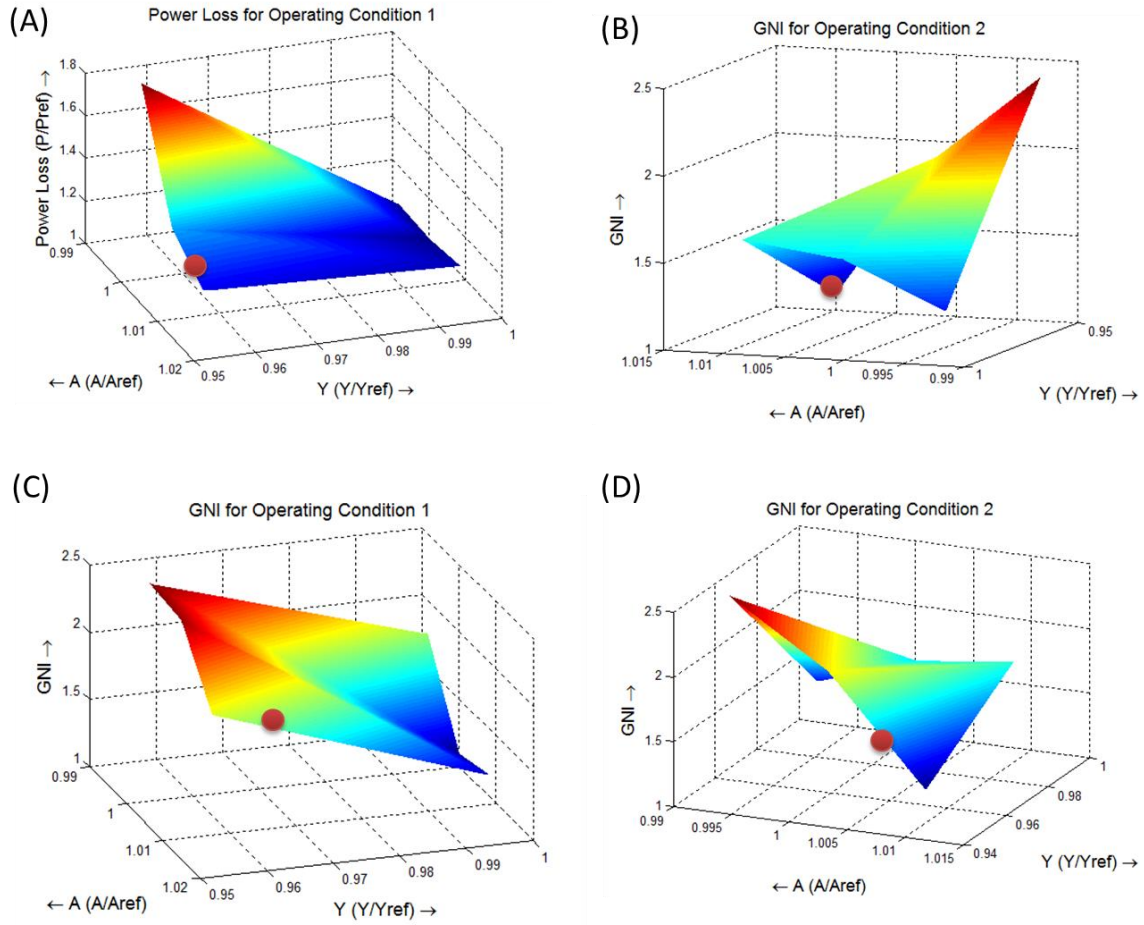

Figure 66: Plots of objective function values at the end of iteration 2. (A) Power loss for OC 1 (B) Power loss for OC 2 (C) GNI for OC 1 (D) GNI for OC 2. The focal point of the iteration is highlighted as a red circle.

The poll step in the second iteration with changed search directions yielded a new focal point as marked in Figure 66. Figure 66 shows the values of the objective functions at the end of this poll step. This iteration was followed by a search step in which the step size of the design grid was halved. The plots of the objective functions at the end of this iteration 3 is shown in Figure 67. The search directions were again changed, but with a refined design grid now. The convergence was reached after 5 iterations of the procedure which included a poll step followed by a search step in the last two iterations. Only the most significant objective function plots with visually noticeable changes in the focal point were shown here in the results section of the optimization procedure.

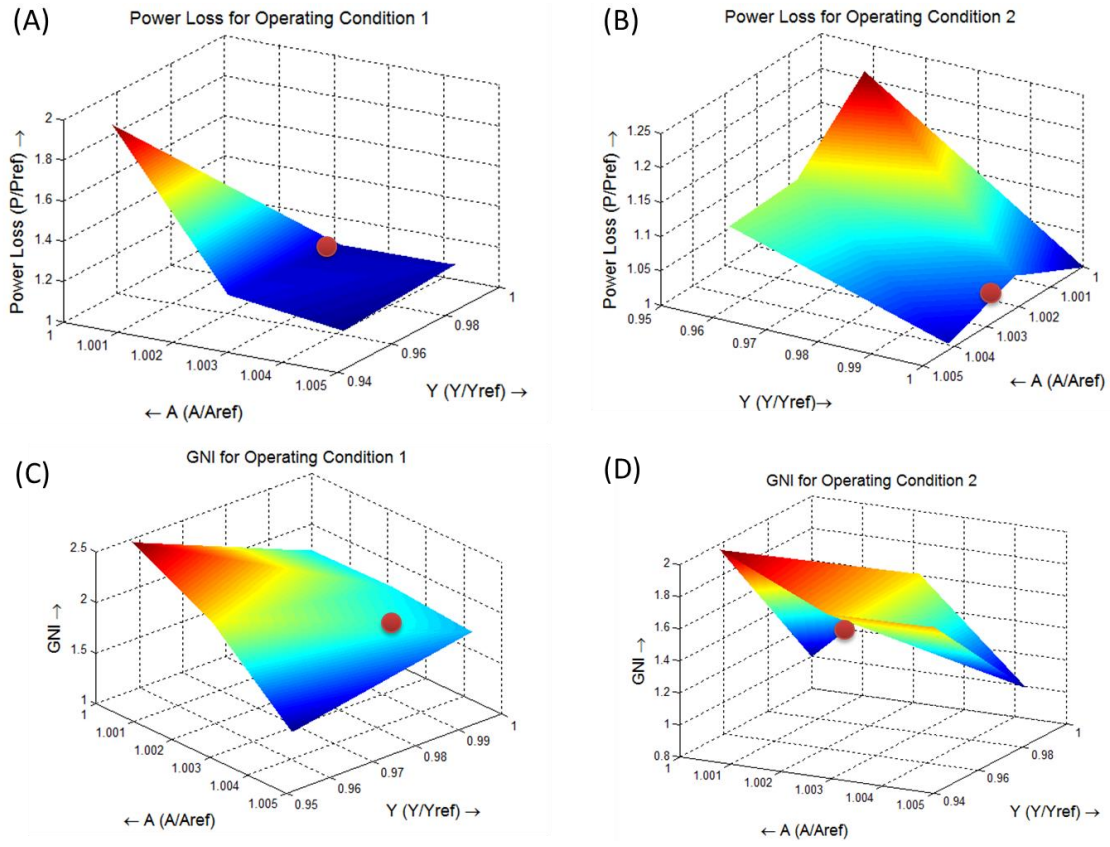

Figure 67: Plots of objective function values at the end of iteration 3. (A) Power loss for OC 1 (B) Power loss for OC 2 (C) GNI for OC 1 (D) GNI for OC 2. The focal point of the iteration is highlighted as a red circle.

The final optimized design grid point was found at ${}^{A}/_{A_{Ref}} = 1.0053$ and ${}^{Y}/_{Y_{Ref}} = 0.979$ which is very close to the optimized design point found in 6.1.

The results obtained for the gap film thickness from the FSI-EHD model for the two selected operating conditions with the optimized balance area design are shown in Figure 68. All the film thickness results presented in this study were normalized with the help of the parameter h_{Ref} which is **O** (3 µm) for the reasons of confidentiality. It can be observed from the results that the hydrodynamic effect of the wedge gears aids in increasing the gap heights and promoting good orientation of the lateral gap.

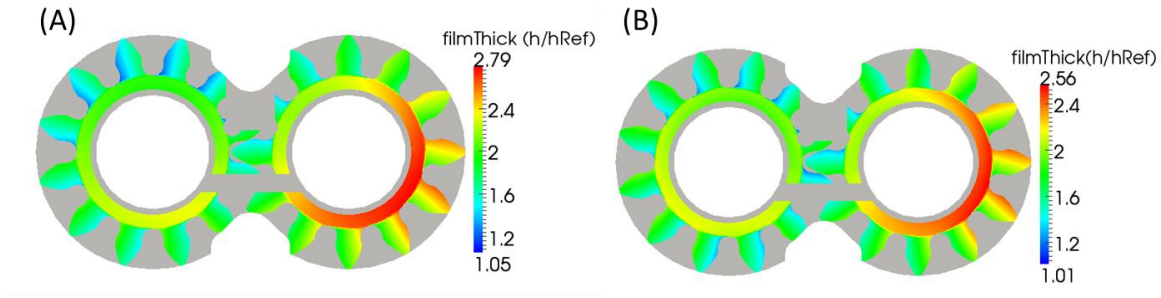

Figure 68: Gap film thickness results with the optimized balance area design for the case of 3 micron wedge depth gears with two input operating conditions at (A) OC 1 (B) OC 2.

A quantitative comparison between the results obtained from the optimization procedure with two and four input operating conditions in terms of the objective functions total power loss from the lateral gap and the GNI of the gap are made in Table 5.

Table 5: Quantitative comparison of total power loss and GNI of the lateral gap between wedged gears (with 3 micron wedge depth) with optimized balance area obtained with two input operating conditions and four input operating conditions.

Operating condition	**Power loss (wrt reference EGM design)**		**GNI (wrt reference EGM design)**	
	Wedged gears with balance area optimized with four input operating conditions	*Wedged gears with balance area optimized with two input operating conditions*	*Wedged gears with balance area optimized with four input operating conditions*	*Wedged gears with balance area optimized with two input operating conditions*
OC1	Reduced by 57.50 %	Reduced by 58.38 %	Increased by 56.77 %	Increased by 54.32 %
OC2	Reduced by 40.28 %	Reduced by 39.44 %	Reduced by 31.37 %	Reduced by 24.43 %

From the Table 5, it can be seen that the power loss and the GNI values obtained between the two optimization procedures with two and four input operating conditions are very

close to each other. Hence, for the sake of saving computation time and cost, using the optimization procedure with two input operating conditions appears to be a feasible option. All the other results presented in this study have been optimized by using two input operating conditions.

6.3.3 5 Micron Wedge Depth with Two Reference Operating Conditions

In the previous two subsections, the optimization procedure developed in this study was applied to design the balance area for a linear sloping wedged gears with 3 μm maximum wedge depth and the potential of using such a tool to develop such novel efficient design was demonstrated. To further illustrate the application of such a tool, a case of wedged gears with 5 μm maximum depth with similar linear sloping profile to the one previously described in 6.1 and 6.3.2 for the same reference EGM, is considered in the present section to optimize its balance area. Two input operating conditions identical to those described in Table 4 were used in the present optimization procedure as well.

The optimization procedure took 6 iterations to converge, which included 4 poll steps followed by two search steps. The reason for this particular optimization taking more number of iterations than the previous optimizations presented in this paper is that the reference EGM with the original balance configuration at 5 micron wedge depth was underbalanced when compared to the other reference configurations considered in this study. This is due to the fact that a 5 micron wedge depth offers a more pronounced hydrodynamic effect which increases the gap heights and thus the lateral leakages from the lubricating gap. This can be seen in the results for gap film thickness later presented in this section in Figure 70 and Figure 71.

The plots of the objective functions, total power loss and the GNI of the lateral lubricating gap at the end of the first iteration are shown in Figure 69 to give a representation of the values of the objective functions obtained in this procedure. The plots of objective functions for the rest of the iteration are not shown here, since similar plots shown in the other optimization studies in this paper provide the trends and directions in which the optimization procedure proceeds. The focal point of the first iteration is marked as a red

circle in Figure 69. The final design grid point was found at $^{A}/_{A_{Ref}} = 1.037$ and $^{Y}/_{Y_{Ref}} = 0.938$ when the convergence was reached in the optimization procedure.

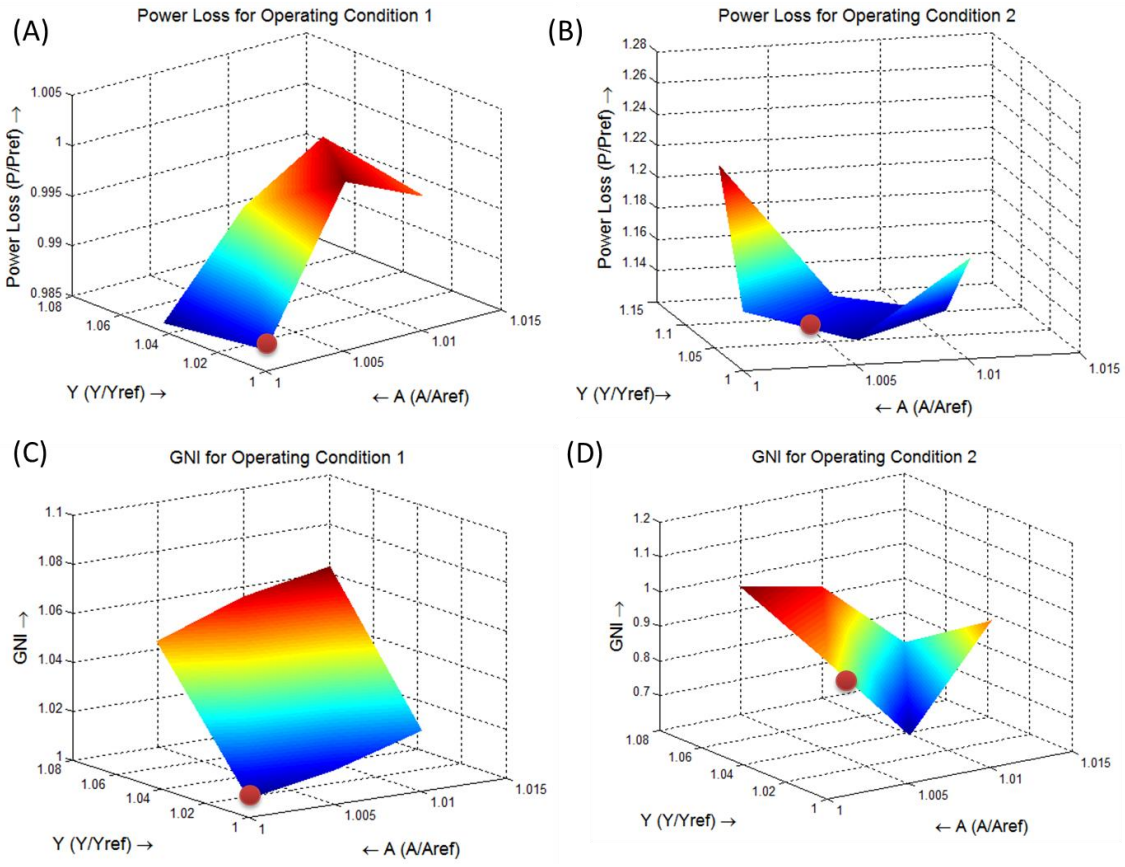

Figure 69: Plots of objective function values at the end of iteration 1. (A) Power loss for OC 1 (B) Power loss for OC 2 (C) GNI for OC 1 (D) GNI for OC 2. The focal point of the iteration is highlighted as a red circle.

The film thickness results in the lateral lubricating gap for the wedge gears with 5 μm maximum wedge depth with the original balance area configuration and new optimized balance area configuration are shown in Figure 70 and Figure 71 respectively. It can be seen visually from these figures that the gap profile and the orientation of the gap has been improved, especially at OC 1. A more rigorous quantitative comparison between these two configurations have been made in Table 6.

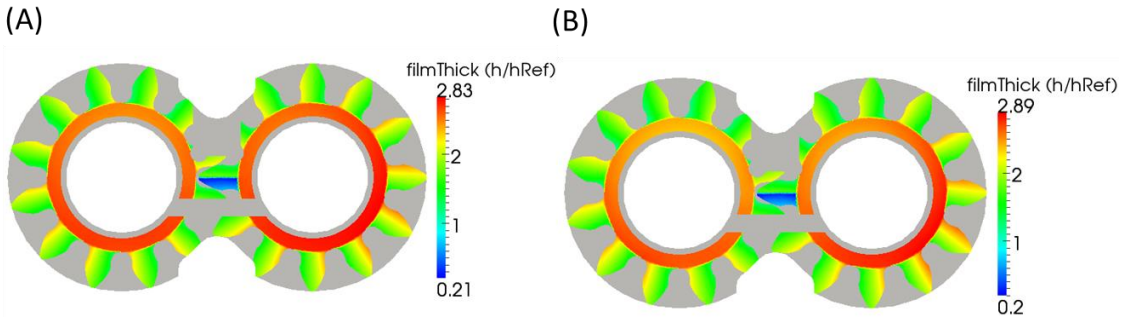

Figure 70: Gap film thickness profiles for wedged gears with 5 micron wedge depth with original balance area configuration at (A) Operating condition 1 (B) Operating condition 2.

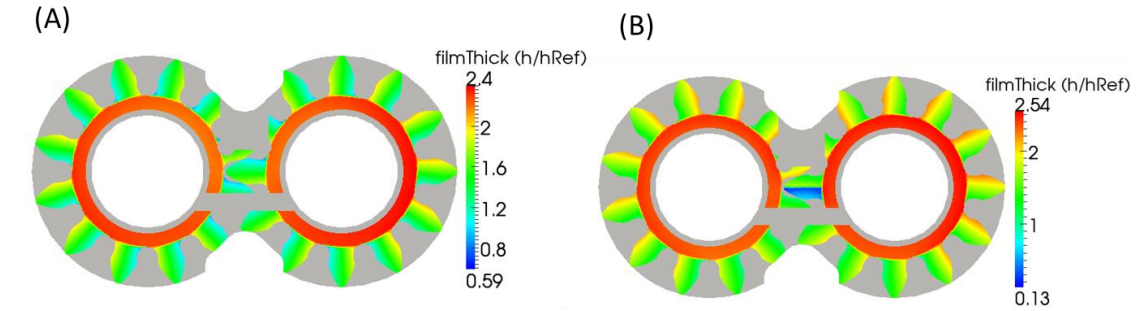

Figure 71: Gap film thickness profiles for wedged gears with 5 micron wedge depth with optimized balance area configuration at (A) Operating condition 1 (B) Operating condition 2.

Table 6: Quantitative comparison of total power loss and GNI of the lateral gap between wedged gears (5 micron maximum wedge depth) with original balance area and optimized balance area design with respect to the reference design without wedged gears.

Operating condition	**Power loss (wrt reference EGM design)**		**GNI (wrt reference EGM design)**	
	Wedged gears with original balance area	*Wedged gears with optimized balance area*	*Wedged gears with original balance area*	*Wedged gears with optimized balance area*
OC1	Reduced by 56.99 %	Reduced by 55.15 %	Increased by 69.99 %	Increased by 59.37 %
OC2	Reduced by 27.83 %	Reduced by 32.61 %	Increased by 19.96 %	Increased by 20.53 %

It can be observed from Table 6 that the lubrication performance of the balance area design has been improved significantly, especially in the power loss values of OC 2 which corresponds to the high pressure high speed condition. It must also be noted that since the current optimization is a multi-objective problem, the resulting optimized balance area configuration represents the best compromise solution across the different objective functions and operating conditions. It is for this reason, a slight increase in the GNI values are found in the optimized design when compared to the original one.

6.3.4 Use of Wedged gears for an Extended Range of Operation

Typically in applications such as injection moulding, a wide range of operation of EGMs between very high and low pressures and speeds. In such a wide range of operation, the axial balance of the EGM becomes a very critical factor in the design. Obtaining an optimal axial balance configuration at all the required operating conditions, becomes a challenging aspect especially with the use of empirical techniques and trial and error experiments. Thus, the optimization tool developed in this research for designing the balance area will prove useful especially in such applications. Furthermore, the hydrodynamic effect provided by adding a wedged profile to the surface of the gears has the potential in improving the performance of EGMs especially at very low speeds. In this section, the capability of the optimization tool to design an optimal balance area for higher values of pressure and between a wide ranges of speeds for a reference EGM with wedged gears is explored.

6.3.4.1 Reference Operating Conditions

Two input operating conditions, both at high pressure but with very low and very high speeds have been chosen for this optimization study and are specified in Table 7. A very low speed of 100 rpm has been chosen for OC 1. A linear sloping wedged profile has been applied to the surface of the gears on each tooth with a maximum wedge depth of 1μm. The hydrodynamic effect of the wedged gears has been shown to perform very well in 6.1 - 6.3.3 and is expected to aid the performance of the selected two operating conditions as well, especially in OC 1 which has a low speed of 100 rpm.

Table 7: Input operating conditions chosen for optimizing the axial balance for an extended operation of the reference EGM.

Operating Condition	Delivery Pressure	Shaft speed
OC 1	$^{p}/_{p_{Ref}} = 0.64$	100 rpm
OC 2	$^{p}/_{p_{Ref}} = 0.64$	2000 rpm

6.3.4.2 Results from the Optimization Procedure

The optimization procedure was initiated with step sizes of $^{\Delta A}/_{A_{Ref}} = 0.0061$ and $^{\Delta Y}/_{Y_{Ref}} = 0.042$. The procedure took 3 iterations to converge, with one poll step followed by two search steps, each of which reduced the step size by half. The plots of the objective functions, power loss and GNI of the lateral gap for both the input operating conditions are shown in Figure 72. The focal point of the iteration is marked as a red circle at all the objective function plots in Figure 72. This focal point did not change for the rest of the procedure and the two succeeding search steps merely reduced the step sizes by half without finding a better design point. Thus, from the numerical procedure, it was found that the best possible design grid point was obtained at $^{A}/_{A_{Ref}} = 1$ and $^{Y}/_{Y_{Ref}} = 1$.

It can be inferred from these results that with the specified step sizes for convergence for both the design parameters A and Y, it was found out that the original balance configuration of the EGM provided the best optimal axial balance across an extended range of operation considered in this case. The use of the optimization procedure helped in verifying this particular fact in this case. Also, it must be noted that an extended range of operation of the reference EGM especially at speeds as low as 100 rpm (considered at OC 1) was possible mainly due to the hydrodynamic effect provided by adding a wedged profile to the gears with a maximum wedge depth of 1 µm. Thus, by considering this profile of the wedged surface for the reference EGM with the original balance configuration, an optimal axial balance for the reference EGM can be achieved for a wide range of operation, especially at very low speeds (~100 rpm).

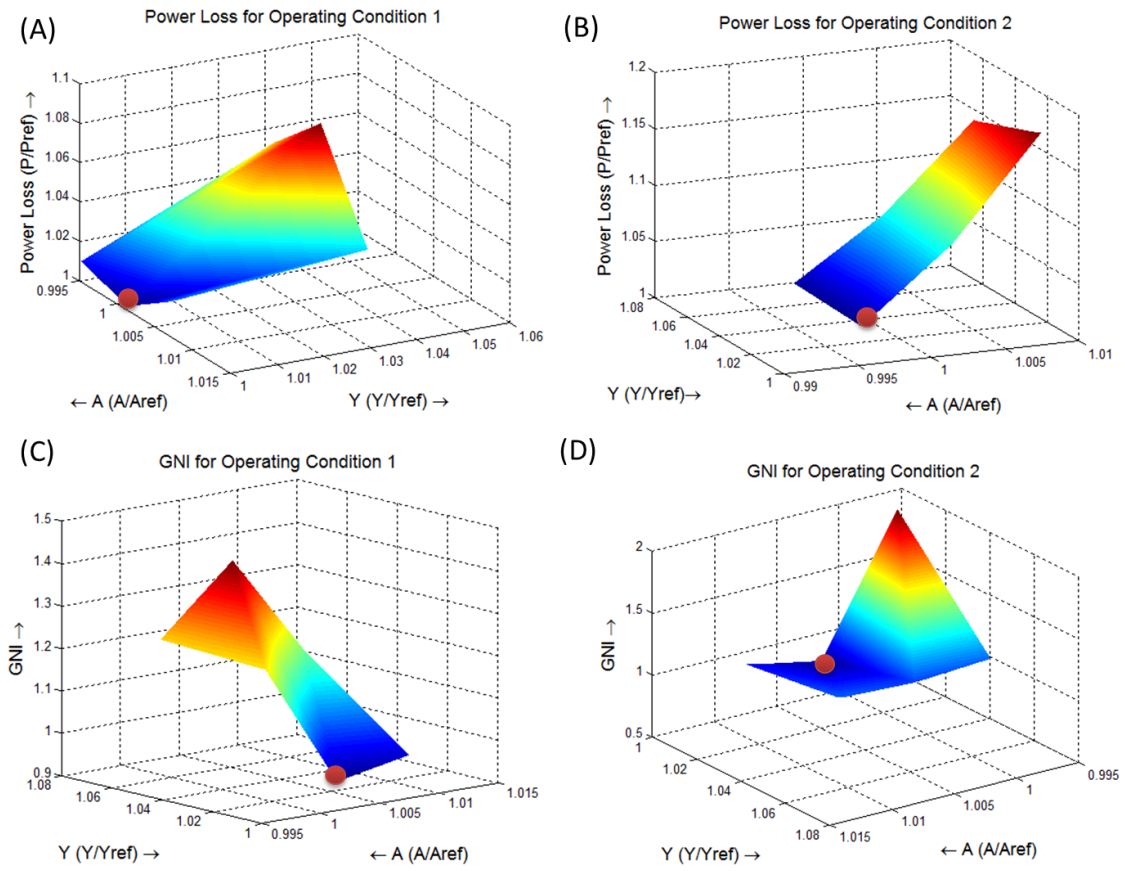

Figure 72: Plots of objective function values at the end of iteration 1. (A) Power loss for OC 1 (B) Power loss for OC 2 (C) GNI for OC 1 (D) GNI for OC 2. The focal point of the iteration is highlighted as a red circle.

The results for the film thickness profiles in the lubricating interface obtained using the FSI-EHD lateral gap model for the nominal reference design of the EGM without the wedged gears at the two operating conditions OC 1 and OC 2 are shown in Figure 73(A) and Figure 73(B) respectively. The film thickness profiles for the optimized balance design of the same reference EGM with the wedged gears (maximum wedge depth of 1 μm) at the two input operating conditions OC 1 and OC 2 are shown in Figure 74(A) and Figure 74(B) respectively.

It can be observed from the film thickness plots that the minimum gap heights at both the operating conditions have been improved by using the wedged gears. In particular, by observing the results for OC 1 closely (from Figure 73(A)), the nominal reference design of the EGM (without the wedge gears) has higher gap heights near the delivery side and

lower gap heights near the suction port. This can be attributed to the fact that the EGM seems to be underbalanced in this case. Thus, by the wedged gears surface, a better axial balance was achieved at this extreme operating condition with a low speed of 100 rpm (OC 1) which can be observed in Figure 74(A). A quantitative comparison of these two cases has been made in Table 8.

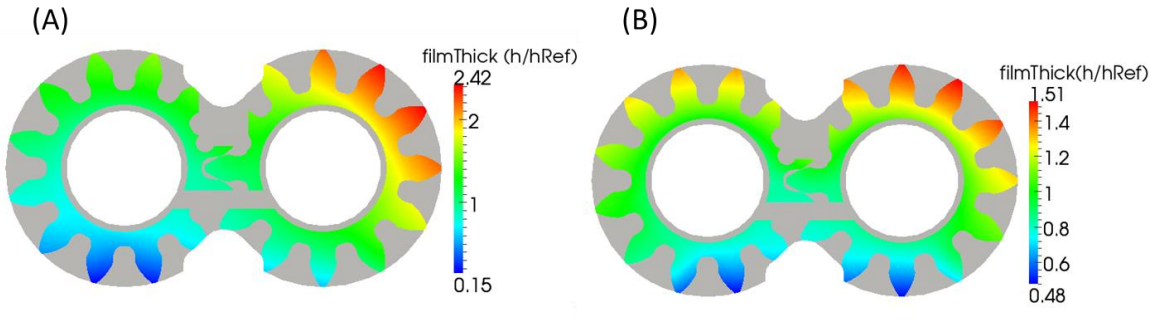

Figure 73: Gap film thickness profiles for the reference EGM without the wedged gears with original balance area configuration at (A) Operating condition 1 (B) Operating condition 2.

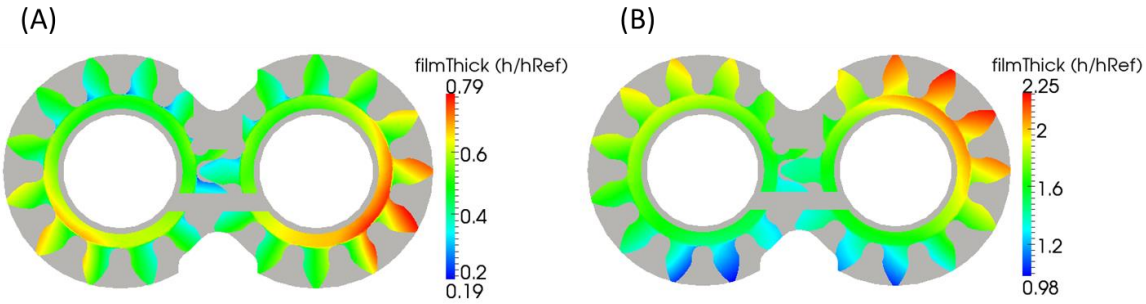

Figure 74: Gap film thickness profiles for the reference EGM with the wedged gears and optimal balance area configuration at (A) Operating condition 1 (B) Operating condition 2.

It can be observed from the table quite significant improvements have been achieved at both the operating conditions in terms of total power loss and GNI in the lateral gap by adding the wedged profile to the surface of the gears.

Table 8: Quantitative comparison of total power loss and GNI of the lateral gap of wedged gears (5 micron maximum wedge depth) with optimized balance area design with respect to the reference design without wedged gears.

Operating condition	**Power loss (wrt to the reference EGM design)**	**GNI (wrt to the reference EGM design)**
OC 1	Reduced by 65.80 %	Reduced by 41.14 %
OC 2	Reduced by 35.04 %	Reduced by 13.88 %

CHAPTER 7. SUMMARY AND CONCLUSION

In the present research study, an automatic numerical procedure was coupled to an advanced FSI-EHD model for lateral lubricating interfaces to design the optimal axial balance for EGMs. The lateral lubricating interfaces in external gear machines are one of the chief sources of power losses, in addition to being frequently the cause of unreliable performance due to wear of parts and seizure. The power losses and the lubricating gap flow itself are dominated by EHD effects. Thus, the effects of fully coupling the solid and the fluid domains in these interfaces need to be properly considered in designing the axial balance in EGMs.

Designing the axial balance in EGMs primarily corresponds to designing the balance area on the lateral bushes and the present research focused on achieving an optimal design of this balance area across a range of operating conditions while fully considering the hydrostatic and hydrodynamic forces acting on the lateral bushing with the help of a FSI model for the lateral gaps. Primarily, the developed numerical procedure aims to achieve an optimal axial balance by minimizing the total power losses in the lateral lubricating gap and ensuring a desired orientation of the lateral gap itself for a wide range of operation of the EGM. The total power losses in the lateral gap include two mutually opposing sources, namely the viscous friction losses and the lateral leakages and the resulting axial balance design should reach an optimal balance between the two. Additionally, in order to account for the non-uniformities and sharp regions of contact in the lateral gap, a factor called the Gap Non-uniformity Index (GNI) was defined in this study. The optimization procedure considers both the power losses and the GNI as part of the objective functions and aims to find the best compromise design solution for the balance area which can minimize both the objective functions at different operating conditions of the EGM. Details of the design

parameters and search methods developed to progress across different iterations in the procedure were presented.

The optimization procedure was shown to be capable of designing the axial balance for different kind balance configurations of EGM, namely both symmetric and asymmetric axial balance EGMs. The results from the optimization procedure for reference EGMs of both configurations were presented and significant improvements to the lubrication performance was achieved in both the cases. Additionally, the optimization tool was also shown in these cases to design both the pressure plate and bearing block design of the lateral bushes.

The potential of the developed optimization tool in investigating novel efficient designs of EGMs, specifically wedged gears in this study, was demonstrated. Adding a linear sloping wedge profile to the surface of the gears was shown provide significant improvements to the lubrication performance in the lateral gaps. Furthermore, when an optimal axial balance using the numerical procedure was designed for these cases, further improvements in power losses and orientation of the gap were observed. Thus, the developed design tool could prove to be very useful in virtually exploring different designs and the possible modifications in these designs. Results from achieving optimal axial balance for specific cases varying the wedge depth in the gear surfaces were presented in this study. The concept of wedge gears along with the developed optimization tool can aid in achieving a stable axial balance of EGMs for an extended field of operation including very high and very low speeds. Such a potential was also demonstrated in this research work.

While the present optimization procedure presents a useful tool for designing the balance areas on lateral bushes, it does not provide the full direct design and shape of the optimized balance area. The optimized results of the procedure include the numerical values of the design parameters considered which need to be used to design the shape of the balance area manually. Integrating the shapes of the various designs considered online with the procedure could be a computationally expensive and time consuming affair with the present method. A possible future development to this procedure could include an efficient way to consider the various shapes of the balance area while finding an optimal design.

However, the optimization procedure developed in this study presents a unique and a first of its kind tool which considers the physical effects of lubricating interfaces in the design process of positive displacement machines. There are few currently existing tools to design the axial balance in EGMs which remains a delicate procedure and such tools are largely empirical, based on experience and expertise. The procedure developed in the current study while coupling an advanced FSI-EHD model for lateral gaps in EGMs to an automatic optimization algorithm thus, creates a unique tool that possesses immense potential to efficiently and virtually design well-balanced EGMs in a fully automatic manner, saving cost, time and efforts.

LIST OF REFERENCES

LIST OF REFERENCES

1. Dhar, S., *A Study of Fluid Structure and Thermal Interactions in the Lubricating Interface Between Gears and Lateral Bushes in External Gear Machines*, Ph.D Thesis, Purdue University, West Lafayette, IN, USA, 2014.
2. Vacca A, Guidetti M. Modelling and experimental validation of external spur gear machines for fluid power applications. Elsevier Simulation and Modelling Practice and Theory. 2011;19:2007-2031.Hooke CJ, Koc E. End plate balance in gear pumps. Paper presented at: Institution of Mechanical Engineers, 1984.
3. Koc E. An investigation into the performance of hydrostatically loaded end-plates in high pressure pumps and motors: movable plate design. Wear. 1991;141:249-265.
4. Koc E, Hooke CJ. Analytical and experimental investigation into the sealing and lubrication mechanisms of the gear ends in pumps. Wear. 1989;135:29-39.
5. Koc E, Hooke CJ. Lubrication and Sealing of Floating End Plates in Gear Pumps. Paper presented at: National Conference on Fluid Power, 1988.
6. Koc E, Hooke CJ. An analysis of the lubrication mechanisms of the bush-type bearings in high pressure pumps. Tribology International. 1997;30:553-560.
7. Borghi M, Milani M, Paltrineiri F, Zardin B. Studying the Axial Balance of External Gear Pumps. Paper presented at: SAE Commercial Vehicle Engineering Congress and Exhibition, 2005.

8. Zecchi M, Vacca A, Casoli P. Numerical analysis of the lubricating gap between bushes and gears in external spur gear machines. Paper presented at: ASME/Bath Symposium on Power Transmission and Motion Control, 2010.

9. Morgridge D, Evans HP, Snidle RW, Yates MK. A study of seal lubrication in an aerospace fuel gear pump including the effects of roughness and mixed lubrication. Tribology Transactions. 2011;54:657-665.

10. Dhar S, Vacca A. A Novel CFD-Axial Motion Coupled Model for the Axial Balance of Lateral Bushings in External Gear Machines. Elsevier Simulation and Modelling Practice and Theory. 2012;26:60-76

11. Dhar S, Vacca A, Lettini A. A Novel Elastohydrodynamic Model for the Lubricating Gaps in External Gear Machines: Evaluation of Axial Balance. Paper presented at: FPNI PhD. Symposium on Fluid Power, 2012.

12. Dhar S, Vacca A. A Fluid Structure Interaction-EHD Model of the Lubricating Gaps in External Gear Machines: Formulation and Validation. Tribology International. 2013;62:78-90.

13. Beecham TE. High Pressure Gear Pumps. Institute of Mechanical Engineers. 1946;154:417-429

14. Bonacini C. Sulla Portata delle Pompe ad Ingranaggi. L'Ingengnere, 1961;9.

15. Manring NH, Kasaragadda SB. The theoretical flow ripple of an external gear pump. ASME Journal of Dynamic Systems Measurement and Control. 2005;125:396-404.

16. Fielding D, Hooke CJ, Foster K, Martin MJ. Sources of Pressure Pulsation from a Gear Pump. Paper presented at: Quiet Oil Hydraulic Systems, 1977.

17. Casoli P, Vacca A, Berta GL. Optimization of Relevant design parameters of external gear pumps. Paper presented at: Japan Fluid Power Symposium, 2008.

18. Casoli P, Vacca A, Franzoni G, Guidetti M. Effects of some relevant design parameters on external gear pumps operating: numerical predictions and experimental investigations. Paper presented at: International Fluid Power Conference (IFK), 2008.

19. Ivantysyn J, Ivantysynova M. Hydrostatic Pumps and Motors. New Delhi: Technip Books International, 2003.

20. Falfari S, Pelloni P. Setup of a 1D model for simulating dynamic behaviour of external gear pumps. Paper presented at: SAE Commerical Vehicle Engineering Congress and Exposition, 2007.

21. Zardin B, Borghi M. Modelling and simulation of external gear pumps and motors. Paper presented at: FPNI PhD. Symposium, 2008.

22. Wustmann W, Helduser S, Wimmer W. CFD Simulation of the reversing process in External Gear Pumps. Paper presented at: International Fluid Power Conference (IFK), 2008.

23. Simerics, Inc. Pumplinx: External Gear Pumps. Available at: http://www.simerics.com/gallery_gear_pump. Accessed June 1, 2014.

24. del Campo D, Castilla R, Raush GA, Gamez Montero PJ, Codina E. Numerical analysis of external gear pumps including cavitation. Journal of fluids engineering. 2012;134(8).

25. Casoli P, Vacca A, Berta GL. A Numerical Model for the Simulation of Flow in Hydraulic External Gear Machines. Paper presented at: Power Transmission and Motion Control, 2007; Bath

26. K. Huang, W. Chang, W. Lian, An Optimization approach to the displacement volumes for external spur gear pumps, Material Science Forum (594), 2008.

27. K. Huang, C. Chen, Kinematic Displacement Optimization of External Helical Gear Pumps, Chung Hua Journal of Science and Engineering, (6), 2008.

28. S wang, H Sakurai, A Kasarekar, The Optimal Design in External Gear Pumps and Motors, IEEE/ASME Transactions on Mechatronics, (16), 2011.

29. Devendran R.S, *A novel optimization methodology for designing external gear machines*, Masters thesis, Purdue University, West Lafayette, IN, USA, 2012

30. Devendran, R. S., & Vacca, A. Optimal design of gear pumps for exhaust gas aftertreatment applications. Simulation Modelling Practice and Theory, 2013:38, 1-19.

31. Seeniraj, G. and Ivantysynova, M. A Multi-Parameter Multi-Objective Approach to Reduce Pump Noise Generation. International Journal of Fluid Power, Vol. 12, 2011.

32. Kim, D. and Ivantysynova, M. Valve plate optimization focusing on noise reduction in the axial piston machine with high volumetric efficiency. Proc. of the 7th FPNI PhD Symposium, Reggio Emilia, Italy, 2012.

33. Ericson L., Johansson A., Ölvander J., and Palmberg J-O, "Prediction and Optimisation of Audible Noise from Fluid Power Machines" in Proceedings of the Seventh International Conference on Fluid Power Transmission and Control, Hangzhou, China, April 7-10, 2009.

34. Ericson L., Ölvander J., and Palmberg J-O., "On Optimal Design of Hydrostatic Machines" in Proceedings of 6th International Fluid Power Conference Dresden, IFK, Dresden, Germany, 2008.

35. Nanbu, T., Ren, N., Yasuda, Y., Zhu, D., & Wang, Q. J. Micro-textures in concentrated conformal-contact lubrication: effects of texture bottom shape and surface relative motion. Tribology Letters, 29(3), 241-252, 2008.

36. Wang, X., Kato, K., & Adachi, K. The lubrication effect of micro-pits on parallel sliding faces of SiC in water. Tribology transactions, 45(3), 294-301, 2002.

37. Křupka, I., & Hartl, M. The effect of surface texturing on thin EHD lubrication films. Tribology International, 40(7), 1100-1110, 2007.

38. Wang, Q. J., & Zhu, D. Virtual texturing: modeling the performance of lubricated contacts of engineered surfaces. Journal of tribology, 127(4), 722-728, 2005.

39. Ivantysynova, M., & Baker, J. Power loss in the lubricating gap between cylinder block and valve plate of swash plate type axial piston machines. Int J Fluid Power, 10(2), 29-43, 2009.

40. Vacca, A., Dhar, S., & Opperwall, T. A coupled lumped parameter and CFD approach for modeling external gear machines. Paper presented at: SICFP2011– The Twelfth Scandinavian International Conference on Fluid Power, 2011.

41. OpenFOAM: The Open Source CFD toolbox. Available at: www.openfoam.com. Accessed June 1, 2014.

42. GNU Scientific Library. Available at: http://www.gnu.org/software/gsl/. Accessed June 1, 2014.

43. ANSYS, Inc. Available at: http://www.ansys.com/. Accessed June 1, 2014.

44. Hamrock, B. J., Schmid, S. R., & Jacobson, B. O. Fundamentals of fluid film lubrication (Vol. 169). CRC press, 2004.

45. Jasak, H., & Weller, H. G. Application of the finite volume method and unstructured meshes to linear elasticity. International journal for numerical methods in engineering, 48(2), 267-287, 2000.

46. Zecchi, M., Vacca, A., & Casoli, P. Numerical analysis of the lubricating gap between bushes and gears in external spur gear machines. In Proc. ASME Symposium on Power Transmission and Motion Control, 2010.

47. Audet, C., Savard, G., & Zghal, W. Multiobjective optimization through a series of single-objective formulations. SIAM Journal on Optimization, 19(1), 188-210, 2008.

48. Torczon, V. On the convergence of the multidirectional search algorithm. SIAM journal on Optimization, 1(1), 123-145, 1991.

49. Torczon, V., & Trosset, M. W. From evolutionary operation to parallel direct search: Pattern search algorithms for numerical optimization. Computing Science and Statistics, 396-401, 1998.

50. Audet, C., Savard, G., & Zghal, W. A mesh adaptive direct search algorithm for multiobjective optimization. European Journal of Operational Research, 204(3), 545-556, 2010.